Requantization of time-dependent mean field for pairing collective motion in superfluid nuclei

Fang Ni

February 2019

Requantization of time-dependent mean field for pairing collective motion in superfluid nuclei

Fang Ni
Doctral Program in Physics

Submitted to the Graduate School of
Pure and Applied Sciences
in Partial Fulfillment of the Requirements
for the Degree of Doctor of Philosophy in
Science

at the
University of Tsukuba

Abstract

The low-lying excited 0^+ states in most of nuclei had been traditionally considered as either β vibration or two-phonon excitation associated with quadrupole vibrations. However, plenty of recent experimental data indicate that not only quadrupole correlations but also pairing correlations play important roles in such excited 0^+ states. The competition between quadrupole correlations and pairing correlations causes complex and mysterious structure for the low-lying excited 0^+ states. We aim to understand such excited 0^+ states based on the time-dependent mean-field (TDMF) theory. Because quantum fluctuation is large in low-lying excitation region, we need to treat the collective motion in large-amplitude regime. However, the theoretical framework to describe pairing collective motions in the large-amplitude regime is not yet established. The nature of low-lying pairing collective motions is still unclear.

We aim at developing a new theoretical framework to describe large-amplitude collective motions associated with nuclear pairing. In our approach, the low-lying excited states are obtained in two steps: (1) solve TDMF equation to obtain the classical trajectories; (2) quantize such classical trajectories to obtain the excited states. The step 2 is called "requantization". First, we consider the pairing collective motions in multi-level pairing model. The pairing models can be classified into two classes, integrable and non-integrable systems. The former one corresponds to the two-level system and the latter one corresponds to the system with three levels or more.

In the integrable system, the requantization of TDMF is particularly feasible because we can easily find the periodic orbits. We apply three different requantization methods, canonical quantization, Fourier decomposition of the time-dependent observables, and stationary phase approximation (SPA) to the path integral. Comparing each requantization method with the exact solution, respectively, SPA turns out to be the most accurate among the three and can describe the excited states quantitatively, including two-particle transition strength. Because the requantized wave functions from SPA are given in terms of the microscopic degrees of freedom, the transition matrix elements can be calculated directly.

Unfortunately, the application of the SPA to the non-integrable system is not straightforward because finding the periodic orbits is an extremely difficult task. We propose a new theoretical approach which makes the SPA to be applicable to non-integrable systems, that is, combining the SPA with the adiabatic self-consistent collective coordinate (ASCC) method (ASCC+SPA). The concept is that we employ the ASCC to extract an integrable subspace from original TDMF phase space, and apply the SPA to the integrable subspace. We apply the ASCC+SPA to the low-lying excited 0^+ states in three-level system and Pb isotopes system. We find that the ASCC+SPA can properly describe the pairing collective motions.

We also examine the validity of the pairing collective model which assumes the pairing gap parameter and gauge angle as the phenomenological collective coordinates. We check the one-to-one correspondence between the collective coordinates self-consistently determined with the ASCC and those assumed in the collective model. We find the collective coordinate describing pairing vibration has no one-to-one correspondence between the two, in both integrable and non-integrable systems. The applicability of the collective model is limited for the nuclear pairing.

With the development of computational power and numerical techniques, the ASCC+SPA is a

promising tool to elucidate the structure of mysterious low-lying excited 0^+ states in nuclei, in near future.

Part of the thesis is based on the results reported in the following publications:

1. *Comparative study of the requantization of the time-dependent mean field for the dynamics of nuclear pairing*, F. Ni and T. Nakatsukasa, Phys. Rev. C **97**, 044310 (2018)

2. *Low-lying collective excited states in nonintegrable pairing models based on the stationary-phase approximation to the path integral*, F. Ni, N. Hinohara and T. Nakatsukasa, Phys. Rev. C **98**, 064327 (2018)

Contents

Chapter 1

Introduction

1.1 Pairing correlation in theoretical and experimental aspects

1.1.1 Superfluid nuclei

Mean-field model is a standard tool to describe the structure of atomic nuclei. The idea of mean-field model is based on the primary theoretical framework of the shell model introduced by Mayer and Jensen in 1949. Mean field picture indicates that the nucleus can be described in single-particle motion in the mean field potential created by the whole nucleons in the nucleus. Although the many-body correlations among the nucleons are extremely complex, the single-particle motion picture can well reproduce the basic properties (e.g. radius, binding energy, separation energy, magic number) in most of nuclide.

Of course, single-particle motion picture cannot describe the nuclear system perfectly. To describe the nuclear structure more precisely, residual interactions need to be taken account. In the 1950s, nuclear physicists found one of the most important residual interactions, pairing correlation. A clear peace of evidence for pairing correlation detected from experiment is the separation energy difference between odd nuclei and even nuclei. Fig. 1.1 shows the separation energies for Sn, Sb, and Te isotopes as a function of neutron number. The isotopes in even number of neutron have about $2 \sim 3$ MeV larger separation energies than the isotopes in the odd number of neutron. It is odd-even staggering (OES) effect, which is detected in whole mass region of nuclei (Fig. 1.2). In this figure, 2Δ corresponds to the separation energy difference between even-even nuclei and odd mass number nuclei. The approximate value is $2\Delta \approx 24A^{-1/2}$ MeV, which indicates a two-body attractive interaction should be included based on the single-particle motion picture. In addition, the spin-parity of the ground states in even-even nuclei are $J^\pi = 0^+$ states and most of the odd-even nuclei have the same spin-parity as their single-particle orbit which the last nucleon fulfills in. These phenomena indicate that the ground states consist of coupled $J^\pi = 0^+$ pairs in even-even nuclei, and coupled $J^\pi = 0^+$ pairs except one nucleon (one proton and one neutron) in the last single-particle orbit in odd-even (odd-odd) nuclei. The two-body attractive interaction which couples two identical nucleons into $J^\pi = 0^+$ state is called pairing correlation.

To describe pairing correlation in nuclei, a theoretical framework beyond the mean-field model seems to be necessary because pairing correlation is two-body interaction. However, there is a tricky approximated theory, BCS theory, enable us to describe pairing correlation within mean-field model. In BCS theory, the superfluid (superconductive) ground state is described in superposed states with different particle number. The particle number in superfluid ground state is not good quantum number, hence, the ground state breaks symmetry in the space, namely U(1) gauge space. The corresponding order parameter, pairing gap Δ, has finite value. Based on BCS theory, because the energy of each particle in a $J^\pi = 0^+$ pair is $E_k = \sqrt{(\epsilon_k - \lambda)^2 + \Delta^2}$, where ϵ_k is single-particle energy, λ is Fermi energy, the lowest single-particle excited state corresponds to one-pair broken state with minimum excitation energy 2Δ. In fact, pairing gap corresponds to the separation energy difference between

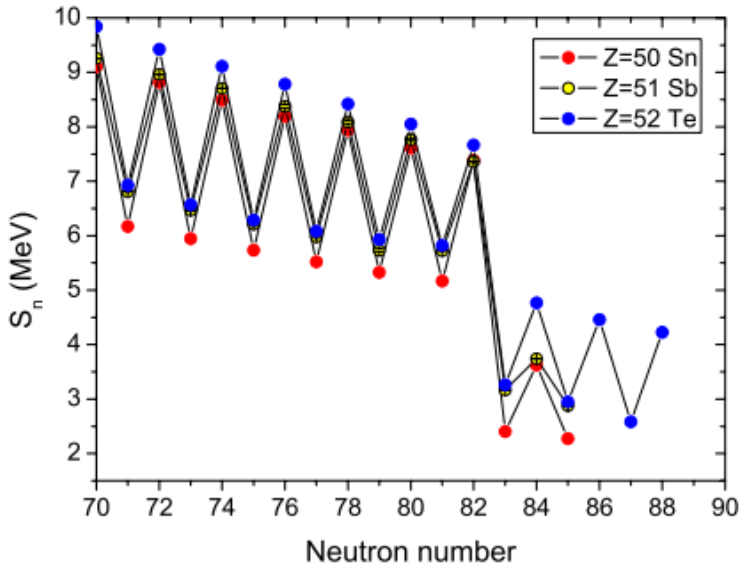

Figure 1.1: Separation energy for Sn, Sb, Te isotopes as a function of neutron number obtained from experimental data. The figure is taken from [1].

even-even nuclei and odd-even nuclei. Thus, BCS theory can explain the OES effect caused from pairing correlation.

After BCS theory was firstly introduced by J. Bardeen, L. Cooper, and J. R. Schrieffer in 1957, it was immediately generalized to Hartree-Fock-Bogoliubov (HFB) theory. HFB theory is the natural extension of Hartree-Fock (HF) theory by introducing Bogoliubov transformation. Under the Bogoliubov transformation, the particles are generalized to quasiparticles, and the mean-field is extended to generalized form including pairing field. After HFB theory had been applied to nuclear physics in 1958, the structure of ground states in nuclei was examined by plenty of studies. Up to now, HFB theory is the standard mean-field theory to describe nuclear structure including pairing correlation.

1.1.2 Pairing collective motion

Due to the superfluid state breaks the symmetry in the U(1) gauge space, there are two types of elementary modes of excitation for pairing collective motion in nuclei. The elementary modes of excitation are Nambu-Goldstone (NG) mode, pairing rotational mode, recovering the broken symmetry in the U(1) gauge space, and Higgs mode, pairing vibrational mode, fluctuating around the energy minimum point.

First, we discuss the pairing rotation. In classical picture, pairing rotation is the motion which the system rotates in the U(1) gauge space (red bi-direction arrow in Fig. 1.4). The motion is described by the coordinate, gauge angle Φ, and the corresponding momentum, total particle number N. Needless to say, N is a constant of motion. In finite many-body quantum system, if we assume the ground state of N_0 particle system as the "ground state", the ground states in $N = N_0 \pm 2, N_0 \pm 4, \cdots$ correspond to the "excited states" in the pairing rotational mode. The excitation energy is $E^{\rm pair}_{\rm rot} = \frac{(N-N_0)^2}{2\mathcal{J}}$, where $\mathcal{J}$ is the pairing-rotational moment of inertia. In experiment, the pairing rotational band is observed in even-even isotopic chain or even-even isotonic chain in open-shell nuclei. A clear observation is detected in Sn isotopes shown in Fig. 1.4. Excluding a constant value and linear term with respect to mass number A, we can find the energies of ground states consist of a parabolic line - pairing rotational band. Recently, the systematic study for the pairing-rotational moment of inertia has been done in Ref. [3]. The experimental moments of inertia obtained from two neutron(proton) separation energies

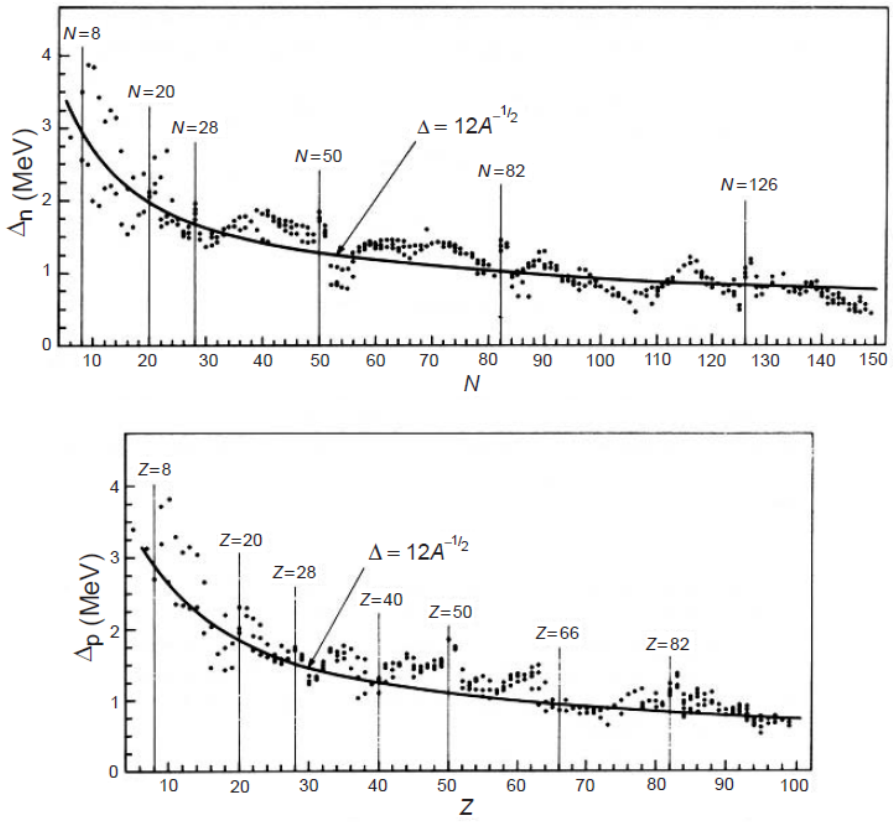

Figure 1.2: The odd-even mass differences Δ_n, Δ_p for neutrons and protons (Zeldes *et al. Mat. Fys. Skr. Dan. Vid. Selsk.*, 3, no. 5 (1967)).

have excellent correspondence with the theoretical moments of inertia obtained from NG mode in quasiparticle random phase approximation (QRPA) [4], not only for the spherical nuclei, but also for the deformed nuclei. Because the pairing-rotational moments of inertia are free from ambiguities caused from odd-even system, they are supposed to be excellent indicators of pairing correlation rather than pairing gaps.

Next, we discuss the pairing vibration. We emphasize that there are two types of pairing vibrations, one vibrating around a normal ground state ($\Delta \approx 0$), and the other vibrating around a superfluid ground state ($\Delta \neq 0$). The properties of the two are quite different. Here, we only focus on the latter case. In classical picture, the system vibrates around the energy minimum point perpendicular to the rotational motion. Depending on the intrinsic structure, various pairing vibrations exists in one nucleus. In quantum picture, if we assume the ground state of N_0 particle system as the "ground state", the excited states in $N = N_0, N_0 \pm 2, N_0 \pm 4, \cdots$ correspond to the "excited states" of pairing vibrational mode. The excitation energy is $E^{\rm pair}_{\rm vib} = n_\alpha \hbar\omega$, where n_α is the number of phonon and α is the label to distinguish different pairing vibrational modes. Because 2Δ is the minimum energy to break one-pair, the collectivity is dominant when $E^{\rm pair}_{\rm vib} < 2\Delta$. Thus, low-lying excited 0^+ states in even-even nuclei have strong collectivity associated with pairing vibration. Except the region around the magic number, excited 0^+ states below 2Δ exist in most of even-even nuclei. However, it is difficult to observe the signatures for pairing vibration directly from experiment. The properties of pairing vibration in nuclei are not well understood up to now.

The signatures for pairing collective motion can also be observed from the two-neutron(proton) transfer reaction [5], such as (p,t), (t,p), and $(^3\mathrm{He},n)$. The cross sections of two particle transfer reaction strongly depend on the matrix elements of $J^\pi = 0^+$ pair-transition operators (e.g. pair-

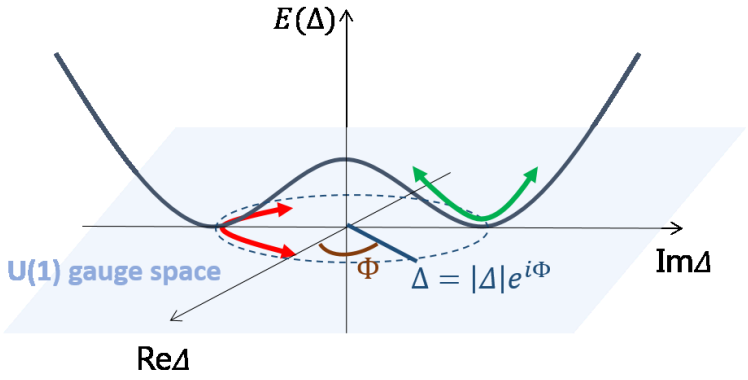

Figure 1.3: Schematic picture of pairing collective motion with superfluid ground state. Red bi-direction arrow indicates pairing rotation, which rotates in Φ direction along the energy minimum circle degenerating at an absolute value of pairing gap $|\Delta| \neq 0$, in the U(1) gauge space. Green bi-direction arrow indicates pairing vibration, which vibrates in $|\Delta|$ direction around one of the degenerated energy minimum points.

additional transition: $\sigma(P_{ad}; 0^+_\alpha(N) \rightarrow 0^+_\beta(N+2)) \sim |\langle N+2, \beta| \sum_k a^\dagger_k a^\dagger_{\bar{k}} |N, \alpha\rangle|^2)$. From theoretical prediction, the pairing correlation enhances $\sigma(g.s. \rightarrow g.s.)$ and decreases $\sigma(g.s. \rightarrow 0^+_{ex})$ significantly, hence, $\sigma(g.s. \rightarrow 0^+_{ex})/\sigma(g.s. \rightarrow g.s.) \ll 1$ is expected in superfluid system. One example of (p,t) reactions is demonstrated in Fig. 1.4. The intraband transition is dominant with respect to the interband transition. Thus, the cross sections of two-neutron transfer reaction is consistent with theoretical prediction. In general, the ratio $\sigma(g.s. \rightarrow 0^+_{ex})/\sigma(g.s. \rightarrow g.s.)$ for two-neutron(proton) transfer reaction is excellent indicator to describe the collectivity of the pairing dynamics.

1.1.3 Mysterious excited 0^+ states and pairing dynamics

In most of nuclei, the structure of excited 0^+ states in a low-lying region (a few MeV excitations) is complex and unclear [6]. The reason is that not only pairing correlations but also deformations and multipole correlations influence the excited 0^+ states significantly. The various correlations competing with each other construct plenty of mysterious excited 0^+ states. We present several examples for these excited 0^+ states observed from experiment.

After the concept of pairing vibration was introduced [7], they encountered the problem for the large asymmetry cross sections between (p,t) and (t,p) reactions in actinide region (e.g. Th, U, Pu, Cm) observed from experiment. In low-lying energy region, the cross section of $\sigma(g.s. \rightarrow 0^+_{ex})$ is about 15% of $\sigma(g.s. \rightarrow g.s.)$ for (p,t) reaction [8, 9], while the signal of $\sigma(g.s. \rightarrow 0^+_{ex})$ is extremely weak for (t,p) reaction [10]. To explain such phenomena, not only pairing vibration but also the necessity of the shape coexistence (oblate shape and prolate shape existing in one state) was suggested [11, 12]. Another interpretation for such phenomena is using microscopic interaction, including multipole pairing correlations and quadrupole particle-hole interactions [13]. Although the approaches between these studies are different, they reproduced the asymmetry cross sections of two-neutron transfer reaction in actinide region. These studies hinted the importance of the quadrupole correlations in low-lying excited 0^+ states.

We can interpret the excited 0^+ states from common viewpoint, liquid drop with surface vibration. Bohr collective model, which is the well-known and successful model describing the quadrupole collective motions in nuclei [14] based on the idea of liquid drop. The 0^+_2 state in the model corresponds to β vibration and the first 2^+ state in $K=2$ bands corresponds to γ vibration, in quadrupole deformed nuclei. Also, their rotational bands exist in each vibrational mode. The nuclei in rare earth region

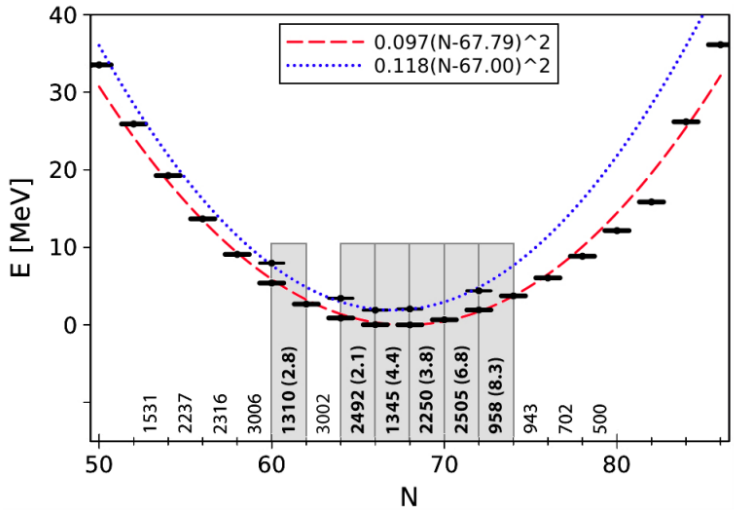

Figure 1.4: Experimental energies of the $J^\pi = 0^+$ states of the Sn isotopes (ground states and pairing vibrational states), populated in (p,t) reactions. The heavy drawn horizontal lines represent the values of the expression $E = -B(^A_{50}\mathrm{Sn}_N) + E_{exc} + 8.124A + 46.33$ MeV, where $B(^A_{50}\mathrm{Sn}_N)$ is the binding energy of the Sn isotopes of mass number A, and E_{exc} is the weighted [with $\sigma(0^+_i)$] average energy of the excited 0^+ states below 3 MeV. The dashed and dotted lines represent the parabolas given in the insets, corresponding to the ground state and to the (average) excited state-based pairing rotational bands. The absolute values of the $g.s. \rightarrow g.s.$ integrated cross sections (in μb units) are given (perpendicular) to the abscissa, as a function of N. The values in the shaded areas correspond to the experimental values, while the remaining values correspond to theoretical predictions. For the first group (experimental), the relative (in %)(p,t), pairing vibrational, cross sections $\sum_i \sigma(g.s. \rightarrow 0^+_i)$ normalized with respect to the ground state cross sections are in parenthesis. The figure is taken from Ref. [2].

(e.g. Sm, Gd, Dy, Er, Yb, Hf, W), well deformed nuclei, had been traditionally considered as the typical examples for the quadrupole collective motions. With the development for extracting $B(E2)$ values from experiment, however, the doubt whether 0^+_2 states in rare earth region is β vibration had arisen in the last decades [15, 16, 17]. They found that only a part of $B(E2)$ values related to the 0^+_2 states agree with the predicted $B(E2)$ values in pure β vibration picture. Moreover, for $E0$ transition, very few 0^+_2 states satisfies the range of $\rho^2(E0)$ values which the β vibrational picture predicts. On the other hand, they detected various cross sections $\sigma(g.s. \rightarrow 0^+_2)$ in both (t,p) and (p,t) reactions. These results suggest that $|0^+_2\rangle$ in rare earth region are not pure β vibrational states, but some states mixing with pairing correlations.

The mystery of excited 0^+ states exist not only in deformed nuclei, but also in spherical nuclei. A best example is the structure of 0^+_2 or 0^+_3 states in Cd isotopes observed in recent experiment [18]. The lower part of Fig. 1.5 shows the excitation energy and $B(E2)$ transition strength in ^{112}Cd. Comparing with the typical values for the ideal quadrupole harmonic vibration in spherical nuclei shown in the upper part of Fig. 1.5, we can find that the observed excitation energy spectra have good coincidence with phonon excitation picture. The 0^+_2 or 0^+_3 states seem to be interpreted as two-phonon or three-phonon excitation. However, the $B(E2)$ values are quite different between the two, especially for the no observed decay from $0^+_{2\mathrm{ph}}$ to 2^+_1 state. Such phenomena are also found in other Cd isotopes. The configuration of these 0^+ states are supposed to be not pure phonon excitation, but proton pair-excitation between $2p_{1/2}$ and $1g_{9/2}$ orbits from the hint of the configurations of Ag isotopes [6]. Therefore, pairing may play an important role in their excited 0^+ states.

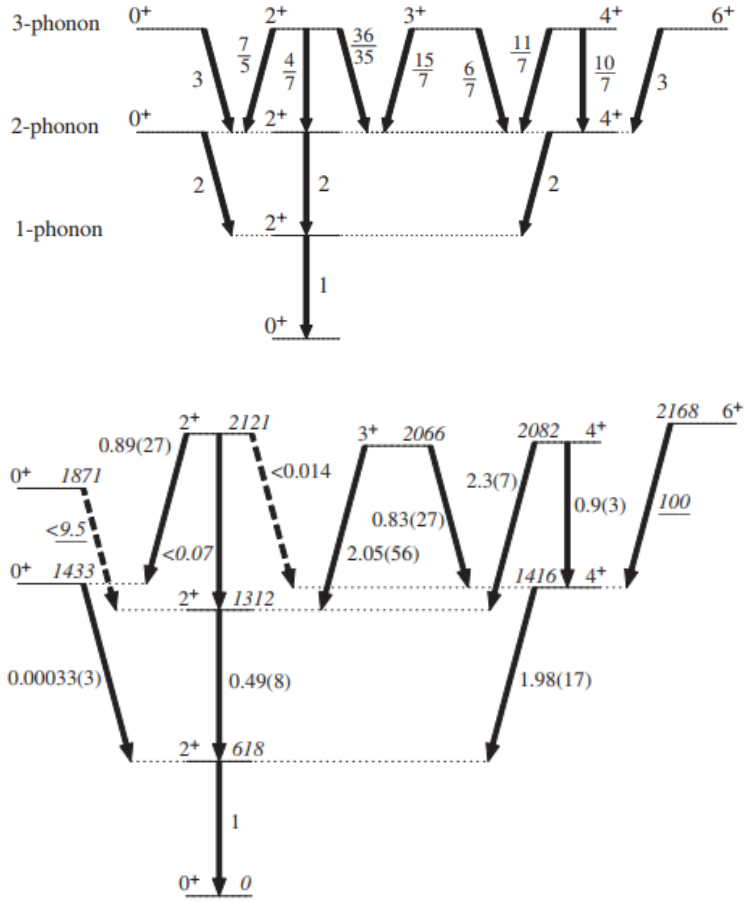

Figure 1.5: $B(E2)$ values, relative to the $B(E2; 2_1^+ \rightarrow 0_1^+)$ value, and energy spectra in phonon excitation picture. Upper panel: expected $B(E2)$ values for a quadrupole harmonic vibrator. Lower panel: data observed for ^{112}Cd. Dashed transitions indicate an unobserved transition. The figure is taken from Ref. [18].

1.2 Motivation of this study

We aim to understand the low-lying excited 0^+ states ($\sim$ a few MeV excitations) from nuclear many-body theory. As mentioned above, pairing correlation plays a significant role in such excited 0^+ states. We need to understand the nature of the pairing dynamics in nuclei. We discuss the theoretical approach to describe the pairing dynamics in the following.

1.2.1 Theoretical problem

Time-dependent mean-field (TDMF) theory is a standard theory to describe the nuclear dynamics. In principle, TDMF enables us to describe the collective motions from the microscopic degrees of freedom without any artificial parameters. Inclusion of the pairing correlation leads to the time-dependent Hartree-Fock-Bogoliubov (TDHFB) theory, which has been utilized for plenty of nuclear structure and reaction studies [19].

Quasiparticle random phase approximation (QRPA) theory, which corresponds to the small amplitude approximation of TDHFB, is known as the most common approach to describe the structure of collective excited states. From a number of studies, the giant resonances (locating at a few MeV $\sim$ dozens of MeV excitations with broad width) can be well described by the QRPA [20, 21, 22, 23]. With density functional formalism, recently, QRPA equation can be solved in finite amplitude method

(FAM) [24]. FAM, which reduces the computational time significantly, enables the linear response calculation for deformed nuclei in allowable computational time. The QRPA is not only useful to predict the collective motions which have not been observed, such as those in exotic nuclei, but also can become the basic concept of a theoretical framework beyond the linear regime. On the other hand, the QRPA description for the low-lying collective excited states is not as good as the giant resonances. The effects of anharmonic vibration and shape coexistence are often important in low-energy region [6], while QRPA is nothing but harmonic approximation. For example, the excitation energies of 0_2^+ states in the rare-earth region have large deviation from the QRPA in realistic nuclear effective interaction [25].

To describe the low-lying excited states, especially for the excited 0^+ states, we need to introduce large-amplitude motions beyond the linear regime. Collective model, which is designed by a couple of collective coordinates and their collective potential and mass parameters, is useful for describing the large-amplitude dynamics. The most popular phenomenological collective model is Bohr collective model, five-dimensional collective Hamiltonian (5DCH) with the quadrupole deformation parameters (β, γ) and the Euler angles (ϕ, θ, ψ). It has been applied to describe the low-lying excited states in realistic nuclei, with their collective potential and mass parameters constructed from the microscopic degrees of freedom [19]. However, the pairing degrees of freedom are not explicitly included in the Bohr collective model. As discussed in Sec. 1.1.2, the pairing vibrational degrees of freedom supposed to be a key ingredient to understand the low-lying excited 0^+ states. We have great interest for the collective coordinates describing the pairing corrective motions.

The discussion for the collective model describing the pairing collective motions is not so much. The first study was introduced by Bes. et al. [26]. They constructed a phenomenological pairing collective model by two degrees of freedom, the pair deformation parameter (pairing gap) Δ and the global gauge angle Φ. After the pairing collective model was formulated, it was combined with the Bohr collective Hamiltonian and applied to describe the nuclear structure [27, 28, 29]. In Ref. [28], the excitation energy and $B(E2)$ transition are improved by introducing pairing degrees of freedom. On the other hand, the wave function of ground state from collective model looks like unusual because the gap parameter Δ_{vib} at the peak of the pairing collective wave function is smaller than the pairing gap Δ_{eq} obtained from BCS equation.

The question is that whether the pair deformation parameter Δ is proper to describe the pairing vibration, as the quadrupole deformation parameters $Q_{2\mu}(\mu = \pm 2, \pm 1, 0)$ describing the quadrupole surface vibration. From the nature viewpoint, the time evolutions of $Q_{2\mu}$ correspond to nuclear vibrations in liquid drop picture, while the time evolution of Δ is difficult to be imagined as a shape vibration. We need to explore more to understand the nature of pairing dynamics in large-amplitude regime.

1.2.2 Our approach

To understand the pairing dynamics in nuclei, we think that it is necessary to develop a theoretical framework describing the large-amplitude collective motions associated with nuclear pairing. Discussion for the collective coordinates describing the pairing collective motions from the TDHFB dynamics itself without any assumption is essential. Apart from the realistic nuclear system, as the first step, we study the pairing collective motions in pairing model, which only contains the monopole pairing correlation in two-body interaction. In this model, the dynamics obtained from the TDHFB degrees of freedom are pure pairing collective motions.

In fact, the number of the TDHFB degrees of freedom equal to the number of the single-particle level, in pairing model. Furthermore, the TDHFB degrees of freedom consist of one constant of motion, pairing rotation, and other intrinsic degrees of freedom. One-level system, which contains only one pairing rotational mode, is well understood (seniority scheme in the textbook [30]). All we have to do is to study the multi-level system. We divide the multi-level system into two classes, two-level system and the system with three levels or more. The former one is two-dimensional integrable system. We

have two decoupled coordinates to describe pairing rotation and pairing vibration, respectively. The latter one is non-integrable system. The coordinates describing the pairing vibrational modes are not explicit. However, adiabatic self-consistent collective coordinate (ASCC) method enables us to find an approximate collective subspace decoupled from other intrinsic degrees of freedom, without any artificial assumption [31, 32]. The ASCC is possible to describe the pairing collective motions in non-integrable system.

With the collective coordinates, we quantize them to obtain the collective excited states. We call this procedure as "requantization". The typical requantization method is Pauli's prescription, a type of canonical quantization, which has been applied to requantize the collective Hamiltonian, such as 5DCH [33] and pairing collective Hamiltonian [26]. However, there is no guarantee whether Pauli's prescription is proper. In addition, Pauli's prescription is not available for the general collective Hamiltonian including the higher-order terms of momenta. Moreover, canonical quantization is not the only approach for requantization. Actually, the requantized results depend on the requantization methods significantly, especially for the pairing collective motions. After trial and error, eventually, we find that the requantization approach following the path integral form is most proper. A stationary-phase approximation (SPA) to the path integral, one of the requantization methods, can describe the pairing collective motions quantitatively. The detailed information is shown in Chap. 3. On the other hand, SPA itself is available only for the integrable system. In order to apply SPA to the general non-integrable system, we construct a new theoretical framework, ASCC+SPA, which can describe the pairing dynamics properly. Moreover, the ASCC+SPA is available not only for pairing collective motions, but also for any types of collective motions. It is the first discussion for the application of the SPA in requantization of TDHFB. In this thesis, the keyword "SPA" emerges frequently.

1.3 Outline of this thesis

This thesis is organized as follows. Chap. 2 is the preparation for the main discussion of the thesis. We show the pairing model in this chapter. Because pairing model is exact solvable model, we give the recipe for the exact solution in the former part. In the latter part, we derive the TDHFB equation for the pairing Hamiltonian in explicit form.

The main achievements of our study are shown in Chap. 3 and Chap. 4. Chap. 3 discuss the pairing collective motions in integrable system (two-level system). We applied three different requantization methods, canonical quantization, Fourier decomposition, and SPA to describe the pairing collective motions. The obtained excitation energies and wave functions from each method are compared with exact solution. Chap. 4 refers the pairing collective motions in non-integrable system. According to the achievement in Chap. 3, we propose a new requantization method, ASCC+SPA. We explain the theoretical framework of ASCC+SPA in the former part, and discuss the result for pairing collective motions from ASCC+SPA in the latter part.

Also, we discuss the validity of the collective model treatment associated with nuclear pairing in Chap. 5. We analyze the one-to-one correspondence between the pairing gap parameter and the collective coordinate obtained from TDHFB dynamics itself in both integrable system and non-integrable system.

In Chap. 6, we summarize our achievements from the study. Moreover, we discuss the remaining problems and perspective of the ASCC+SPA, toward the realistic nuclear system.

Chapter 2

Pairing model

We introduce the pairing model in this chapter. The Hamiltonian of pairing model is

$$\hat{H} = \sum_{\alpha=1}^{L} \epsilon_\alpha \hat{n}_\alpha - g \sum_{\alpha\beta} \hat{S}^+_\alpha \hat{S}^-_\beta, \tag{2.1}$$

where

$$\hat{n}_\alpha = \sum_m \hat{a}^\dagger_{j_\alpha m} \hat{a}_{j_\alpha m} \tag{2.2}$$

$$\hat{S}^+_\alpha = \sum_{m>0} \hat{a}^\dagger_{j_\alpha m} \hat{a}^\dagger_{j_\alpha \overline{m}}, \quad \hat{S}^-_\alpha = \hat{S}^{+\dagger}_\alpha. \tag{2.3}$$

In L single-particle level system, each single-particle energy ϵ_α possesses $(2\Omega_\alpha)$-fold degeneracy ($\Omega_\alpha = j_\alpha + 1/2$) and $\sum_{m>0}$ indicates the summation over $m = 1/2, 3/2, \cdots$, and $\Omega_\alpha - 1/2$. $\overline{m}$ indicates the time reversal quantum number with respect to m. The strength of pairing correlation is represented by coupling constant g. We also define a seniority ν_α, which is the number of unpaired particles in each level. The total number of unpaired particles is $\nu = \sum_\alpha \nu_\alpha$. The unpaired particles play a part in Pauli blocking effect.

In one-level system ($L = 1$), the pairing dynamics is well understood. The analytic solution of the total energy is

$$E_\nu(N) = \epsilon N - \frac{1}{4} g (N - \nu)(2\Omega - N - \nu + 2). \tag{2.4}$$

The pairing rotational band created by the pairing correlation is completely parabolic with the pairing-rotational moment of inertia $2/g$. Also, the excited states in a specified N is only described by the quantum number ν. For example, the first excited state in even particle system is $\nu = 2$ state, which corresponds to one $J^\pi = 0^+$ pair broken state.

The non-explicit dynamics arises in multi-level pairing model ($L \geq 2$). The pairing rotational mode includes higher order terms of N due to the shell effect. In addition, several pairing vibrational modes emerge. The pairing vibration is not single-particle motion specified by ν_α, but a collective motion arisen from $J^\pi = 0^+$ pairs. In order to solve the multi-level pairing Hamiltonian, we explain the numerical exact solution. Also, we derive the TDHFB equation to study the pairing collective motions based on the mean-field picture.

2.1 Exact solution

The eigenvalues and eigenvectors can be solved exactly in pairing model. There are two major methods to obtain the exact solutions, diagonalization in quasispin space and Richardson equation.

2.1.1 Diagonalization in quasispin space

We introduce SU(2) quasispin operators fulfilling the follows commutation relation

$$[\hat{S}^0_\alpha, \hat{S}^+_\beta] = \delta_{\alpha\beta}\hat{S}^+_\alpha, \qquad [\hat{S}^+_\alpha, \hat{S}^-_\beta] = 2\delta_{\alpha\beta}\hat{S}^0_\alpha. \tag{2.5}$$

If we set

$$\hat{S}^0_\alpha = \frac{1}{2}(\sum_m \hat{a}^\dagger_{j_\alpha m}\hat{a}_{j_\alpha m} - \Omega_\alpha) \tag{2.6}$$

and $\hat{S}^+_\alpha, \hat{S}^-_\alpha$ as in Eq. (2.3), the commutation relation (2.5) is fulfilled. Using quasispin operators, the Hamiltonian can be represented by quasispin operators

$$\hat{H} = \sum_\alpha \epsilon_\alpha(2\hat{S}^0_\alpha + \Omega_\alpha) - g\sum_{\alpha\beta}\hat{S}^+_\alpha\hat{S}^-_\beta. \tag{2.7}$$

Therefore, any states $|\psi\rangle$ belong to SU(2)$\otimes\cdots\otimes$SU(2) Hilbert space, and can be expanded in the basis $|S_1, S^0_1; \cdots; S_\alpha, S^0_\alpha; \cdots\rangle$

$$|\psi\rangle = \sum_{S^0_1,\cdots S^0_\alpha,\cdots} c_{S^0_1,\cdots S^0_\alpha,\cdots}|S_1, S^0_1; \cdots; S_\alpha, S^0_\alpha; \cdots\rangle\,. \tag{2.8}$$

We consider the physical meaning of the quasispin space. Because S^+_α and S^-_α correspond to the creation and annihilation operators with respect to the $J^\pi = 0^+$ pairs in each level, the quasispin space is specified in a fixed combination of $\{\nu_\alpha\}$. Also, S^0_α is related to the occupation number in each level. $S^0_\alpha = -S_\alpha$ is the minimum value corresponding no $J^\pi = 0^+$ pair in the level α and $S^0_\alpha = S_\alpha$ is the maximum value corresponding full of $J^\pi = 0^+$ pairs in the level α. Because ν_α plays a part in Pauli blocking effect in the level, the absolute value of quasispin S_α is

$$S_\alpha = \frac{1}{2}(\Omega_\alpha - \nu_\alpha). \tag{2.9}$$

The dimension of the model space is $D = \prod_\alpha(2S_\alpha + 1)$. However, $[\hat{H}, \hat{N}] = 0$ indicates that the Hamiltonian is block diagonal with respect to the total particle number N. The model space can be reduced after we extract the combination of $\{S^0_\alpha\}$ fulfilling

$$N = \sum_\alpha(2S^0_\alpha + 2S_\alpha + \nu_\alpha). \tag{2.10}$$

For example, we consider the dimension of a system with single-particle levels between the magic number 50 and 82. Under spherical symmetry, we have five single-particle levels, $d_{5/2}$, $g_{7/2}$, $s_{1/2}$, $d_{3/2}$, and $h_{11/2}$. The corresponding degeneracy is $\{\Omega_\alpha\} = \{3, 4, 1, 2, 6\}$. If we only consider the case for $\nu_\alpha = 0$, the dimension for the system is $D = 840$. On the other hand, the dimension is reduced under a fixed N, such as 105 for $N = 14$ and 91 for $N = 20$.

2.1.2 Richardson equation

As mentioned above, diagonalizing the Hamiltonian is simple method to obtain the exact solution. However, diagonalization procedure is time consuming when the model space becomes large. The calculation time is proportional to the cubes of the dimension of the model space. For example, if we consider the system between the magic number 50 and 82, the calculation time in deformed system is $\sim 10^5$ times as much as the case in spherical system because the dimension for the deformed system is $D = 2^{16} = 65536$.

The alternative method to obtain the exact solution is to solve Richardson equation. The idea was introduced by R. W. Richardson [34, 35, 36, 37, 38]. We divide the total energy into two parts

$$E = \langle\psi|\hat{H}|\psi\rangle \tag{2.11}$$

$$= \sum_{\alpha} \epsilon_\alpha \nu_\alpha + \sum_{m=1}^{M} E_m. \tag{2.12}$$

The first term is the energy of unpaired particles, and the second term is the total energy of $J^\pi = 0^+$ pairs. The pair-energy E_α is derived from the non-linear equations

$$1 - g\sum_{\alpha} \frac{\Omega_\alpha - \nu_\alpha}{2\epsilon_\alpha - E_\alpha} + 2g \sum_{n(\neq m)}^{M} \frac{1}{E_n - E_m} = 0, \tag{2.13}$$

where M indicates the number of $J^\pi = 0^+$ pairs equaling to the numbers of the non-linear equations. We note that E_m can become not only real numbers, but also complex conjugate pairs when $M \geq 2$.

We solved the non-linear equations numerically in general. If we input a set of initial values E_m^0 into the equations, the values will converge by using proper numerical algorithm such as Newton-Raphson method. The difficult point is that we cannot directly specify the index of excitation from the obtained excitation energy because the energy $\sum_{m=1}^{M} E_m$ is possible to converged to any excited states. After plenty of studies for the numerical techniques, recently, such difficulty was solved in Ref. [39]. They employed a simple hybrid polynomial to simplify the guess of the initial values, and obtained the proper energies easily in very short computational time. This approach is useful not only for the energy in ground state, but also for the low-lying excitation energies

Another challenging problem is how to calculate the wave functions. The eigenvectors can be also calculated numerically by using the obtained E_m. Because the dimension of the eigenvectors is huge in general, we need to calculate the matrix elements for a specific operator we interest (e.g. occupation number operator $\hat{n}_\alpha$, two-particle transition operator $\hat{S}_\alpha^\pm$). The expectation value of such operators can be obtained by solving non-linear equations for a specific operator [38]. However, there is no general method to calculate the off-diagonal part of operators. The development for solving Richardson equations is still necessary.

2.2 TDHFB dynamics

We apply time-dependent mean-field (TDMF) theory to examine the classical picture of the pairing dynamics. With pairing correlation, TDMF theory attributes to TDHFB theory. The TDHFB equation can be derived from the time-dependent variational principle,

$$\delta\mathcal{S} = 0, \quad \mathcal{S} \equiv \int \langle\phi(t)|i\frac{\partial}{\partial t} - \hat{H}|\phi(t)\rangle\, dt, \tag{2.14}$$

where $|\phi(t)\rangle$ is time-dependent generalized Slater determinant (coherent state)

$$|\phi(t)\rangle = \mathcal{R}\exp\left(\sum_{k<k'} Z_{kk'}(t)\hat{\beta}_k^\dagger\hat{\beta}_{k'}^\dagger\right)|\Phi_0\rangle\,, \tag{2.15}$$

where $\beta_k^\dagger$ is quasiparticle creation operator and $\mathcal{R}$ is normalization factor. $|\Phi_0\rangle$ is generally chosen as ground state or vacuum state. $Z_{kk'}(t)$ is time-dependent complex number determined by TDHFB equation.

2.2.1 Hamilton's equation

We derive the TDHFB equation in pairing model. First, we consider the time-dependent coherent state. Because the noticeable phenomenon is the pairing collective motions for $J^\pi = 0^+$ pairs in pairing model, we describe the time-dependent coherent state in SU(2) quasispin operators

$$|Z(t)\rangle = \prod_\alpha \left(1 + |Z_\alpha(t)|^2\right)^{-S_\alpha} \exp[Z_\alpha(t)\hat{S}^+_\alpha]\,|0\rangle\,. \tag{2.16}$$

Here, we choose $|\Phi_0\rangle = |0\rangle$ corresponding to the vacuum (zero particle) state. In the quasispin representation, $|0\rangle = \prod_\alpha |S_\alpha, -S_\alpha\rangle$. The coherent state is the extension of BCS trail wave function, which consists of the superposition of different particle number states. Z_α are complex numbers. $|Z_\alpha| = 0$ corresponds to empty occupation and $|Z_\alpha| = \infty$ corresponds to full occupation for $J^\pi = 0^+$ pairs in the level α.

With the transformation $Z_\alpha = \tan\frac{\theta_\alpha}{2} e^{-i\chi_\alpha}$ $(0 \le \theta \le \pi,\ 0 \le \chi < 2\pi)$, the Lagrangian and the expectation value of Hamiltonian become

$$\mathcal{L}(t) = \langle Z(t)|i\hbar\frac{\partial}{\partial t} - \hat{H}|Z(t)\rangle = \sum_\alpha j_\alpha\dot{\chi}_\alpha - \hat{\mathcal{H}}(\chi, j), \tag{2.17}$$

$$\begin{aligned}\mathcal{H}(\chi, j) &\equiv \langle Z(t)|\hat{H}|Z(t)\rangle \\ &= \sum_\alpha \epsilon_\alpha\nu_\alpha + \sum_\alpha 2\epsilon_\alpha j_\alpha - g\sum_\alpha\left((\Omega_\alpha - \nu_\alpha)j_\alpha - j^2_\alpha + \frac{j^2_\alpha}{\Omega_\alpha - \nu_\alpha}\right) \\ &\quad - 2g\sum_{\alpha<\beta}\sqrt{j_\alpha j_\beta(\Omega_\alpha - \nu_\alpha - j_\alpha)(\Omega_\beta - \nu_\beta - j_\beta)}\cos(\chi_\alpha - \chi_\beta),\end{aligned} \tag{2.18}$$

where χ_α are chosen as the canonical coordinates and j_α are the conjugate momenta defined in

$$j_\alpha \equiv \frac{\partial\mathcal{L}}{\partial\dot{\chi}_\alpha} = S_\alpha(1 - \cos\theta_\alpha). \tag{2.19}$$

The detailed derivations are shown in Appendix A. The canonical variables (χ, j) have clear physical meaning. χ_α represent a kind of gauge angle of each level, and j_α correspond to the occupation number in each level

$$\langle Z|\hat{n}_\alpha|Z\rangle = \nu_\alpha + 2j_\alpha. \tag{2.20}$$

From (2.19), we can find that $0 \le j_\alpha \le 2S_\alpha$, where $j_\alpha = 0$ corresponds to empty occupation and $j_\alpha = 2S_\alpha$ corresponds to full occupation for $J^\pi = 0^+$ pairs in the level α. Using canonical variables, the TDHFB equations attribute to the Hamilton's equations

$$\dot{\chi}_\alpha = \frac{\partial\mathcal{H}}{\partial j_\alpha}, \quad \dot{j_\alpha} = -\frac{\partial\mathcal{H}}{\partial\chi_\alpha}. \tag{2.21}$$

2.2.2 Constant of motion

The number of the TDHFB degrees of freedom is same as the number of the single-particle levels. However, there is one constant of motion, pairing rotation. Using (2.20), the total particle number can be written in

$$N = \langle Z|\hat{N}|Z\rangle = \nu + 2J, \tag{2.22}$$

where J is defined in

$$J \equiv \sum_\alpha j_\alpha. \tag{2.23}$$

Because ν is nothing but quantum number, we often use J instead of N to specify the total particle number in the following. We confirm that the total particle number is conserved by checking the Poisson Bracket

$$\begin{aligned}\{\mathcal{H}, J\}_{PB} &= \sum_{\alpha}\left(\frac{\partial \mathcal{H}}{\partial \chi_\alpha}\frac{\partial J}{\partial j_\alpha} - \frac{\partial \mathcal{H}}{\partial j_\alpha}\frac{\partial J}{\partial \chi_\alpha}\right) \\ &= \sum_{\alpha}\frac{\partial \mathcal{H}}{\partial \chi_\alpha} \\ &= \sum_{\alpha} 2g \sum_{\beta\neq\alpha}\sqrt{j_\alpha j_\beta(\Omega_\alpha - \nu_\alpha - j_\alpha)(\Omega_\beta - \nu_\beta - j_\beta)}\sin\left(\chi_\alpha - \chi_\beta\right) \\ &= 0. \end{aligned} \tag{2.24}$$

Actually, J correspond to a conjugate momentum with respect to a global gauge angle Φ. We note that Φ is not necessarily becoming $\Phi = \sum_\alpha \chi_\alpha/L$ because the explicit form of Φ depends on the coordinate transformations. In other words, the condition of total particle number conservation cannot determine the form of Φ uniquely.

The canonical variables (Φ, J) describe the pairing rotation. The pairing rotational band emerges in the particle number chain $(\cdots, N-2, N, N+2, \cdots)$. The last term in (2.18) contains the higher order terms with respect to N. It is related to the shell effect. In single-level system, the last term in (2.18) disappears and (2.18) attributes to (2.4). The pairing rotational band is exactly parabolic. In multi-level system, the coupling constant g and single-particle energy ϵ_α affects significantly to the last term in (2.18). The parabolic structure will be broken when the shell effect is strong. The examples for the energy spectra are shown in Appendix D.

For convenience, we decouple the pairing rotational mode in the following chapters. The degrees of freedom is $L-1$ in L level system. In multi-level pairing model, therefore, the dynamics is integrable for $L = 2$ and non-integrable for $L \geq 3$. We discuss the integrable system and non-integrable system in Chapter 3 and 4, respectively.

Chapter 3

Requantization of TDHFB in integrable system

In integrable system, the periodic trajectories are explicit. The requantization of the TDHFB is feasible in such case. In two-level system, the degrees of freedom equal to the number of the constants of motion, total particle number and energy, hence, two-level pairing model is integrable. The main achievement from the study for the integrable system is, we find that the requantization method, stationary-phase approximation (SPA) to the path integral, can quantitatively reproduce the collective excited 0^+ states.

First, we derive the explicit canonical coordinates for each constant of motion in two-level system. We discuss the integrable TDHFB dynamics with some specific examples in Sec. 3.1. Next, we introduce three different requantization methods to obtain the excited states. We discuss the concept and detailed derivation for each requantization method, respectively, in Sec. 3.2, The obtained results from each requantization method are shown in Sec. 3.3.

3.1 Classical dynamics in two-level system

3.1.1 TDHFB dynamics

To describe the one-dimensional time-dependent motion, pairing vibration, by an explicit coordinate, we transform the coordinates χ_α into global gauge angle Φ and relative gauge angle ϕ

$$\Phi \equiv \frac{\chi_1 + \chi_2}{2}, \qquad \phi \equiv \chi_2 - \chi_1. \tag{3.1}$$

These ranges are $0 \leq \Phi \leq 2\pi$ and $-2\pi \leq \phi \leq 2\pi$. Their conjugate momenta (J, j) are given by

$$J = \frac{\partial \mathcal{L}}{\partial \dot{\Phi}} = j_1 + j_2, \qquad j = \frac{\partial \mathcal{L}}{\partial \dot{\phi}} = \frac{j_2 - j_1}{2}. \tag{3.2}$$

As in (2.20), j corresponds to the relative occupation number

$$j = \frac{\nu_2 - \nu_1}{2} + \frac{n_2 - n_1}{4}. \tag{3.3}$$

As discussed in 2.2.2, we note that $\Phi \equiv c_1\chi_1 + c_2\chi_2,\ \phi \equiv \chi_2 - \chi_1$ $(c_1 + c_2 = 1,\ 0 < c_1, c_2 < 1)$ can decouple the pairing rotational mode. One of the choice, $c_1 = c_2 = 1/2$ as in (3.1), is the simplest transformation. After the coordinate transformation, the Lagrangian and Hamiltonian in terms of these canonical variables $(\phi, j; \Phi, J)$ are given by

$$\mathcal{L} = J\dot{\Phi} + j\dot{\phi} - \mathcal{H}(\phi, j; J) \tag{3.4}$$

$$\begin{aligned}\mathcal{H}(\phi, j; J) = &\sum_{\alpha=1,2} \epsilon_\alpha \nu_\alpha + \sum_{\alpha=1,2} 2\epsilon_\alpha j_\alpha - g \sum_{\alpha=1,2} \left((\Omega_\alpha - \nu_\alpha) j_\alpha - j_\alpha^2 + \frac{j_\alpha^2}{\Omega_\alpha - \nu_\alpha} \right) \\ &- 2g\sqrt{j_1 j_2 (\Omega_1 - \nu_1 - j_1)(\Omega_2 - \nu_2 - j_2)} \cos\phi,\end{aligned} \tag{3.5}$$

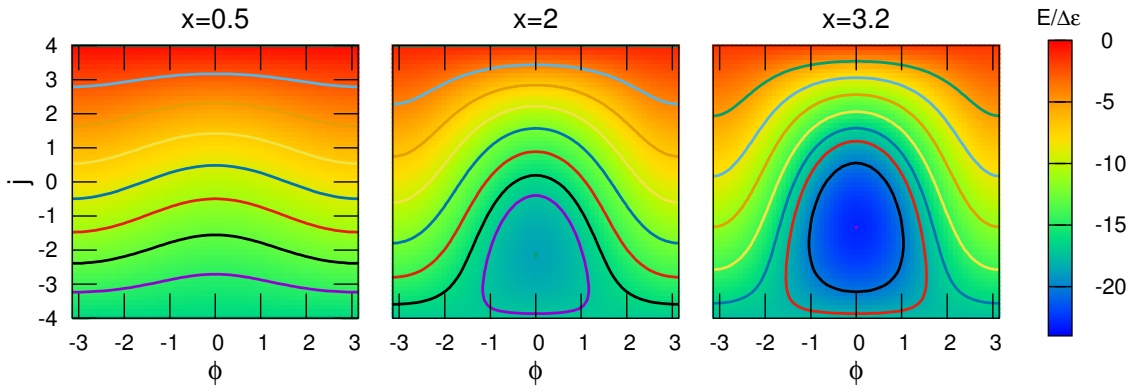

Figure 3.1: Energy contour plot for $\Omega_1 = \Omega_2 = 8$ and $N = 16$. The lines indicate the TDHFB trajectories fulfilling the EBK quantization condition of Eq. (3.20). The figure is taken from Ref. [40].

with

$$j_1 = \frac{J}{2} - j, \qquad j_2 = \frac{J}{2} + j. \tag{3.6}$$

The TDHFB equation can be written in a form of the classical equations of motion:

$$\frac{d\Phi}{dt} = \frac{\partial \mathcal{H}}{\partial J}, \qquad \frac{dJ}{dt} = -\frac{\partial \mathcal{H}}{\partial \Phi}, \tag{3.7}$$

$$\frac{d\phi}{dt} = \frac{\partial \mathcal{H}}{\partial j}, \qquad \frac{dj}{dt} = -\frac{\partial \mathcal{H}}{\partial \phi}. \tag{3.8}$$

Because J and the total energy E are constants of motion, the TDHFB trajectories with given J and E are determined in the two-dimensional phase space (ϕ, j) with the condition

$$\mathcal{H}(\phi(t), j(t); J) = E. \tag{3.9}$$

We demonstrate an example of the classical trajectories in two-level system. Fig. 3.1 shows the contour lines fulfilling (3.9), which correspond to the classical trajectories, with $\Omega_1 = \Omega_2 = \Omega = 8$, $\nu = 0$, and $N = 2\Omega = 16$ with three deferent coupling constant g. The dimensionless coupling constant x is defined as $x = 2g\Omega/(\epsilon_2 - \epsilon_1)$ (See Appendix B.1). The phase transition from normal state to superfluid state occurs at $x = 1$ in closed shell ($N = 2\Omega$). At $x < 1$ corresponding the left panel in Fig. 3.1, the trajectory of ground state is $j = -4$ independent from ϕ. It is consistent with the fully occupied lower level $n_1 = N$ and the empty upper level $n_2 = 0$. For the dynamical states, the trajectories are open with gentle slopes. At $x > 1$ corresponding the middle and right panels in Fig. 3.1, the trajectory of ground state becomes a point at $\phi = 0$, $j = j_0$ ($-4 < j_0 < 4$). With superfluid ground state, the dynamical states have two types, closed trajectory and open trajectory. The closed trajectory appears around $(\phi, j) = (0, j_0)$ at low-energy region. On the other hand, the open trajectory with steep slope appears at high-energy region relatively. The stronger pairing correlation is, the higher transition energy from closed trajectory to open trajectory is. The structure of the excited states between closed trajectory and open trajectory is quite different. The excited states with closed trajectories correspond to "condensed states" similar to the superfluid ground states. The chain of the "condensed states" consists of a rotational band, as shown in Appendix D. Also, they enhance the matrix element of two-particle transfer reaction significantly. We show the feature of these excited states in Sec. 3.3.

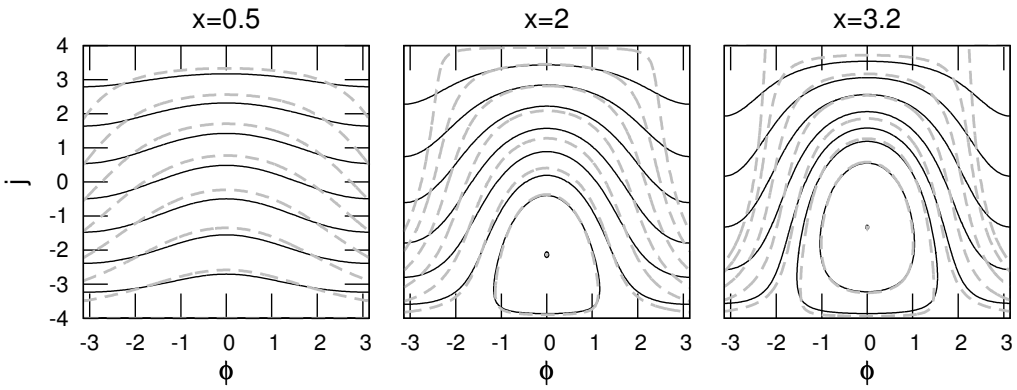

Figure 3.2: Energy contour plot in the same system as Fig. 3.1. Black solid lines correspond to TDHFB trajectories and gray dashed lines correspond to ATDHFB trajectories.

3.1.2 TDHFB dynamics in adiabatic[1] limit

In general, the frequency of the collective motion is much smaller than the frequency in single-particle motion. The slow velocity of the collective motion enable us to expand the TDHFB Hamiltonian up to second order with respect to the collective momentum. We discuss the TDHFB dynamics in adiabatic approximation.

From (3.5), we find that the classical Hamiltonian is even function with respect to ϕ. With time reversal $t \to -t$, Eq. (3.8) is invariant under $j \to j$ and $\phi \to -\phi$, which indicates that j is time-even and ϕ is time-odd. Thus, we switch the coordinate and momentum

$$(\phi, j) \to (j, -\phi), \tag{3.10}$$

to make the coordinate time-even. The classical Hamiltonian under adiabatic approximation becomes

$$\mathcal{H}(j, \phi) \approx V(j) + \frac{1}{2} B^{-1}(j) \phi^2, \tag{3.11}$$

where

$$\begin{aligned} V(j) = \mathcal{H}(\phi = 0, j) = &\sum_{\alpha=1,2} \epsilon_\alpha \nu_\alpha + \sum_{\alpha=1,2} 2\epsilon_\alpha j_\alpha - g \sum_{\alpha=1,2} \left((\Omega_\alpha - \nu_\alpha) j_\alpha - j_\alpha^2 + \frac{j_\alpha^2}{\Omega_\alpha - \nu_\alpha} \right) \\ &- 2g\sqrt{j_1 j_2 (\Omega_1 - \nu_1 - j_1)(\Omega_2 - \nu_2 - j_2)} \end{aligned} \tag{3.12}$$

$$B^{-1}(j) = \left. \frac{\partial^2 \mathcal{H}}{\partial \phi^2} \right|_{\phi=0} = 2g\sqrt{j_1 j_2 (\Omega_1 - \nu_1 - j_1)(\Omega_2 - \nu_2 - j_2)}. \tag{3.13}$$

Of course, $V(j)$ is potential and $B(j)$ is mass parameter. We define a classical trajectory obtained from (3.11) as adiabatic TDHFB (ATDHFB) trajectory. Because the closed trajectories appear around the energy minimum point $(\phi, j) = (0, j_0)$, we expect that adiabatic approximation performs excellent for closed trajectories.

We compare the difference of the classical trajectories between TDHFB and ATDHFB. Fig. 3.2 shows both TDHFB and ATDHFB trajectories in the same system as in Fig. 3.1. For weak pairing correlation ($x < 1$), both results are similar, especially at the low-energy region. For strong pairing

[1] In this thesis, the word "adiabatic" means that the collective motion is slow compared with the single-particle motion.

correlation ($x > 1$), both results are almost identical for closed trajectories. The opened trajectories are also well reproduced near the closed trajectories. The deviation becomes large at the high-energy region. We conclude that ATDHFB is excellent approximation at low-energy region for both open and closed trajectories.

3.2 Requantization methods

To obtain quantum states from TDHFB dynamics, quantization of the TDHFB trajectories, namely, requantization is necessary procedure. We emphasize that there are infinite quantum pictures corresponding to one classical picture. Different quantization methods lead to different quantum states. The straightforward requantization method is canonical quantization, which is commonly applied into nuclear collective model. Here, we apply the canonical quantization to describe the excited states.

3.2.1 Stationary phase approximation to the path integral

TDHFB trajectory corresponds to a stationary-phase limit of the path integral formulation. The idea for constructing excited states from TDHFB trajectories based on the path integral formulation was proposed in Ref. [41, 42, 43, 44, 45, 46]. It recovers quantum fluctuations missing in the mean-field level, and possibly enables us to describe large-amplitude collective tunneling phenomena. The requantization of the TDHFB is particularly feasible for integrable systems, because the system is described by separable action-angle variables (I_k, ϕ_k), leading to the Einstein-Brillouin-Keller (EBK) quantization condition. However, for non-integrable systems in general, it is difficult to find suitable periodic orbits to quantize. A possible solution to this difficulty is to find a decoupled collective subspace spanned by a single coordinate and its conjugate momentum [19]. Since the one-dimensional system is integrable, the quantization is practicable.

Here, we formulate the stationary-phase approximation to the path integral (SPA). Starting an arbitrary state $|\psi(0)\rangle$ at time $t = 0$, the time-dependent full quantum state can be written in the path integral form ($\hbar = 1$)

$$\begin{aligned} |\psi(t)\rangle =& e^{-i\hat{H}t} |\psi(0)\rangle \\ =& \int d\mu(Z'') \, |Z''\rangle \int d\mu(Z') \int_{Z(0)=Z'}^{Z(t)=Z''} \mathcal{D}\mu[Z(\tau)] e^{i\mathcal{S}[Z(\tau)]} \psi(Z'), \end{aligned} \tag{3.14}$$

where $\psi(Z) \equiv \langle Z|\psi(0)\rangle$ and the invariant measure $d\mu(Z)$ is defined by the unity condition,

$$\int d\mu(Z) \, |Z\rangle \, \langle Z| = 1. \tag{3.15}$$

In Eq. (3.14), $\mathcal{S}[Z(\tau)]$ is the action (2.14) along a given path $Z(\tau)$ with the initial coherent state $|Z(0)\rangle = |Z'\rangle$ and the final state $|Z(t)\rangle = |Z''\rangle$, then, the integration $\int \mathcal{D}\mu[Z(\tau)]$ is performed over all possible paths $|Z(\tau)\rangle$ between them. Among all trajectories in the path integral, the lowest stationary-phase approximation $\delta S_{\rm cl} = 0$ selects the TDHFB (classical) trajectories[2].

$$|\psi(t)\rangle \approx \int d\mu(Z') \, |Z'_{\rm cl}(t)\rangle \, e^{i\mathcal{S}_{\rm cl}(Z'_{\rm cl}(t), Z')} \psi(Z'), \tag{3.16}$$

where the TDHFB trajectory starting from $|Z'\rangle$ ends at $|Z'_{\rm cl}(t)\rangle$ at time t. The action $\mathcal{S}_{\rm cl}(Z_f, Z_i)$ is calculated along this classical trajectory connecting $Z_i = Z'_{\rm cl}(0) = Z'$ and $Z_f = Z'_{\rm cl}(t)$.

$$\begin{aligned} \mathcal{S}_{\rm cl}(Z'_{\rm cl}(t), Z') \equiv& \int_0^t \langle Z_{\rm cl}(t)| i\frac{\partial}{\partial t} - H|Z_{\rm cl}(t)\rangle \, dt \\ =& \mathcal{T}[Z_{\rm cl}] - \mathcal{H}(Z', Z'^*)t, \end{aligned} \tag{3.17}$$

[2]In this formulation, the stationary-phase approximation agrees with the TDHF(B) trajectories, while that to the auxiliary-field path integral of Refs. [41, 42] leads to the TDH(B) without the Fock potentials.

with the action integral $\mathcal{T}[Z_{\rm cl}]$

$$\mathcal{T}[Z_{\rm cl}] \equiv \int_0^t \langle Z_{\rm cl}(t)|i\frac{\partial}{\partial t}|Z_{\rm cl}(t)\rangle\, dt. \tag{3.18}$$

In the last equation of Eq. (3.17), we used the fact that the TDHFB trajectory conserves the energy, $\mathcal{H}(Z_{\rm cl}(t), Z^*_{\rm cl}(t)) = \mathcal{H}(Z', Z'^*)$.

The energy eigenstates correspond to stationary states, $\langle Z|\psi(t)\rangle \propto \langle Z|\psi(0)\rangle = \psi(Z)$, which can be constructed by superposing the coherent states along a periodic TDHFB trajectory $Z^{(k)}_{\rm cl}$ as [44, 45, 47]

$$|\psi_k\rangle = \oint d\mu(Z^{(k)}_{\rm cl})\, |Z^{(k)}_{\rm cl}\rangle\, e^{i\mathcal{T}[Z^{(k)}_{\rm cl}]}. \tag{3.19}$$

The single-valuedness of the wave function leads to the quantization condition (k: integer)

$$\begin{aligned}\mathcal{T}_\circ[Z^{(k)}_{\rm cl}] &= \oint \langle Z_{\rm cl}(t)|i\frac{\partial}{\partial t}|Z_{\rm cl}(t)\rangle\, dt \\ &= 2k\pi.\end{aligned} \tag{3.20}$$

The state evolves in time as $|\psi_k(t)\rangle = |\psi_k\rangle\, e^{-iE_k t}$, with the energy of the k-th periodic trajectory, $E_k = \mathcal{H}(Z^{(k)}_{\rm cl}, Z^{(k)*}_{\rm cl})$.

Finding TDHFB trajectories satisfying the quantization condition (3.20) is an extremely difficult task in general. It is better founded and more practical if the classical system is completely integrable. In integrable systems, M complex variables $Z(t)$ can be transformed into the action-angle variables;

$$\begin{aligned}Z(t) &= \{Z_\alpha(t); \alpha = 1, \cdots, M\} \\ &\to \{E; v_1, \cdots, v_{M-1}; \theta_1(t), \cdots, \theta_M(t)\},\end{aligned} \tag{3.21}$$

where the variables E and v define an invariant torus, while $\theta(t)$ parameterize the coordinates on the torus. The integration path of Eq. (3.20) is now taken as topologically independent closed path on the torus, namely the EBK quantization condition. There are M independent closed paths and M quantum numbers, $k = (k_1, \cdots, k_M)$, to specify the stationary energy eigenstate. These are associated with M invariant variables, $\{E_k; v^{(k)}_1, \cdots, v^{(k)}_{M-1}\}$. Using the invariant measure

$$d\mu(Z) = \rho(E, v, \theta) dE dv_1 \cdots dv_{M-1} d\theta_1 \cdots d\theta_M, \tag{3.22}$$

the k-th semiclassical wave function can be calculated as

$$|\psi_k\rangle \propto \oint d\theta_1 \cdots \oint d\theta_M\ \rho(E_k, v^{(k)}, \theta) e^{i\mathcal{T}[E_k, v^{(k)}, \theta]}\, |E_k, v^{(k)}, \theta\rangle\, . \tag{3.23}$$

Here, we omit the integration with respect to the invariant variables, E and v.

We apply the SPA approach to the two-level pairing model. The invariant measure in SU(2)⊗SU(2) is

$$\begin{aligned}d\mu(Z) &= \prod_{\alpha=1,2} \frac{2S_\alpha + 1}{\pi}(1 + |Z_\alpha|^2)^{-2} d({\rm Re}Z_\alpha) d({\rm Im}Z_\alpha) \\ &= \prod_{\alpha=1,2} \frac{2S_\alpha + 1}{4\pi} d(\cos\theta_\alpha) d\chi_\alpha \\ &= \left(\prod_{\alpha=1,2} \frac{1 + (2S_\alpha)^{-1}}{2\pi} \right) d\Phi dJ d\phi dj.\end{aligned} \tag{3.24}$$

In the last equation, we transform the canonical coordinates by Eqs. (3.1) and (3.2). Since the particle number $J = (N - \nu)/2$ and the total energy E are invariant, the two-level pairing model is integrable. Thus, we can construct the semiclassical wave function using Eq. (3.23). From (3.4), the action integral is given by

$$\begin{aligned}\mathcal{T}_k(\Phi, \phi; J) &= J\Phi + \int_0^t j(t')\frac{d\phi}{dt'}dt' \\ &\equiv \mathcal{T}_{J,E_k}(\Phi, t),\end{aligned} \tag{3.25}$$

where the integration is performed on the k-th closed trajectory of Eq. (3.20), and the variables (ϕ, j) are transformed into (t, E). The semiclassical wave function fulfilling the EBK quantization condition becomes

$$|\psi_k^J\rangle \propto \oint d\Phi \oint dt e^{i\mathcal{T}_{J,E_k}(\Phi,t)} |\Phi, t\rangle_{J,E_k} \tag{3.26}$$

$$\propto \sum_{m=0}^{J} C_m^{(E_k,J)} |S_1, -S_1 + m; S_2, -S_2 + (J - m)\rangle\,, \tag{3.27}$$

with $S_\alpha = (\Omega_\alpha - \nu_\alpha)/2$ and the coefficients

$$\begin{aligned}C_m^{(E_k,J)} =& \binom{J}{m} \int_0^T dt \exp\left(i\int^t j(t')\dot{\phi}(t')dt' - i(J/2 - m)\phi(t)\right) \\ &\times A(j_1, S_1, m)A(j_2, S_2, J - m),\end{aligned} \tag{3.28}$$

$$A(j, S, m) = \left(\frac{j}{2S}\right)^{m/2} \left(\frac{2S - j}{2S}\right)^{S-m/2} \sqrt{\frac{(2S)!m!}{(2S - m)!}},$$

where T is the period of the closed trajectory. The TDHFB-requantized wave functions (3.27) are eigenstates of the total particle number. This is due to the integration over the global gauge angle Φ, which makes the particle number projection not only for the ground state but also for excited states. See Appendix C.1 for detailed derivation of Eq. (3.27).

Since we obtain the microscopic wave function of every eigenstate, the expectation values and the transition matrix elements for any operator can be calculated in a straightforward manner. In Sec. 3.3, we show those of the pair-addition operator $\hat{S}^+$ which characterize properties of the pair condensates.

Let us note the periodic conditions of the coordinates and the quantization condition. We have three types of periodic conditions. (1) $\Phi \to \Phi \pm 2\pi$ with fixed ϕ. The quantization condition (3.20) becomes

$$2\pi J = 2k\pi, \tag{3.29}$$

which determines nothing but the total particle number J. (2) $\phi \to \phi$ with fixed Φ. The quantization condition (3.20) becomes

$$\oint j d\phi = 2k\pi, \tag{3.30}$$

which determines the excited states for closed TDHFB trajectories (e.g., 3.1). (3) $(\Phi, \phi) \to (\Phi \pm \pi, \phi \pm 2\pi)$ and $(\Phi, \phi) \to (\Phi \pm \pi, \phi \mp 2\pi)$. because the two original variables, (χ_1, χ_2), are independent periodic variables of the period 2π, in addition to the trivial periodicity of 2π for Φ and of 4π for ϕ. The former (latter) corresponds to $\chi_2 \pm 2\pi$ ($\chi_1 \pm 2\pi$) with χ_1 (χ_2) being fixed. The quantization condition (3.20) becomes

$$\begin{aligned}&\mathcal{T}_{J,E_k}(\Phi \pm \pi, \phi \pm 2\pi; J) = \mathcal{T}_{J,E_k}(\Phi, \phi; J) + 2m\pi \\ \Leftrightarrow \quad &\pm J\pi + \int_{-\pi}^{\pi} j d\phi = 2m\pi,\end{aligned} \tag{3.31}$$

which determines the excited states for open TDHFB trajectories (e.g., Fig. 3.1). This leads to the following:

$$\int_{-\pi}^{\pi} j d\phi = \begin{cases} 2k\pi & \text{for } J = 2n, \\ (2k+1)\pi & \text{for } J = 2n+1, \end{cases} \tag{3.32}$$

where m, k and $n > 0$ are integer numbers.

3.2.2 Canonical quantization

In the pairing collective model, the canonical quantization with Pauli's prescription was adopted in previous studies [26, 27, 28, 29]. Assuming magnitude and phase of the pairing gap as collective coordinates, a collective Hamiltonian was constructed in the second order in momenta. Then, the Hamiltonian was quantized by the canonical quantization with Pauli's prescription. In this section, we apply similar quantization method to the TDHFB Hamiltonian (3.5). The main difference is that the collective canonical variables are not assumed in the present case, but are obtained from the TDHFB dynamics itself.

It is not straightforward to apply Pauli's prescription to the present case, because the TDHFB Hamiltonian (3.5) is not limited to the second order in momenta. The application of Pauli's prescription for the adiabatic TDHFB Hamiltonian (3.11) is discussed in Appendix B.2. Here, we adopt a simple symmetrized ordering, as

$$\begin{aligned} \mathcal{H}(\hat{\phi}, \hat{j}; \hat{J}) = & \sum_{\alpha=1,2} \epsilon_\alpha \nu_\alpha + \sum_{\alpha=1,2} 2\epsilon_\alpha j_\alpha - g \sum_{\alpha=1,2} \left((\Omega_\alpha - \nu_\alpha) j_\alpha - j_\alpha^2 + \frac{j_\alpha^2}{\Omega_\alpha - \nu_\alpha} \right) \\ & - g \left\{ \sqrt{j_1 j_2 (\Omega_1 - \nu_1 - j_1)(\Omega_2 - \nu_2 - j_2)} \cos\hat{\phi} \right. \\ & \left. + \cos\hat{\phi} \sqrt{j_1 j_2 (\Omega_1 - \nu_1 - j_1)(\Omega_2 - \nu_2 - j_2)} \right\}. \end{aligned} \tag{3.33}$$

To fulfill the canonical quantization condition

$$[\hat{\Phi}, \hat{J}] = i, \qquad [\hat{\phi}, \hat{j}] = i, \tag{3.34}$$

as in (3.6), j_α contain J and j which are replaced by

$$\hat{J} = -i \frac{\partial}{\partial \Phi}, \qquad \hat{j} = -i \frac{\partial}{\partial \phi}. \tag{3.35}$$

Since Φ is a cyclic variable, we write the collective wave function $\Psi(\Phi, \phi)$ as eigenstates of the number of $J^\pi = 0^+$ pairs J in a separable form

$$\Psi_k^{(J)}(\Phi, \phi) = \frac{1}{\sqrt{2\pi}} e^{iJ\Phi} \psi_k^{(J)}(\phi). \tag{3.36}$$

Then, the problem is reduced to the one-dimensional Schrödinger equation for the motion in the relative angle ϕ. the Schrödinger equation is

$$H\left(\phi, -i\frac{d}{d\phi}; J\right) \psi_k^{(J)}(\phi) = E_k^{(J)} \psi_k^{(J)}(\phi). \tag{3.37}$$

The wave function should have a periodic property with respect to the variable ϕ; $\psi_k(\phi) = \psi_k(\phi + 4\pi)$. For the adopted simple ordering of Eq. (3.33), it is convenient to use the eigenstates of $\hat{j}$ as the basis to diagonalize the Hamiltonian. They are

$$\chi_j(\phi) = \frac{1}{\sqrt{4\pi}} e^{i\phi j}, \qquad \text{with } j\text{: integer or half integer.} \tag{3.38}$$

Since the Hamiltonian (3.33) contains only terms linearly proportional to $e^{\pm i\phi}$, the basis states χ_j with half-integer difference in j are not coupled with each other. Thus, the eigenstates of Eq. (3.37) can be expanded as

$$\psi_k^{(J)}(\phi) = \sum_{j=j_{\min},j_{\min}+1,\cdots}^{j_{\max}} c_{k,j}^{(J)} \chi_j^{(J)}(\phi). \tag{3.39}$$

According to the relation $j = (j_2 - j_1)/2$ in Eq. (3.2), we adopt the (half-)integer values of j for $J = 2n$ ($J = 2n + 1$) with integer n. This is consistent with the quantization condition (3.32). The coupling term with different j in Eq. (3.33) vanishes for $j_\alpha = 0$ and $j_\alpha = \Omega_\alpha - \nu_\alpha$, which restricts values of j in a finite range of $j_{\min} \le j \le j_{\max}$.

In order to estimate the two-particle transfer matrix elements, we construct the corresponding operators as follows. The classical form of matrix elements are obtained as

$$\begin{aligned} S^+(\Phi, J; \phi, j) &= \langle Z|\hat{S}^+|Z\rangle \\ &= \frac{1}{2}\left(\sqrt{j_1(\Omega_1 - \nu_1 - j_1)}e^{-i\phi/2} + \sqrt{j_2(\Omega_2 - \nu_2 - j_2)}e^{i\phi/2}\right)e^{i\Phi} \qquad (3.40) \\ S^-(\Phi, J; \phi, j) &= \langle Z|\hat{S}^-|Z\rangle \\ &= \frac{1}{2}\left(\sqrt{j_1(\Omega_1 - \nu_1 - j_1)}e^{i\phi/2} + \sqrt{j_2(\Omega_2 - \nu_2 - j_2)}e^{-i\phi/2}\right)e^{-i\Phi}. \qquad (3.41) \end{aligned}$$

Again, we adopt a simple symmetrized ordering for the quantization:

$$\begin{aligned} S^\pm(\hat{\Phi}, \hat{J}; \hat{\phi}, \hat{j}) =& \frac{1}{4}\left(\sqrt{j_1(\Omega_1 - \nu_1 - j_1)}e^{\mp i\hat{\phi}/2} + \sqrt{j_2(\Omega_2 - \nu_2 - j_2)}e^{\pm i\hat{\phi}/2}\right)e^{\pm i\hat{\Phi}} \\ &+ \frac{1}{4}e^{\pm i\hat{\Phi}}\left(e^{\mp i\hat{\phi}/2}\sqrt{j_1(\Omega_1 - \nu_1 - j_1)} + e^{\pm i\hat{\phi}/2}\sqrt{j_2(\Omega_2 - \nu_2 - j_2)}\right). \end{aligned} \tag{3.42}$$

The exponential factors $e^{\pm i\Phi}$ change the total particle number $N \to N \pm 2$ ($J \to J \pm 1$), while $e^{\pm i\phi/2}$ change the relative numbers, $j_2 - j_1 \to j_2 - j_1 \pm 1$. Using these operators, the pair-addition transition strengths are calculated as

$$\begin{aligned} B(P_{\rm ad}; k \to k') &= |\,\langle J', k'|S^+(\hat{\Phi}, \hat{J}; \hat{\phi}, \hat{j})|J, k\rangle\,|^2 \\ &= \left|\frac{1}{2\pi}\int_0^{2\pi} d\Phi \int_{-2\pi}^{2\pi} d\phi \psi_{k'}^{(J')*}(\phi)e^{-iJ'\Phi}S^+(\hat{\Phi}, \hat{J}; \hat{\phi}, \hat{j})\psi_k^{(J)}(\phi)e^{iJ\Phi}\right|^2, \end{aligned} \tag{3.43}$$

which automatically vanishes for $J' \neq J + 1$.

3.2.3 Fourier decomposition

The requantization and calculation of the matrix elements can be also performed using the time-dependent solutions of the TDHFB. It was proposed and applied to the two-level pairing model [48], which we recapitulate in this subsection.

The TDHFB provides a time-dependent solution $Z(t)$ starting from a given initial state $Z(0)$. The energy eigenvalues and the corresponding closed trajectories are determined from the EBK quantization condition (3.20). The pair transfer matrix elements are evaluated as the Fourier components of the time-dependent mean values $S^\pm(t) = S^\pm(Z(t))$, Eqs. (3.40) and (3.41). Since the global gauge angle Φ is a cyclic variable, the motion in the relative gauge angle ϕ is independent from Φ. Thus, we calculate the time evolution of $\phi(t)$, and find the period of the k-th closed trajectory T satisfying Eq. (3.20). Then, the Fourier component,

$$\tilde{S}^\pm(E_k; \omega) = \frac{1}{T}\int_0^T dt e^{i\omega t} S^\pm(t), \tag{3.44}$$

corresponds to the pair transfer matrix element from the state k to k' when $\omega = 2\pi(k'-k)/T$. The pair-addition transition strengths are calculated as

$$B(P_{\rm ad}; k \to k') = \left| \tilde{S}^+ \left(E_k; \frac{2\pi}{T}\Delta k \right) \right|^2, \tag{3.45}$$

with $\Delta k = k' - k$. In this approach, the transition between the ground states of neighboring nuclei ($N \to N+2$) corresponds to the stationary component ($k = 0$ and $\Delta k = 0$), namely the expectation value in the BCS approximation.

The derivation of Eq. (3.44) is based on the wave packet in the classical limit [49]. The TDHFB state is assumed to be a superposition of eigenstates $|\phi_k^N\rangle$ in a narrow range of energy $E_{k_0} - \Delta E < E_k < E_{k_0} + \Delta E$,

$$|Z(t)\rangle = \sum_N \sum_k c_k^N \, |\phi_k^N\rangle \, e^{-iE_k t}, \tag{3.46}$$

where the eigenenergies are evenly spaced and the coefficients c_k^N slowly vary with respect to k and N. The expectation value of $S^\pm$ is

$$S^\pm(t) = \sum_N \sum_{k,k'} c_{k'}^{N+2*} c_k^N \, \langle \phi_{k'}^{N+2} | \hat{S}^\pm | \phi_k^N \rangle \, e^{i(E_{k'} - E_k)t}. \tag{3.47}$$

The matrix element $\langle \phi_{k'}^{N+2} | \hat{S}^\pm | \phi_k^N \rangle$ quickly disappears as $|k' - k|$ increases, while it stays almost constant for the small change of k and N with $|k' - k|$ being fixed. Thus, we may approximate $c_{k'}^{N+2} \approx c_k^N$, $E_{k'} - E_k \approx \omega_0 \Delta k$, and that $\langle \phi_{k'}^{N+2} | \hat{S}^\pm | \phi_k^N \rangle \approx \langle \phi_{k_0+\Delta k}^{N+2} | \hat{S}^\pm | \phi_{k_0}^N \rangle$

$$\begin{aligned} S^\pm(t) &\approx \sum_N \sum_k \left| c_k^N \right|^2 \sum_{\Delta k} \langle \phi_{k_0+\Delta k}^{N+2} | \hat{S}^\pm | \phi_{k_0}^N \rangle \, e^{i\omega_0 \Delta k t} \\ &= \sum_{\Delta k} \langle \phi_{k_0+\Delta k}^{N+2} | \hat{S}^\pm | \phi_{k_0}^N \rangle \, e^{i\omega_0 \Delta k t}, \end{aligned} \tag{3.48}$$

where k_0 is a representative index value of the superposition in Eq. (3.46). From this classical wave packet approximation, we obtain Eq. (3.44). It is not trivial to justify the approximation for small values of Ω and for transitions around the ground state.

3.3 Result

In this section, we study the seniority-zero states ($\nu_1 = \nu_2 = 0$) in the two-level system with equal degeneracy, $\Omega_1 = \Omega_2 = \Omega$. Since all the properties are scaled with the ratio, $g/\Delta\epsilon$, where $\Delta\epsilon$ is the level spacing $\Delta\epsilon = \epsilon_2 - \epsilon_1$, we use the dimensionless parameter x defined in Appendix (B.6) to control the strength of the pairing correlation.

We apply the requantization methods in Sec. 3.2. In the following, the stationary-phase approximation to the path integral in Sec. 3.2.1 is denoted as "SPA", the Fourier decomposition method (Sec. 3.2.3) as "FD", and the canonical quantization with periodic boundary condition (Sec. 3.2.2) as "CQ". Note that the SPA and the FD produce the same eigenenergies which are based on the EBK quantization rule.

3.3.1 Large-Ω cases

In the limit of $\Omega \to \infty$, we expect that the classical approximation becomes exact. Here, we adopt $\Omega = 50$ with $N = 100$ (closed-shell configuration) and $N = 50$ (mid-shell configuration).

Calculated excitation energies are shown in Fig. 3.3. The results of SPA/FD and CQ are compared with the exact values. At the weak pairing limit of $x \to 0$, the excitation energies are multiples of

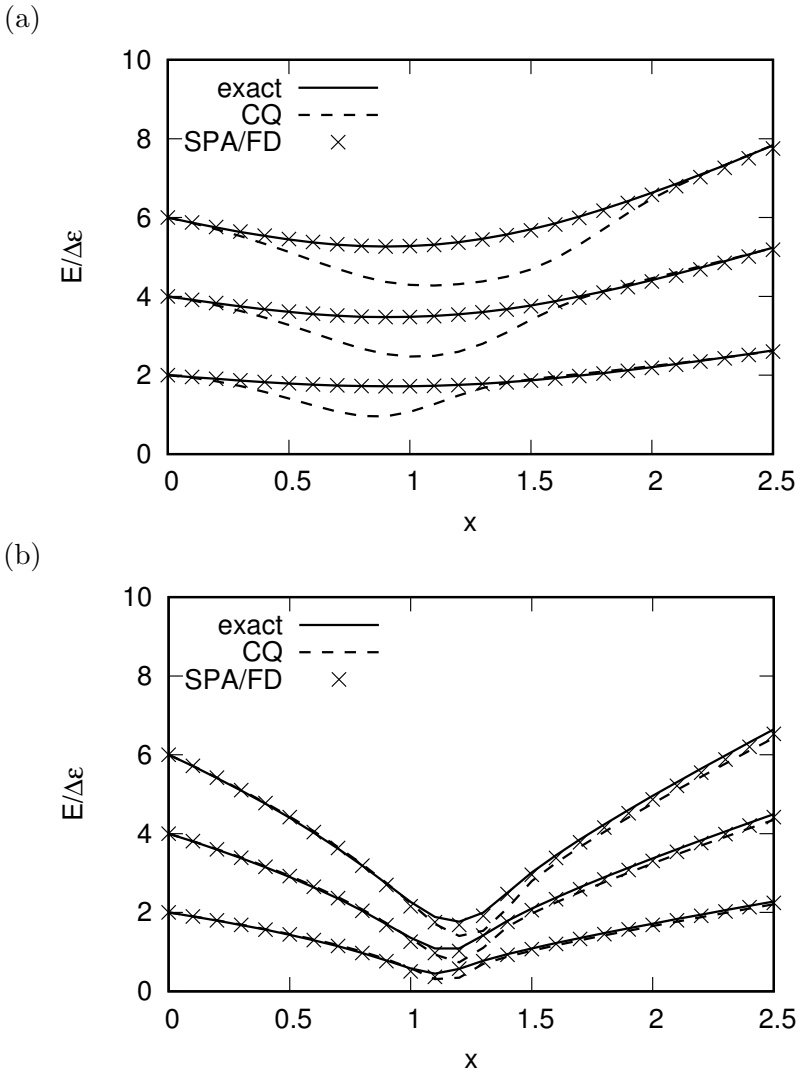

Figure 3.3: Excitation energies of $|0_2^+\rangle$, $|0_3^+\rangle$ and $|0_4^+\rangle$ for $\Omega = 50$ systems with (a) $N = 50$ and (b) $N = 100$ as functions of the dimensionless parameter x of Eq. (B.6). The figure is taken from Ref. [40].

$2\Delta\epsilon$, which correspond to pure $2n$-particle-$2n$-hole excitations. Both the weak and the strong pairing limits are nicely reproduced by all the calculations, while the CQ method produces excitation energies slightly lower than the exact values in an intermediate region around $x = 1$. It is somewhat surprising to see that the deviation is larger for the case of the mid-shell configuration ($N = 50$) than the closed shell ($N = 100$). Here, we emphasize that all of the requantization methods reproduce the pairing vibrational states with normal ground state ($N = 2\Omega$, $x < 1$), while QRPA theory cannot describes them.

The deviation in the CQ method is mainly due to the zero-point energy in the ground state. Since we solve the collective Schrödinger equation (3.37) with the quantized Hamiltonian of Eq. (3.33), the zero-point energy $\Delta E > 0$ is inevitable in the CQ method. The ΔE is associated with the degree of localization of the wave function. Thus, the magnitude of ΔE for "bound" states are different from that for "unbound" states. See Fig. 3.1. In the strong pairing limit, the potential minimum is deep enough to bound both ground and excited states. Conversely, all the states are unbound in the weak limit. In both limits, ΔE for ground and excited states are similar, and they are canceled for the excitation energy. However, near $x = 1$, the ground state is bound, while the excited states are unbound. In this case, ΔE is larger in the ground state than in the excited states, which makes

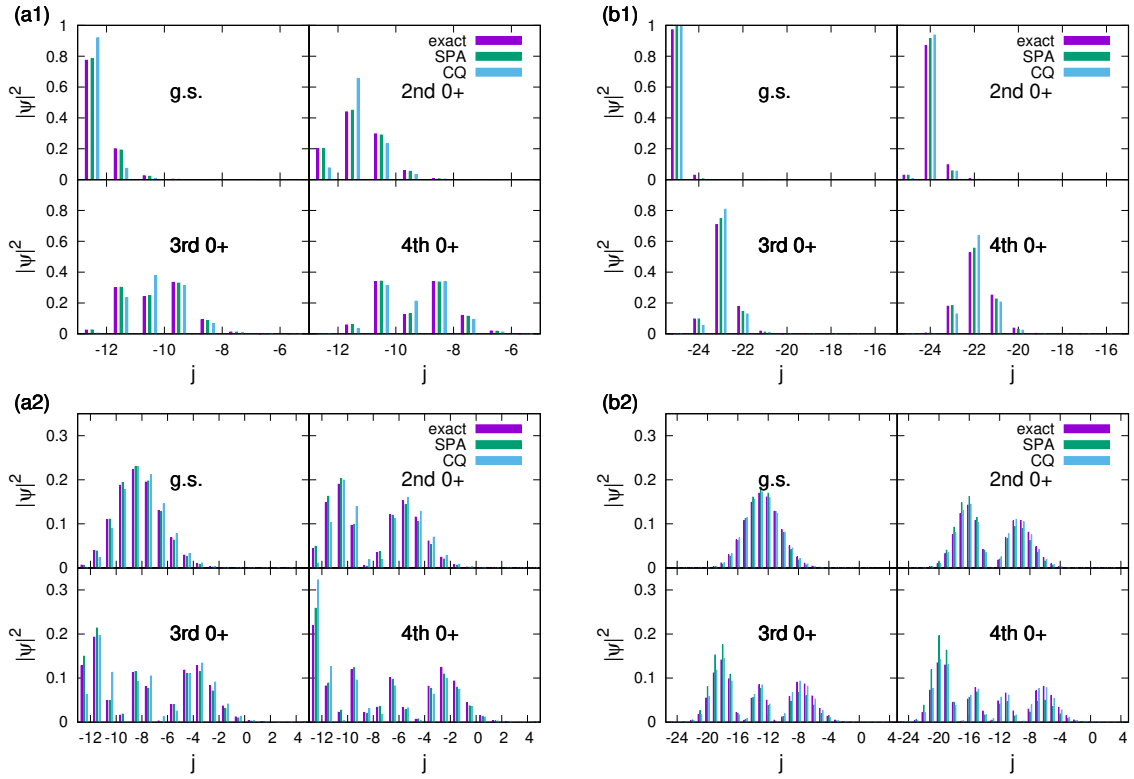

Figure 3.4: Occupation probability in excited 0^+ states as a function of j for $\Omega = 50$ systems with (a) $N = 50$ and (b) $N = 100$. The upper and lower panels display the results for $x = 0.5$ and $x = 2$, respectively. The three vertical bars at each j from the left to the right represent the squared components of the wave functions from exact, SPA, and CQ calculations, respectively. The left end of the horizontal axis at $j = j_{\min}$ corresponds to a component with $(n_1, n_2) = (N, 0)$. The next at $j = j_{\min} + 1$ corresponds to the one with $(n_1, n_2) = (N - 2, 2)$, and so on. The figure is taken from Ref. [40].

the excitation energy smaller. This also explains the difference between the mid-shell and closed-shell configurations. In the closed shell, all the states are unbound for $x < 1$, while, in the mid-shell, there is a region in $x < 1$ where the ground state is bound but the excited state is unbound.

The obtained wave functions in the SPA and the CQ can be decomposed in the $2n$-particle-$2n$-hole components in Fig. 3.4. In the SPA, it is done as Eq. (3.27) and the normalized squared coefficients $|C_m^{(E_k,J)}|^2$ are plotted in Fig. 3.4. For the CQ, $|c_{k,j}^{(J)}|^2$ in Eq. (3.39) are shown. Here, m and j are related to each other, $2j = J - 2m$. They show excellent agreement with the exact results, not only for the ground state but for excited states. We find the SPA is even more precise than the CQ.

Next, let us discuss the transition matrix elements. Here, we discuss $k = 0$ (ground state) and $k = 1$ (1st excited $\nu = 0$ state). The FD calculation is based on the time evolution of the expectation value $S^+(t)$ with fixed (J, Φ) in Eq. (3.44). For $(N, k) \to (N + 2, k')$ transitions, we basically adopt the trajectories for the initial state, namely, the one with $J = N/2$ satisfying the k-th EBK quantization condition. The $k \to k$ ($\Delta k = 0$) transitions correspond to the intraband transitions of the pair-rotational band, when the state is deformed in the gauge space (pair deformation). For the ground-state band ($k = 0$), this is nothing but the expectation value at the BCS wave function, with the constant value of S^+. Since the constant S^+ provides only $\Delta k = 0$ intraband transitions, for the interband transition of $(N, k = 0) \to (N + 2, k = 1)$ transitions, the trajectory satisfying the EBK condition of $k = 1$ is used to perform the Fourier decomposition (3.44) of $\omega = 2\pi/T$.

The calculated pair-addition strengths $B(P_{\rm ad})$ are shown in Fig. 3.5 for $N = 48 \to 50$, and in Fig. 3.6 for $N = 98 \to 100$. Near the closed-shell configuration ($N = 98 \to 100$), the pair-addition

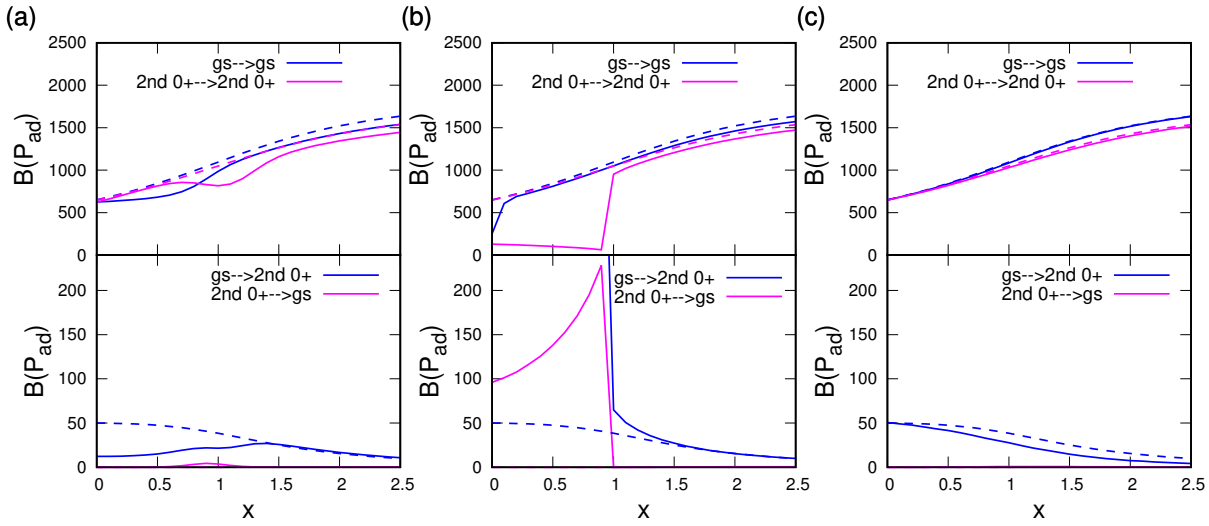

Figure 3.5: The strength of pair additional transition $B(P_{\rm ad}; k \to k')$ for $\Omega = 50$ systems from $N = 48$ to 50. Left panels: results of the CQ method; Middle panels: FD; Right panels: SPA. Dashed lines represent exact calculation. Upper panels show the intraband transitions of $|0_1^+\rangle \to |0_1^+\rangle$ and $|0_2^+\rangle \to |0_2^+\rangle$, while lower panels show the interband transition of $|0_1^+\rangle \to |0_2^+\rangle$ and $|0_2^+\rangle \to |0_1^+\rangle$. The figure is taken from Ref. [40].

strengths for the intraband transitions ($\Delta k = 0$) drastically increase around $x = 1$. This reflects a character change from the pair vibration ($x \lesssim 1$) to the pair rotation ($x \gtrsim 1$). The $B(P_{\rm ad}; k \to k)$ in the pair-rotational transitions are about 20 times larger than those in the vibrational transitions. The interband $B(P_{\rm ad}; 0 \to 1)$ are similar to the $B(P_{\rm ad}; 0 \to 0)$ in the vibrational region ($x \lesssim 1$), because they both change the number of pair-phonon quanta by one unit. In contrast, $B(P_{\rm ad}; 1 \to 0)$, which change the phonon quanta by three, are almost zero. In the pair-rotational region ($x \gg 1$), $B(P_{\rm ad}; 1 \to 0)$ and $B(P_{\rm ad}; 0 \to 1)$ are roughly identical. This is because both $B(P_{\rm ad}; 1 \to 0)$ and $B(P_{\rm ad}; 0 \to 1)$ correspond to one-phonon excitation in "deformed" cases ($x \gg 1$).

In the mid-shell region ($N = 48 \to 50$), the intraband $B(P_{\rm ad}; k \to k)$ are smoothly increase as x increases. Their values are larger than the interband strengths by about one (two) order of magnitude at $x \sim 0$ ($x \sim 2.5$), indicating the pair-rotational character. The interband $B(P_{\rm ad}; 0 \to 1)$ show a gradual decrease as a function of x, while $B(P_{\rm ad}; 1 \to 0)$ are negligibly small, even at $x \gg 1$. This presents a prominent difference from the closed-shell case.

All the features of the pair-transfer strengths are nicely reproduced in the SPA method, for both the closed- and mid-shell configurations. The CQ method qualitatively agrees with the exact calculation. For instance, the order-of-magnitude difference between intraband and interband transitions. However, the precision of the CQ method is not so good, especially around $x = 1$. The FD method properly describes the main features in the superfluid phase, while it fails for the normal phase ($x \lesssim 1$). In the mid-shell configuration, the ground state is always in the superfluid phase at $x > 0$, while the $k = 1$ excited state corresponds to the open (closed) trajectory at $0 < x \lesssim 1$ ($x \gtrsim 1$). For the open trajectory, the FD produces wrong values. However, somewhat surprisingly, the SPA, which uses these open trajectories for the construction of wave functions, reproduces main features of the exact results.

3.3.2 Small-Ω cases

Next, we discuss systems with smaller degeneracy $\Omega = 8$. Again, we study systems near the closed-shell and the mid-shell configurations.

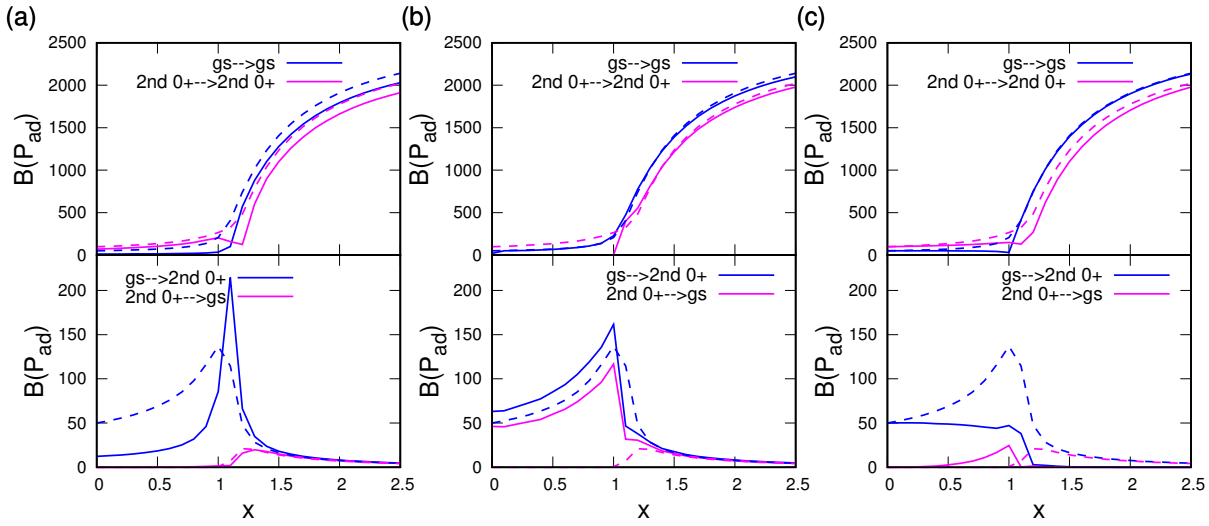

Figure 3.6: The same as described in the caption of Fig. 3.5 but for $N = 98 \to 100$. The figure is taken from Ref. [40].

(a) Mid-shell configuration

The calculated excitation energies are shown in Fig. 3.7 for the $N = 8$ case. The SPA/FD reproduces the exact calculation in the entire region of x, not only for the lowest but also for higher excited states. The CQ reproduces the exact result in a weak pairing region ($x \lesssim 1$), while it underestimates the excitation energies at $x \gtrsim 1$. Analogous to the case of $\Omega = 50$, this is mainly due to effect of the zero-point energy ΔE. The ground-state energy in the CQ calculation is bound at $x \gtrsim 1$. However, because of the weak collectivity with $N = 8$, the first excited state stays unbound even at the maximum x in Fig. 3.7. Therefore, the energy shift $\Delta E > 0$ is larger in the ground state, which makes the excitation energy smaller.

The wave functions are plotted in Fig. 3.8. At the weak pairing case of $x = 0.5$, both the SPA and the CQ reproduce the exact result. At $x = 2$, the squared coefficients of the ground state has an asymmetric shape peaked at the lowest j, which suggests that the state is not deeply bound in the potential. It is in contrast to the symmetric shape in Fig. 3.4. The wave functions obtained by the CQ method has noticeable deviation from the exact results. On the other hand, the SPA wave functions are almost identical to the exact ones.

The pair-addition transition strengths from $N = 6$ to $N = 8$ are shown in Fig. 3.9. The intraband $k \to k$ transitions increase and the interband $k = 0 \to 1$ transitions decrease as functions of x. Their relative difference becomes more than one order of magnitude at $x \gtrsim 2$. Thus, even at relatively small Ω and N, the intraband transitions in the pair rotation is qualitatively different from the interband transitions.

We find the excellent agreement between the SPA and the exact calculations. The first excited state corresponds to the open trajectory which turns out to almost perfectly reproduce the exact wave function. In contrast, this open trajectory produces results far from the exact one in the FD method. It produces almost vanishing the intraband $B(P_{\rm ad}; 1 \to 1)$. The $B(P_{\rm ad}; 0 \to 0)$ shows a qualitative agreement for its behavior, but is significantly underestimated. The CQ method also underestimates the intraband transitions.

For the mid-shell configurations, the SPA is dominantly superior to the CQ and the FD methods.

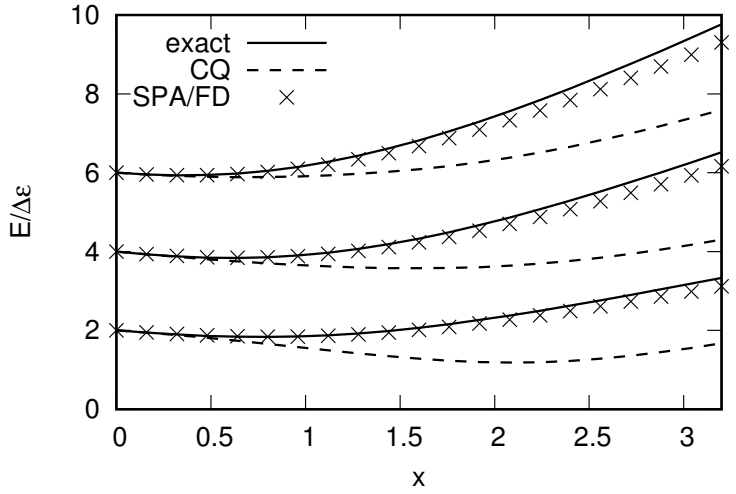

Figure 3.7: Excitation energies of $|0_2^+\rangle$, $|0_3^+\rangle$ and $|0_4^+\rangle$ for $\Omega = N = 8$ systems as functions of x. The figure is taken from Ref. [40].

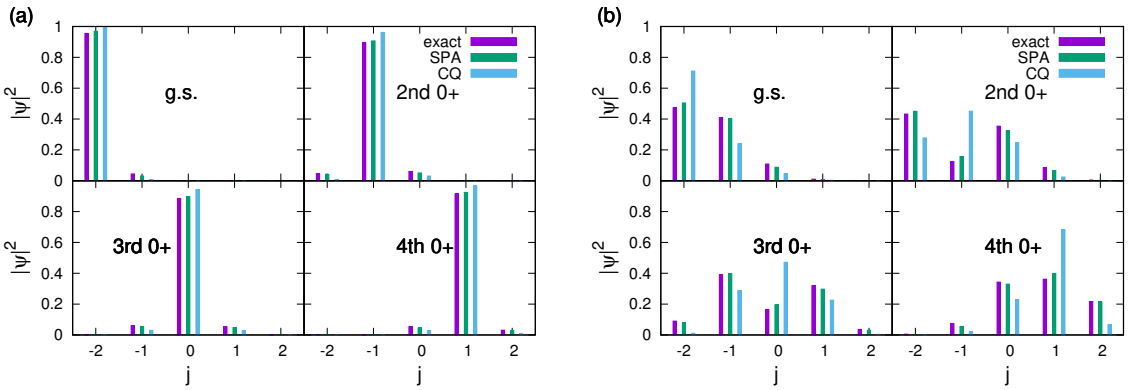

Figure 3.8: Occupation probability in excited 0^+ states as a function of j for $\Omega = N = 8$ systems. The panels (a) and (b) display the results for $x = 0.5$ and $x = 2$, respectively. See also the caption of Fig. 3.4. The figure is taken from Ref. [40].

(b) Closed-shell configuration

In the closed shell with $N = 16$, the minimum-energy trajectory changes at $x = 1$ from $j = -4$ (normal phase) to the BCS minimum $j > -4$ and $\phi = 0$ (superfluid phase). At the transitional point ($x = 1$), the harmonic approximation is known to collapse, namely to produce zero excitation energy. In Fig. 3.10, this collapsing is avoided in all the calculations (SPA/FD and CQ). The behaviors of the lowest excitation agree with the exact calculations, while the CQ method substantially underestimates those for higher states. This is again due to the difference in the zero-point energy in the ground and the excited states. In the CQ calculation, the first excited state is bound at $x \gtrsim 2$, but the second excited state is unbound for $x \lesssim 3.2$.

Near the transition point from the open to closed trajectories, the wave functions calculated with the SPA and CQ methods somewhat differ from the exact ones. In Fig. 3.11, the wave functions at $x = 0.5$ and 2 are presented. They agree with exact calculation at $x = 0.5$. In contrast, we find some deviations for the first excited state ($k = 1$) at $x = 2$. This is because the $k = 1$ trajectory corresponding to the first excited state changes its character from open to closed at $x \approx 1.8$. Therefore, the first excited wave function is difficult to reproduce in the SPA, although the wave functions for the

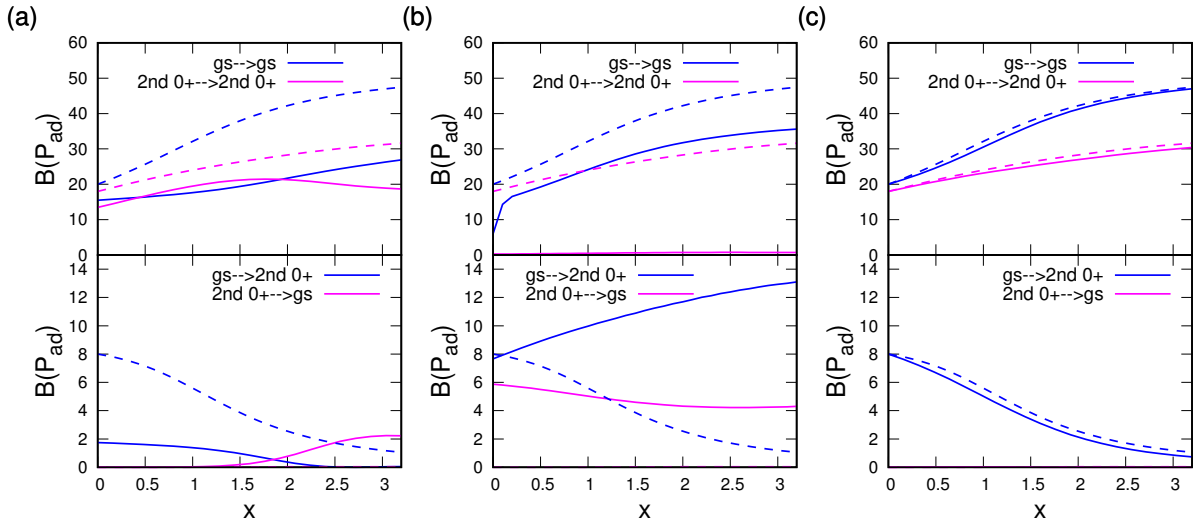

Figure 3.9: The same as described in the caption of Fig. 3.5 but for $N = 6 \to 8$ with $\Omega = 8$. The figure is taken from Ref. [40].

ground and higher excited states show reasonable agreement. The similar disagreement is observed for the ground state near $x = 1$.

Singular behaviors near the transition points can be also observed in the pair-addition transition strengths ($N = 14 \to 16$) shown in Fig. 3.12. At $x = 1$, the intraband $B(P_{\rm ad}; 0 \to 0)$ shows a kink in the SPA, and $B(P_{\rm ad}; 1 \to 1)$ shows another kink at $x \approx 1.8$. These exactly correspond to the transition points from open to closed trajectories. Nevertheless, the overall behaviors are well reproduced and the values at the weak and strong pairing limit are reasonably reproduced in the SPA. The CQ calculation also shows smoothed kink-like behaviors near the transition points. However, it underestimates the intraband $B(P_{\rm ad}; k \to k)$. The FD method does not have a kink for $B(P_{\rm ad}; 0 \to 0)$, because $S^+(t)$ is calculated for an $N = 14$ system. Both intraband and interband transitions in the FD calculations reasonably agree with the exact results at $x \gtrsim 1.8$. The $k = 1$ state is not properly reproduced at $x \lesssim 1.8$ with the open trajectory.

For the closed-shell configurations, the SPA and the FD methods provide reasonable description for the pair-transfer transition strengths.

From these studies, we find only the SPA reproduce the exact solution quantitatively in all of the two-level systems. The SPA is the best requantization method among the three.

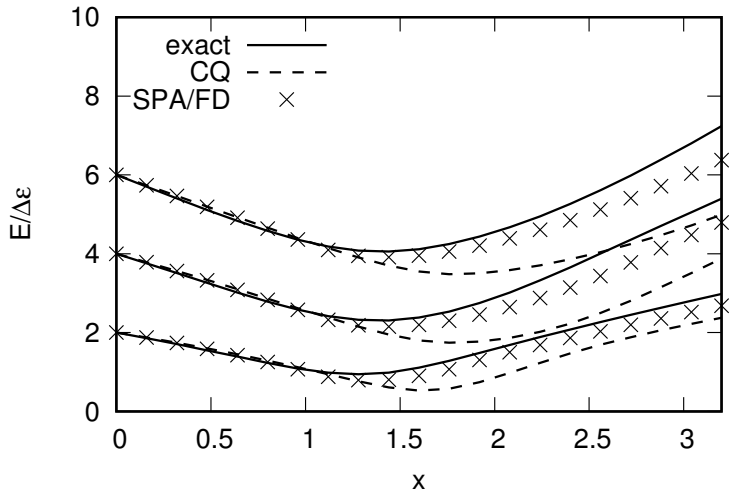

Figure 3.10: The same as described in the caption of Fig. 3.7 but for $N = 2\Omega = 16$. The figure is taken from Ref. [40].

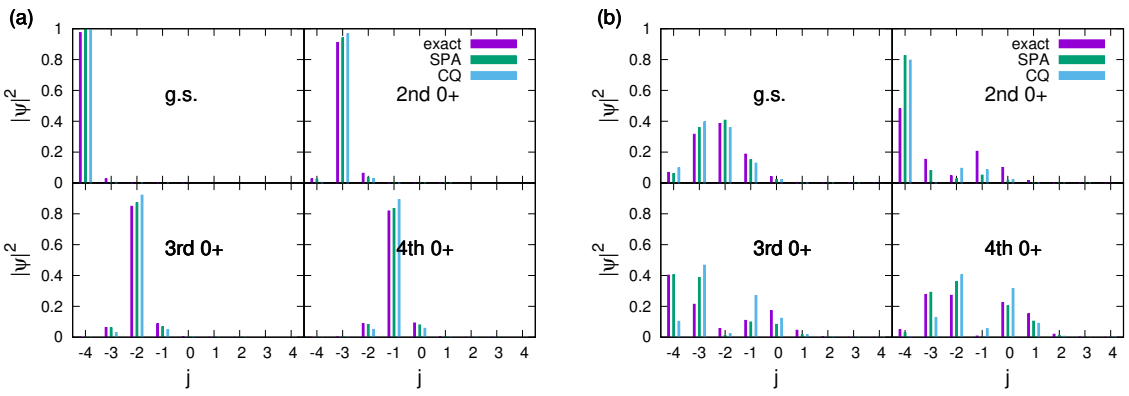

Figure 3.11: The same as described in the caption of Fig. 3.8 but for $N = 2\Omega = 16$. The figure is taken from Ref. [40].

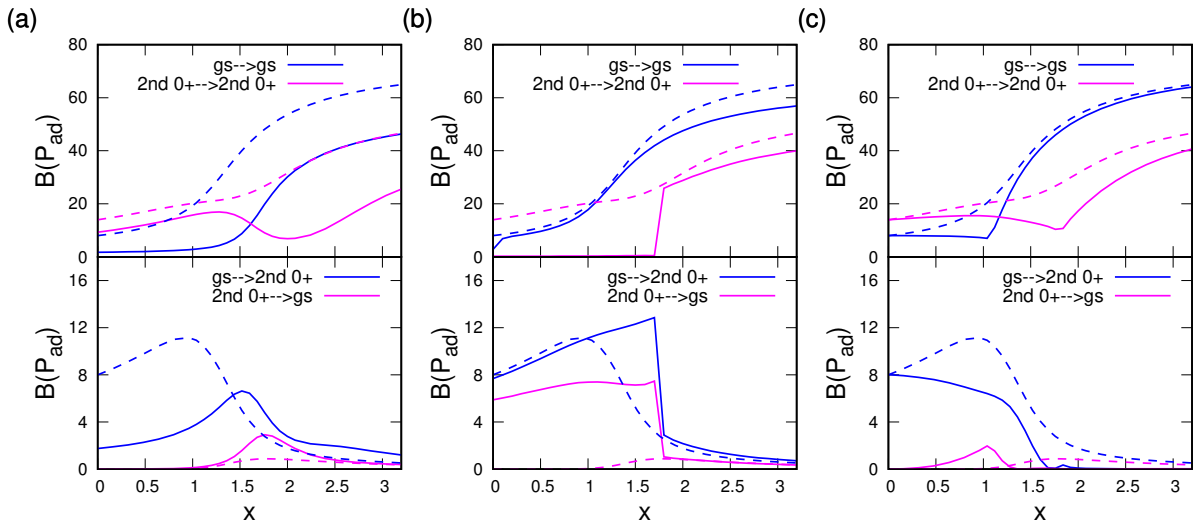

Figure 3.12: The same as described in the caption of Fig. 3.5 but for $N = 14 \rightarrow 16$ with $\Omega = 8$. The figure is taken from Ref. [40].

Chapter 4

Requantization of TDHFB in non-integrable system

The stationary-phase approximation (SPA) to the path integral [47] gives quantitative results not only for the excitation energies, but also for the wave functions and two-particle-transfer strengths, from the study of the requantization of the TDHFB in two-level pairing model,. The quantized states obtained in the SPA have two advantages; first, the wave functions are given directly in terms of the microscopic degrees of freedom, and second, the restoration of the broken symmetries are automatic. In the pairing model, the quantized states are eigenstates of the particle-number operator. On the other hand, applications of the SPA have been limited to integrable systems. This is because we need to find separable periodic trajectories on a classical torus. Since the nuclear systems, of course, correspond to non-integrable systems, a straightforward application of the SPA is not possible.

In this chapter, we propose a new approach of the SPA applicable to the non-integrable systems, which is based on the extraction of the one-dimensional (1D) collective coordinate using the adiabatic self-consistent collective coordinate (ASCC) method. Since the 1D system is integrable, the collective subspace can be quantized with the SPA. The optimal degree of freedom associated with a slow collective motion is determined self-consistently inside the TDHFB space, without any assumption. Thus, our approach of the ASCC+SPA to the pairing model basically consists of two steps: (1) find a decoupled 1D collective coordinate of the pair vibration, in addition to the pair rotational degrees of freedom. (2) apply the SPA independently to each collective mode.

We introduce the theoretical framework of the ASCC, SPA, and their combination, ASCC+SPA in Sec. 4.1. In Sec. 4.2, we provide some details in the application of the ASCC+SPA to the multi-level pairing model. We give the numerical results in Sec. 4.3, including neutron pair vibrations in Pb isotopes.

4.1 Theoretical framework of ASCC+SPA in non-integrable system

4.1.1 Adiabatic self-consistent collective coordinate method and 1D collective subspace

ASCC was developed from the basic idea of the self-consistent collective coordinate (SCC) method [50], which can maximum decouple a collective subspace from TDMF phase space. Because the collective coordinates are obtained from TDMF dynamics itself without any assumption in ASCC, they are superior than the phenomenological collective coordinates in the collective models. In this subsection, we recapitulate the ASCC method to find a 1D collective coordinate, following the notation of Ref. [32].

As is seen in Sec. 4.3, the TDHFB equations can be interpreted as the classical Hamilton's equations of motion with canonical variables $\{\xi^\alpha, \pi_\alpha\}$. Each point in the phase space (ξ^α, π_α) corresponds to a generalized Slater determinant (coherent state). Assuming slow collective motion, we expand the Hamiltonian $\mathcal{H}(\xi, \pi)$ with respect to the momenta π up to second order. The TDHFB Hamiltonian is

written as

$$\mathcal{H} = V(\xi) + \frac{1}{2}B^{\alpha\beta}(\xi)\pi_\alpha\pi_\beta \tag{4.1}$$

with the potential $V(\xi)$ and the reciprocal mass parameter $B^{\alpha\beta}(\xi)$ defined by

$$V(\xi) = \mathcal{H}(\xi, \pi = 0), \tag{4.2}$$

$$B^{\alpha\beta}(\xi) = \left.\frac{\partial^2\mathcal{H}(\xi,\pi)}{\partial\pi_\alpha\partial\pi_\beta}\right|_{\pi=0}. \tag{4.3}$$

The Einstein's convention for summation with respect to the repeated upper and lower indices is assumed hereafter.

For multi-level pairing models in Sec. 4.2, there is a constant of motion in the TDHFB dynamics, namely the average particle number $q^n \equiv J = \langle\hat{N} - \nu\rangle/2$. Since the particle number $\hat{N}$ is time-even Hermitian operator, we treat J as a coordinate, and its conjugate gauge angle, p_n, as a momentum. Since q^n is a constant of motion, the Hamiltonian does not depend on p_n. On the other hand, the gauge angle p_n changes in time, which corresponds to the pair rotation, a Nambu-Goldstone (NG) mode associated with the breaking of the gauge (particle-number) symmetry. We assume the existence of 2D collective subspace Σ_2 (4D phase space), described by a set of canonical variable $(q^1, q^2 = q^n; p_1, p_2 = p_n)$, which is well decoupled from the rest of degrees of freedom, $\{q^a, p_a\}$ with $a = 3, \cdots$. The collective Hamiltonian is given by imposing $q^a = p_a = 0$, namely by restricting the space into the collective subspace

$$\mathcal{H}_{\rm coll}(q, p; q^n) = \bar{V}(q^1, q^n) + \frac{1}{2}\bar{B}^{11}(q^1, q^n)p_1^2. \tag{4.4}$$

Since there exist two conserved quantities, q^n and $\mathcal{H}_{\rm coll}$, this 2D system is integrable. We can treat the collective motion of (q^1, p_1) separately from the pair rotation (q^n, p_n).

In the collective Hamiltonian (4.4), the variable q^n is trivially given as the particle number, which is expanded up to second order in the momenta π,

$$q^n = f^n(\xi) + \frac{1}{2}f^{(1)n\alpha\beta}\pi_\alpha\pi_\beta. \tag{4.5}$$

To obtain the non-trivial collective variables (q^1, p_1), we assume the point transformation[1],

$$q^1 = f^1(\xi), \tag{4.6}$$

and ξ^α on the subspace Σ_2 is given as $\xi^\alpha = g^\alpha(q^1, q^n, q^a = 0)$. The momenta on Σ_2 are transformed as

$$p_1 = g^\alpha_{,1}\pi_\alpha, \quad p_n = g^\alpha_{,n}\pi_\alpha, \tag{4.7}$$

$$\pi_\alpha = f^1_{,\alpha}p_1 + f^n_{,\alpha}p_n, \tag{4.8}$$

where the comma indicates the partial derivative ($f^1_{,\alpha} = \partial f^1/\partial\xi^\alpha$). The canonical variable condition leads to

$$f^i_{,\alpha}g^\alpha_{,j} = \delta^i_j, \tag{4.9}$$

where $i, j = 1$ and n. The collective potential $\bar{V}(q^1, q^n)$ and the collective mass parameter $\bar{B}_{11}(q^1, q^n) = [\bar{B}^{11}(q^1, q^n)]^{-1}$ can be given by

$$\bar{V}(q^1, q^n) = V(\xi = g(q^1, q^n, q^a = 0)), \tag{4.10}$$

$$\bar{B}^{11}(q^1, q^n) = f^1_{,\alpha}\tilde{B}^{\alpha\beta}(\xi)f^1_{,\beta}, \tag{4.11}$$

[1]We may lift the restriction to the point transformation, as Eq. (4.5) [51]. In this chapter, we neglect these higher-order terms, such as $f^{(1)1\alpha\beta}\pi_\alpha\pi_\beta/2$.

where $\tilde{B}^{\alpha\beta}$ are defined as

$$\tilde{B}^{\alpha\beta}(\xi) = B^{\alpha\beta}(\xi) - \bar{V}_{,n} f^{(1)n\alpha\beta}(\xi). \tag{4.12}$$

Decoupling conditions for the collective subspace Σ_2 lead to the basic equations of the ASCC method [31, 32], which determine tangential vectors, $f^1_{,\alpha}(\xi)$ and $g^\alpha_{,1}(q)$.

$$\delta H_M(\xi, \pi) = 0, \tag{4.13}$$

$$\mathcal{M}^\beta_\alpha f^1_{,\beta} = \omega^2 f^1_{,\alpha}, \qquad \mathcal{M}^\beta_\alpha g^\alpha_{,1} = \omega^2 g^\beta_{,1}. \tag{4.14}$$

The first equation (4.13) is called moving-frame Hartree-Fock-Bogoliubov (HFB) equation. The moving-frame Hamiltonian $\mathcal{H}_M$ is

$$\mathcal{H}_M(\xi, \pi) = \mathcal{H}(\xi, \pi) - \lambda_1 q^1(\xi) - \lambda_n q^n(\xi, \pi). \tag{4.15}$$

The second equation (4.14) is called moving-frame QRPA equation. The matrix $\mathcal{M}^\beta_\alpha$ in the moving-frame QRPA equation (4.14) can be rewritten as

$$\mathcal{M}^\beta_\alpha = \tilde{B}^{\beta\gamma}\left(V_{,\gamma\alpha} - \lambda_n f^n_{,\gamma\alpha}\right) + \frac{1}{2}\tilde{B}^{\beta\gamma}_{,\alpha} V_{,\gamma}. \tag{4.16}$$

The NG mode, $f^n_{,\alpha}$ and $g^\alpha_{,n}$, corresponds to the zero mode with $\omega^2 = 0$. Therefore, the collective mode of our interest corresponds to the mode with the lowest frequency squared except for the zero mode.

In practice, we obtain the collective path according to the following procedure:

1. Find the HFB minimum point ξ^α_i $(i = 0)$ by solving Eq. (4.13) with $\lambda_1 = 0$. Let us assume that this corresponds to $q^1_i = 0$.

2. Diagonalize the matrix $\mathcal{M}^\beta_\alpha$ to solve Eq. (4.14) using Eq. (4.16).

3. Move to the next neighboring point $\xi^\alpha_{i+1} = \xi^\alpha_i + d\xi^\alpha$ with $d\xi^\alpha = g^\alpha_{,1} dq^1$. This corresponds to the collective coordinate, $q^1_{i+1} = q^1_i + dq^1$.

4. At ξ^α_{i+1} (q^1_{i+1}), obtain a self-consistent solution of Eqs. (4.13) and (4.14) to determine ξ^α_{i+1}, $f^1_{,\alpha}$, and $g^\alpha_{,1}$.

5. Go back to Step 3 to determine the next point on the collective path.

We repeat this procedure with $dq^1 > 0$ and $dq^1 < 0$, and construct the collective path. In Steps 2 and 4, we choose a mode with the lowest frequency squared ω^2. Note that ω^2 can be negative. In Step 4, when we solve Eq. (4.13), we use a constraint on the magnitude of $dq^1 = f^1_{,\alpha} d\xi^\alpha$. Since the normalization of $f^1_{,\alpha}$ and $g^\alpha_{,1}$ is arbitrary as far as they satisfy Eq. (4.9), we fix this scale by an additional condition of $\bar{B}^{11}(q^1) = 1$.

4.1.2 Stationary-phase approximation to path integral

For quantization of integrable systems, we can apply the stationary-phase approximation (SPA) to the path integral. Since the collective Hamiltonian (4.4) that is extracted from the TDHFB degrees of freedom is integrable, the SPA is applicable to it. In this manner, we may apply the ASCC+SPA to non-integrable systems in general.

(a) Basic idea of ASCC+SPA

Because the Hamiltonian $\mathcal{H}_{\rm coll}$ of Eq. (4.4) is separable, it is easy to find periodic trajectories on invariant tori. Since the pair rotation corresponds to the motion of p_n with a constant q^n, all we need to do is to find classical periodic trajectories C_k in the (q^1, p_1) space (with a fixed q^n) which satisfy the Einstein-Brillouin-Keller (EBK) quantization rule with a unit of $\hbar = 1$,

$$\oint_{C_k} p_1 dq^1 = 2\pi k, \tag{4.17}$$

where k is an integer number.

At each point in the space $(q^1, q^n; p_1, p_n)$ corresponds to a generalized Slater determinant $|q^1, q^n; p_1, p_n\rangle = |\xi, \pi\rangle$, where (ξ, π) are given as $\xi^\alpha = g^\alpha(q^1, q^n, q^a = 0)$ and $\pi_\alpha = f^1_{,\alpha} p_1 + f^n_{,\alpha} p_n$. According to the SPA (Sec. 3.2.1), the k-th excited state $|\psi_k\rangle$ is constructed from the k-th periodic trajectory C_k, given by $(q^1(t), p_1(t))$, of the Hamiltonian $\mathcal{H}_{\rm coll}$.

$$|\psi_k\rangle \propto \oint dp_n \oint_{C_k} \rho(q,p) dt\, |q,p\rangle\, e^{i\mathcal{T}[q,p]}, \tag{4.18}$$

where (q,p) means $(q^1, q^n; p_1, p_n)$, and the weight function $\rho(q,p)$ is given through an invariant measure $d\mu(q,p)$ as

$$d\mu(q,p) = \rho(q,p) dE dt dq^n dp_n. \tag{4.19}$$

The invariant measure $d\mu(q,p)$ is defined by the unity condition $\int d\mu(q,p)\, |q,p\rangle\, \langle q,p| = 1$. The action integral $\mathcal{T}$ is

$$\mathcal{T}[q,p] \equiv \int_0^t \langle q(t'), p(t')| i \frac{\partial}{\partial t'} |q(t'), p(t')\rangle\, dt'. \tag{4.20}$$

The SPA quantization is able to provide a wave function $|\psi_k\rangle$ in microscopic degrees of freedom, which is given as a superposition of generalized Slater determinants $|q,p\rangle$. In addition, the integration with respect to p_n over a circuit on a torus automatically recovers the broken symmetry, namely the good particle number. However, it relies on the existence of invariant tori. In the present approach of the ASCC+SPA, we first derive a decoupled collective subspace Σ_2 and identify canonical variables (q,p). Because of the cyclic nature of (q^n, p_n), it is basically a 1D system and becomes integrable. In other words, we perform the torus quantization on approximate tori in the TDHFB phase space (ξ, π), which is mapped from tori in the 2D collective subspace (q,p).

(b) Notation and practical procedure for quantization

For the application of the ASCC+SPA method to the pairing model in Sec. 4.2, we summarize some notations and procedures to obtain quantized states.

In Sec. 4.2, the time-dependent generalized Slater determinants (coherent states) are written as $|Z\rangle$ with complex variables $Z_\alpha(t)$. The variables Z_α are transformed into real variables $(j^\alpha, -\chi_\alpha)$ that correspond to (ξ^α, π_α) in Sec. 4.1. The definition and physical meaning of χ_α and j^α are explained in Sec. 2.2. Although it is customary to take the time-odd angle χ_α as a coordinate, we take the number j^α as a coordinate and the angle $-\chi_\alpha$ as a momentum with an additional minus sign. Similarly, the gauge angle Φ and the total particle number J correspond to variables of the pair rotation, $-p_n$ and q^n, respectively. According to the EBK quantization rule (4.17), the ground state with $k = 0$ corresponds to nothing but the HFB state with a fixed particle number $J(= q^n)$. For the k-th excited states, we perform the following calculations:

1. Obtain the 1D collective subspace with canonical variables (q^1, p_1) according to the ASCC in Sec. 4.1.1.

2. Find a trajectory $(q^1(t), p_1(t))$ which satisfies the k-th EBK quantization condition (4.17).

3. Calculate the action integral (4.20) for the k-th trajectory.

4. Construct the k-th excited state using Eq. (4.18).

The ASCC provides the 2D collective subspace (q^1, J) and the generalized coherent states $|\Phi = 0, J; q, p = 0\rangle$. For finite values of momenta, we use Eq. (4.8) to obtain the state $|\Phi, J; q, p\rangle$.

4.2 Application of ASCC+SPA in pairing model

4.2.1 Application of ASCC

We construct a 2D collective subspace Σ_2 from the ASCC method. We expand the classical Hamiltonian up to second order with respect to the momenta, $-\chi_\alpha$

$$\mathcal{H}(j,\chi) \approx V(j) + \frac{1}{2}B^{\alpha\beta}(j)\chi_\alpha\chi_\beta, \tag{4.21}$$

where the potential $V(j)$ and the reciprocal mass parameter $B^{\alpha\beta}(j)$ are given as[2]

$$\begin{aligned} V(j) =& \mathcal{H}(j,\chi=0) \\ =& \sum_\alpha \epsilon_\alpha\nu_\alpha + \sum_\alpha 2\epsilon_\alpha j^\alpha - g\sum_\alpha\left((\Omega_\alpha-\nu_\alpha)j^\alpha - (j^\alpha)^2 + \frac{(j^\alpha)^2}{\Omega_\alpha-\nu_\alpha}\right) \\ & - g\sum_{\alpha\neq\beta}\sqrt{j^\alpha j^\beta(\Omega_\alpha-\nu_\alpha-j^\alpha)(\Omega_\beta-\nu_\beta-j^\beta)}, \end{aligned} \tag{4.22}$$

$$B^{\alpha\beta}(j) = \left.\frac{\partial^2\mathcal{H}}{\partial\chi_\alpha\partial\chi_\beta}\right|_{\chi=0} \tag{4.23}$$

$$= \begin{cases} 2g\sum_{\gamma\neq\alpha}\sqrt{j^\gamma j^\alpha(\Omega_\gamma-\nu_\gamma-j^\gamma)(\Omega_\alpha-\nu_\alpha-j^\alpha)} & \text{for } \alpha=\beta \\ -2g\sqrt{j^\alpha j^\beta(\Omega_\alpha-\nu_\alpha-j^\alpha)(\Omega_\beta-\nu_\beta-j^\beta)} & \text{for } \alpha\neq\beta \end{cases}.$$

We may apply the ASCC method in Sec. 4.1.1 by regarding $\xi \to j$ and $\pi \to -\chi$.

The TDHFB conserves the average total particle number N. We adopt

$$J = \frac{N-\nu}{2} = \sum_\alpha j^\alpha, \tag{4.24}$$

as a coordinate q^n. Since this is explicitly given as the expectation value of the particle-number operator, curvature quantities, such as $f^n_{,\alpha\beta}$ and $f^{(1)n\alpha\beta}$, are explicitly calculable. On the other hand, the gauge angle $\Phi = -p_n$ is not given a priori. Since the ASCC solution provides $g^\alpha_{,n}$ as an eigenvector of Eq. (4.14), we may construct it as Eq. (4.7) in the first order in $\pi = -\chi$. We confirm that the pair rotation corresponds to an eigenvector of Eq. (4.14) with the zero frequency $\omega^2 = 0$.

In the present pairing model, from Eq. (4.24), we find J does not depend on χ. This means $f^{(1)n\alpha\beta} = 0$ in Eq. (4.5), thus, $\tilde{B}^{\alpha\beta} = B^{\alpha\beta}$. The second derivative of J with respect to j also vanishes, which indicates $f^n_{,\gamma\alpha}$ in Eq. (4.16) is zero. The gauge angle Φ is locally determined by the solution of Eq. (4.14).

$$\Phi = g^\alpha_{,n}\chi_\alpha, \tag{4.25}$$

[2]In this thesis, j^α and j_α are identical. Definition of the upper index in j^α is to utilize the Einstein summation convention.

It should be noted [32] that the definition of the collective variables (q^1, p_1) is not unique, because it can be arbitrarily mixed with the pair rotation (q^n, p_n) as

$$q^1 \to q^1 + cq^n, \quad p_n \to p_n - cp_1 \tag{4.26}$$

with an arbitrary constant c. Numerically, this arbitrariness sometimes leads to a problematic behavior in iterative procedure of the ASCC. In order to fix the parameter c, we adopt a condition called "ETOP" in Ref. [52]. We require the following condition to determine c:

$$\sum_\alpha f^1_{,\alpha} = 0, \tag{4.27}$$

where $f^1_{,\alpha}$ is replaced as

$$f^1_{,\alpha} \to f^1_{,\alpha} + cf^n_{,\alpha} \tag{4.28}$$

with Eq. (4.26).

4.2.2 Application of SPA

After deriving the collective subspace Σ_2, we perform the quantization according to the SPA in Sec. 4.1.2. We can identify a series of states $\{|\Phi, J; q^1(t), p_1(t)\rangle\}$ on the trajectory, in the form of Eq. (2.16) with parameters Z_α given at (Φ, J, q^1, p_1) and $q^a = p_a = 0$ for $a \geq 3$, by calculating a trajectory in the (q^1, p_1) space. Since the variables (Φ, J) and (q^1, p_1) are separable, we may take closed trajectories independently in (Φ, J) and (q^1, p_1) sectors, which we denote here as C_Φ and C_1, respectively. The action integral is given by

$$\begin{aligned}
\mathcal{T}(\Phi, J; q^1, p_1) =& \int_{C_\Phi} \langle \Phi(t), J; q^1, p_1 | i\frac{\partial}{\partial t} | \Phi(t), J; q^1, p_1 \rangle \, dt \\
&+ \int_{C_1} \langle \Phi, J; q^1(t), p_1(t) | i\frac{\partial}{\partial t} | \Phi, J; q^1(t), p_1(t) \rangle \, dt \\
=& J\Phi + \int_{C_1} \sum_\alpha j^\alpha d\chi_\alpha \\
\equiv& \mathcal{T}_\Phi(J, \Phi) + \mathcal{T}_1(q^1, p_1; J).
\end{aligned} \tag{4.29}$$

In fact, the gauge-angle dependence is formally given as

$$|\Phi, J; q^1, p_1\rangle = e^{-i\Phi\hat{J}} \, |J; q^1, p_1\rangle \, , \tag{4.30}$$

where

$$\hat{J} = \frac{\hat{N} - \nu}{2} = \sum_\alpha (\hat{S}^0_\alpha + S_\alpha). \tag{4.31}$$

Then, the action for the trajectory C_1 can be also expressed as

$$\mathcal{T}(q^1, p_1; J) = \int_{C_1} \langle J; q^1, p_1 | i\frac{\partial}{\partial t} | J; q^1, p_1 \rangle \, dt. \tag{4.32}$$

In the SU(2) representation, the invariant measure is

$$\begin{aligned} d\mu(Z) &= \prod_\alpha \frac{2S_\alpha+1}{\pi}(1+|Z_\alpha|^2)^{-2} d(\mathrm{Re}\, Z) d(\mathrm{Im}\, Z) \\ &= \prod_\alpha \frac{-(2S_\alpha+1)}{4\pi} d(\cos\theta_\alpha) d\chi_\alpha \\ &= \prod_\alpha \frac{1+(2S_\alpha)^{-1}}{2\pi} d\chi_\alpha dj^\alpha \\ &= \left[\prod_\alpha \frac{1+(2S_\alpha)^{-1}}{2\pi}\right] d\Phi dJ dq^1 dp_1 \prod_a dq^a dp_a, \end{aligned} \tag{4.33}$$

where (q^a, p_a) are the intrinsic canonical variables decoupled from the collective subspace Σ_2. In the last line in Eq. (4.33), we used the invariance of the phase-space volume element in the canonical transformation. According to Eq. (4.33), the weight function $\rho(q,p)$ in Eq. (4.18) is just a constant, thus, treated as the normalization of the wave function.

The coherent state $|\Phi, J; q^1, p_1\rangle = |Z\rangle$ is expanded in the SU(2) quasispin basis as

$$|Z\rangle = e^{-i\Phi\hat{J}} |J; q^1, p_1\rangle = e^{-i\Phi\hat{J}} \sum_{\{m_\alpha\}} B_m(Z) \,|\cdots; S_\alpha, -S_\alpha + m_\alpha, \cdots\rangle\,, \tag{4.34}$$

where the summation is taken over all possible combinations of integer values of $\{m_\alpha\}$ with

$$B_m(Z) = \prod_\alpha \left(\frac{j_\alpha}{2S_\alpha}\right)^{m_\alpha/2} \left(\frac{2S_\alpha - j_\alpha}{2S_\alpha}\right)^{S_\alpha - m_\alpha/2} \sqrt{\frac{(2S_\alpha)!}{m_\alpha!(2S_\alpha - m_\alpha)!}} e^{-im_\alpha\phi_\alpha}, \tag{4.35}$$

where the relative angles are defined as

$$\phi_\alpha \equiv \chi_\alpha - \Phi \tag{4.36}$$

and the lower index m indicates a combination of $\{m_\alpha\}$. From Eq. (4.8) in ASCC, we can directly obtain the relative angles $\phi_\alpha = -f^1_{,\alpha} p_1$. The integer number m_α corresponds to the number of pairs in the level α.

Using Eq. (4.35), the k-th excited state is calculated as

$$\begin{aligned} |\psi_k\rangle &\propto \oint_{C_\Phi} d\Phi \oint_{C_1} dt\, |\Phi, J; q^1, p_1\rangle\, e^{i\mathcal{T}(\Phi, J; q^1, p_1)} \\ &= \sum_{\{m_\alpha\}} \int_0^{2\pi} d\Phi e^{i(J - \sum_\alpha m_\alpha)\Phi} \oint dt e^{i\mathcal{T}_1}(t) B_m(Z) \,|\cdots; S_\alpha, -S_\alpha + m_\alpha, \cdots\rangle \\ &\equiv \sum_{\{m_\alpha\}_J} C_m \,|\cdots; S_\alpha, -S_\alpha + m_\alpha, \cdots\rangle\,. \end{aligned} \tag{4.37}$$

The coefficients C_m are given by

$$C_m = \oint_{C_1} dt e^{i\mathcal{T}_1(t)} B_m(Z(t)). \tag{4.38}$$

In the last line of Eq. (4.37), the summation is restricted to $\{m_\alpha\}$ that satisfy $\sum_\alpha m_\alpha = J$. It is easy to find that J must be integer, according to the quantization rule (4.17) for the (J, Φ) sector.

The SPA for the ground state ($k = 0$) is given by the stationary point in the (q^1, p_1) sector, namely, the HFB state $|\Phi, J; q, p\rangle = e^{-i\Phi\hat{J}} |\mathrm{HFB}\rangle$. Nevertheless, the rotational motion in $\Phi(t)$ is present, which leads to the number quantization (projection). Therefore, Eq. (4.37) becomes

$$|\psi_{\mathrm{g.s.}}\rangle \propto \sum_{\{m_\alpha\}} \int_0^{2\pi} d\Phi e^{i(J - \sum_\alpha m_\alpha)\Phi} \,|\mathrm{HFB}\rangle\,, \tag{4.39}$$

which is identical to the wave function of the particle-number projected HFB state.

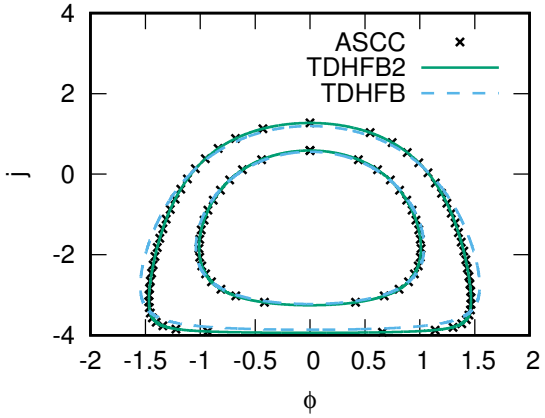

Figure 4.1: Classical trajectories satisfying the EBK quantization condition (4.17) with $k = 1$ and 2 in the (ϕ, j) phase space. The crosses, solid and dashed lines correspond to the results of the ASCC+SPA, TDHFB2+SPA, and TDHFB+SPA, respectively. The crosses for the ASCC+SPA trajectories are plotted every ten calculations ($\delta q = 10dq = 0.1/\sqrt{\epsilon_0}$). The figure is taken from Ref. [53].

4.3 Result

We first apply the ASCC+SPA method to an integrable two-level model, then, to non-integrable multi-level models.

4.3.1 Integrable case: Two-level pairing model

In Sec. 3.3, using the explicit transformation to these separable variables, we examined the performance of the SPA requantization for the two-level model. In this section, we discuss the same model as in Sec. 3.3, but we determine the transformation using the ASCC method and then apply the SPA (ASCC+SPA).

Here, we study the system with the equal degeneracy, $\Omega_1 = \Omega_2 = 8$, the pairing strength $g/\epsilon_0 = 0.2$ ($x = 3.2$), $\nu = 0$, and $N = 16$. In this two-level case, we use the level spacing, $\epsilon_0 \equiv \epsilon_2 - \epsilon_1$, as the unit of energy. The moving-frame QRPA produces the zero mode and another eigenvector with a finite frequency squared $\omega^2 \neq 0$. We follow the latter mode to construct the collective path. In the ASCC calculation, we set the increment of the collective coordinate, $dq = 0.01$, in units of $1/\sqrt{\epsilon_0}$. We confirm that the pair rotation always has a zero frequency on the collective path. On the obtained collective path, we calculate a classical trajectory for the Hamiltonian

$$\mathcal{H}_{\rm coll}(q^1, p_1; J) = \frac{1}{2}p_1^2 + V(q^1, J) \tag{4.40}$$

with $N = 16$, $\nu = 0$. Calculated trajectories that satisfy the EBK quantization condition (4.17) for the first and second excited states (0_2^+ and 0_3^+) are mapped onto the (ϕ, j) plane and shown in Fig. 4.1. We also calculate the trajectories using the explicit transformation of the variables to $(\Phi, J; \phi, j)$, Eq. (3.5), which are shown by dashed lines in Fig. 4.1. We call this "TDHFB trajectories". Small deviation in large ϕ is due to the absence of the higher-order terms in χ_α in the ASCC. In fact, if we calculate the trajectories in the variables $(\Phi, J; \phi, j)$ using the adiabatic TDHFB Hamiltonian Eq. (3.11) ("TDHFB2 trajectories"), we obtain the solid lines in Fig. 4.1, which perfectly agree with the ASCC trajectories.

The action integrals $\mathcal{T}(t)$ corresponding to these closed trajectories are shown in Fig. 4.2. For the 0_2^+ state, all three calculations agree well with each other, while we see small deviation between the full TDHFB and the ASCC/TDHFB2 calculations for the 0_3^+ state.

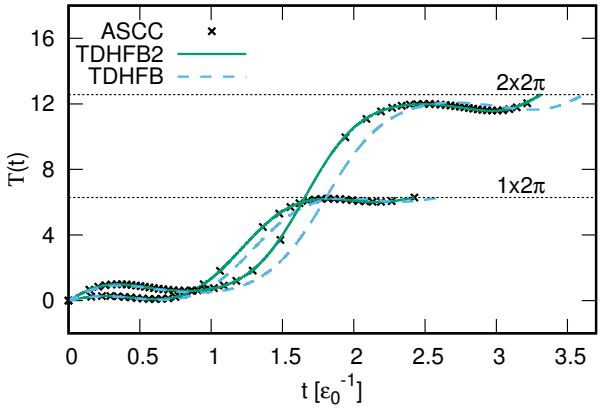

Figure 4.2: Calculated action integrals for the $|0_2^+\rangle$ and $|0_3^+\rangle$ states as functions of time t. The crosses, solid and dashed lines correspond to the ASCC+SPA, the TDHFB2+SPA, and the TDHFB+SPA, respectively. The action integrals are calculated on each trajectory in Fig. 4.1 from $(\phi, j) = (0, j_{\max})$ in the clockwise direction. The crosses for the ASCC+SPA trajectories are plotted every ten calculations ($\delta q = 10dq = 0.1/\sqrt{\epsilon_0}$). The figure is taken from Ref. [53].

The calculated wave functions for the excited 0^+ states are shown in Fig. 4.3. We show the occupation probabilities which are decomposed into the $2n$-particle-$2n$-hole components. The left end of the horizontal axis at $m_2 - m_1 = -8$ ($j = -4$) corresponds to a state with $(m_1, m_2) = (N/2, 0)$ where all the particles are in the lower level $\alpha = 1$. The next one at $m_2 - m_1 = -6$ ($j = -3$) corresponds to the one with $(m_1, m_2) = ((N-2)/2, 1)$, and so on. The results from the TDHFB2+SPA and the ASCC+SPA are identical to each other within numerical error, and they reproduce the TDHFB+SPA calculation well.

By comparing with the full TDHFB calculation with the ASCC+SPA approach in the two-level pairing model, we conclude that the ASCC is reliable for description of low-lying collective states, for which the adiabatic approximation is justifiable. In addition to that, we should note that the pair rotation is properly separated.

4.3.2 Non-integrable case (1): Three-level pairing model

In contrast to the two-level model, the TDHFB for the three-level model is non integrable. We set the parameters of the system as follows: $\nu = 0$, $\Omega_1 = \Omega_2 = \Omega_3 = \Omega = 8$, $\epsilon_1 = -\epsilon_0$, $\epsilon_2 = 0$, $\epsilon_3 = 1.5\epsilon_0$, and $g = 0.2\epsilon_0$. We use the parameter ϵ_0 as the unit energy. For the sub-shell closed configuration of $N = 2\Omega = 16$, the HFB ground state changes from the normal phase to the superfluid phase at $g_c = 0.058\epsilon_0$. We calculate a chain of systems with even particle numbers from $N = 14$ to $N = 24$.

We obtain three eigen frequencies for the moving-frame QRPA equation, on the collective path (Fig. 4.4). First of all, we clearly identify the zero mode with $\omega^2 = 0$ everywhere along the collective path. This means that the pair rotation is separated from the other degrees of freedom in the ASCC. The frequency could become imaginary ($\omega^2 < 0$). Except for the case of sub-shell closure ($N = 2\Omega_1 = 16$), the frequency rapidly increases near the end points. The end points are given by points where the search for the next point on the collective path in Sec. 4.1.1 fails.

We choose the lowest frequency squared mode, except for the zero mode, as a generator of the collective path (q^1). Figure 4.5 shows variation of the occupation probability of each single-particle state, as functions of the collective coordinate q^1 on the collective path. The most striking feature is that the collective path terminates with special configurations which are given by the integer number of occupation. This is the reason why the search for the collective path fails at both the ends. At the

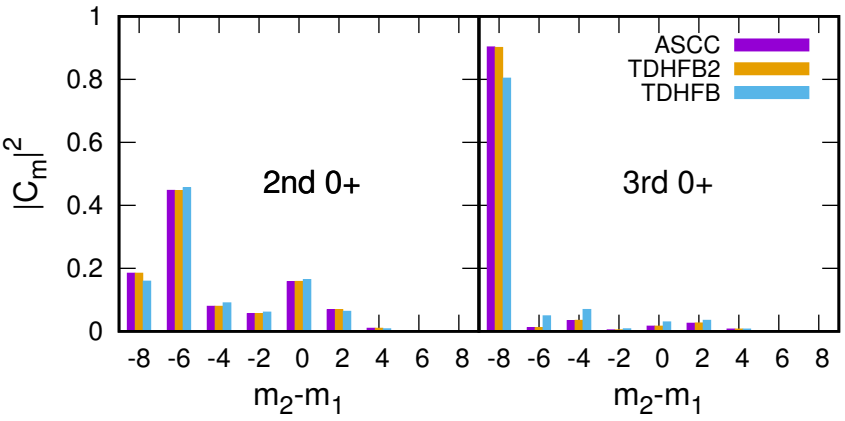

Figure 4.3: Occupation probabilities for the 0_2^+ and 0_3^+ states. The horizontal line indicates the $j = (m_2 - m_1)/2$ of the quasi-spin basis in Eq. (4.37). The vertical bars at each $m_2 - m_1$ from left to right represent $|C_m|^2$ of Eq. (4.38) in the ASCC+SPA, TDHFB2+SPA and TDHFB+SPA calculations, respectively. The figure is taken from Ref. [53].

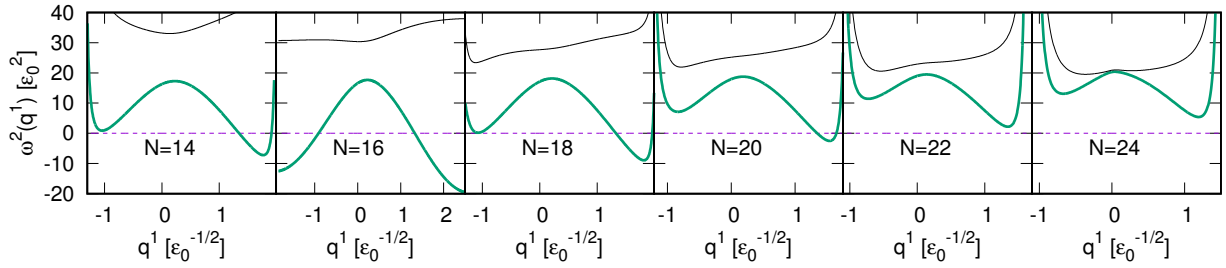

Figure 4.4: Eigenvalues of moving-frame QRPA equation as a function of the collective coordinate q^1, from $N = 14$ to $N = 24$. The thick (green) lines are the modes we choose as the collective coordinate q^1, while the dashed lines correspond to the zero modes (q^n). In each panel, both ends of the horizontal axis corresponds to the ending points of the collective path q^1. The figure is taken from Ref. [53].

end points, the occupation of the level 3 (ϵ_3) vanishes, while those of the levels 1 and 2 become either maximum or minimum. The left end of each panel in Fig. 4.5 corresponds to a kind of "Hartree-Fock" (HF) state which minimizes the single-particle-energy sum, $\sum_\alpha 2j_\alpha\epsilon_\alpha$. The pairing correlation is weakened in both ends of the collective path.

The collective mass with respect to the coordinate q^1 is normalized to unity. The collective potential is shown in Fig. 4.6. The range of q^1 is the largest for the system with $N = 16$. This is because the variation of j^1 and j^2 is the largest in this case.

Based on the collective path determined by the ASCC calculation, we perform the requantization according to the SPA. Table 4.1 shows the excitation energies of the first and second excited states, determined by the EBK quantization condition (4.17). Comparing the result of the ASCC+SPA with that of the exact calculation, we find that the excitation energies are reasonably well reproduced. The ASCC+SPA underestimates the excitation energies only by about 5%.

It should be noted that the second excited state in the collective path corresponds to the 0_4^+ state, not to the 0_3^+ state, in the exact calculation. We examine the interband ($k \neq k'$) pair-addition

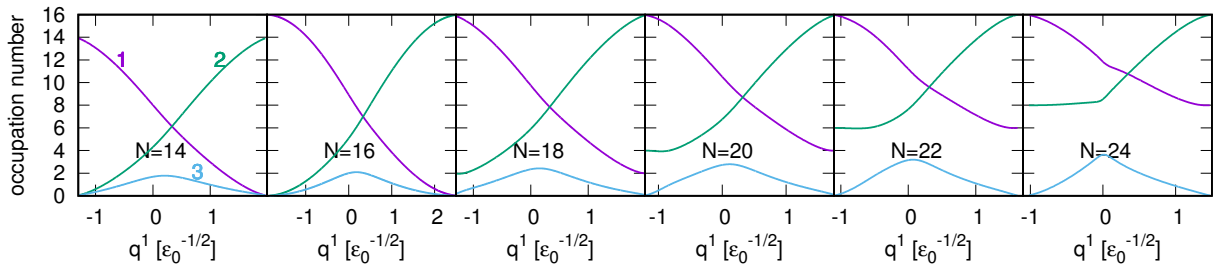

Figure 4.5: The occupation numbers $2j^\alpha$ in each single-particle level α as a function of the collective coordinate q^1, from $N = 14$ to $N = 24$. The purple, green, and blue lines correspond to $\alpha = 1$, 2, and 3, respectively. At the left end point of the collective coordinate in each panel, the configuration corresponds to the "HF-like" states. See text for details. The figure is taken from Ref. [53].

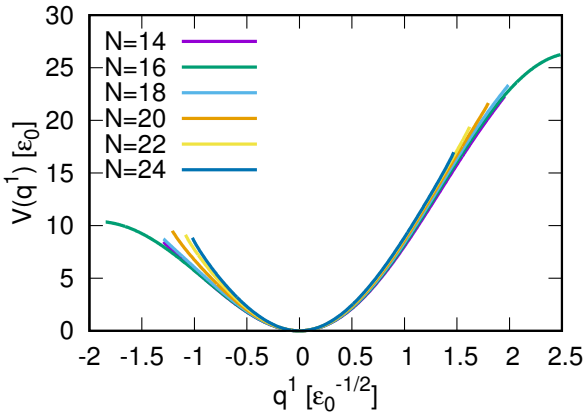

Figure 4.6: Collective potential $V(q^1)$ obtained from the ASCC. We adjust the energy minimum point as $q^1 = 0$ and $V = 0$. The figure is taken from Ref. [53].

transition,

$$B(P_{\rm ad}; k \to k') \equiv \left| \langle 0^+_{k'}; N+2 | \, \hat{S}^+ \, | 0^+_k; N \rangle \right|^2 , \tag{4.41}$$

in the exact solution. $B(P_{\rm ad}; 0^+_2 \to 0^+_3)$ is 10 $\sim$ 100 times smaller than $B(P_{\rm ad}; 0^+_1 \to 0^+_3)$, while $B(P_{\rm ad}; 0^+_1 \to 0^+_2)$ and $B(P_{\rm ad}; 0^+_1 \to 0^+_3)$ are in the same order. The ASCC+SPA produces states in the same family, namely, those belonging to the same collective subspace (path). In the phonon-like picture, we expect similar magnitude of the strengths for $B(P_{\rm ad}; {\rm g.s.} \to \omega_{\rm phon})$ and $B(P_{\rm ad}; \omega_{\rm phon} \to 2\omega_{\rm phon})$, but smaller values of $B(P_{\rm ad}; {\rm g.s.} \to 2\omega_{\rm phon})$. Thus, the 0^+_4 state in the exact calculation corresponds to the two-phonon state in the ASCC+SPA. The 0^+_3 state in the exact calculation may correspond to a collective path associated with another solution of the moving-frame QRPA (thin black line in Fig. 4.4).

Next, we calculate the wave functions, according to Eqs. (4.37) and (4.39). The ground state corresponds to the number-projected HFB state (variation before projection). In contrast, the excited states are given as superposition of generalized Slater determinants in the collective subspace, The pair-addition transition strengths computed using these wave functions of the excited states are shown in Fig. 4.7. For the intraband transition ($k = k'$ in Eq. (4.41)), the ASCC+SPA method well reproduces the strengths of the exact calculation. The ground-to-ground transitions, $B(P_{\rm ad}; 0^+_1 \to 0^+_1)$, are perfectly reproduced, while $B(P_{\rm ad}; 0^+_2 \to 0^+_2)$ are underestimated by about 10% $\sim$ 20%.

Table 4.1: Calculated excitation energies of the first and the second excited states in units of ϵ_0. In the exact calculation, the second excited state in the ASCC+SPA corresponds to the 0_4^+ state. See text for details. The table is taken from Ref. [53].

N	14	16	18	20	22	24
ASCC+SPA (1st exc.)	3.87	3.90	3.97	4.09	4.23	4.33
Exact	4.09	4.13	4.20	4.30	4.44	4.60
ASCC+SPA (2nd exc.)	7.42	7.42	7.60	7.92	8.26	8.47
Exact	7.65	7.71	7.88	8.15	8.49	8.74

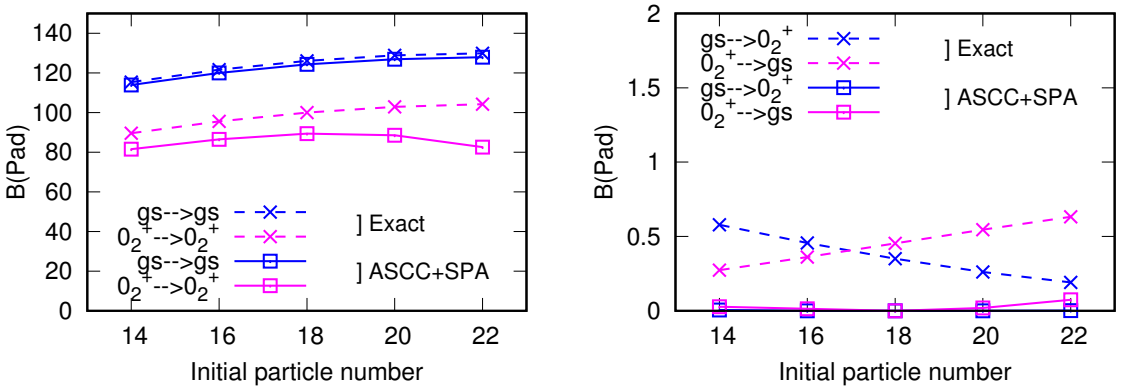

Figure 4.7: Calculated strength of pair-addition transition (4.41) from $N = 14$ to $N = 22$. The solid (dashed) lines correspond to the ASCC+SPA (exact) calculation. The horizontal line indicates the particle number of the initial states. The left panel shows the intraband transitions, $0_1^+ \to 0_1^+$ and $0_2^+ \to 0_2^+$, while the right panel shows the interband transitions, $0_1^+ \to 0_2^+$ and $0_2^+ \to 0_1^+$. The figure is taken from Ref. [53].

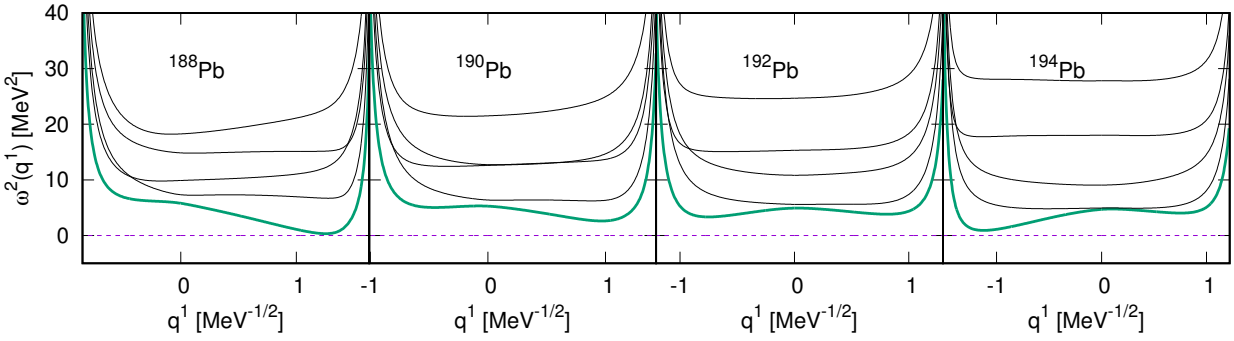

Figure 4.8: The same as described in the caption of Fig. 4.4 but for Pb isotopes. The figure is taken from Ref. [53].

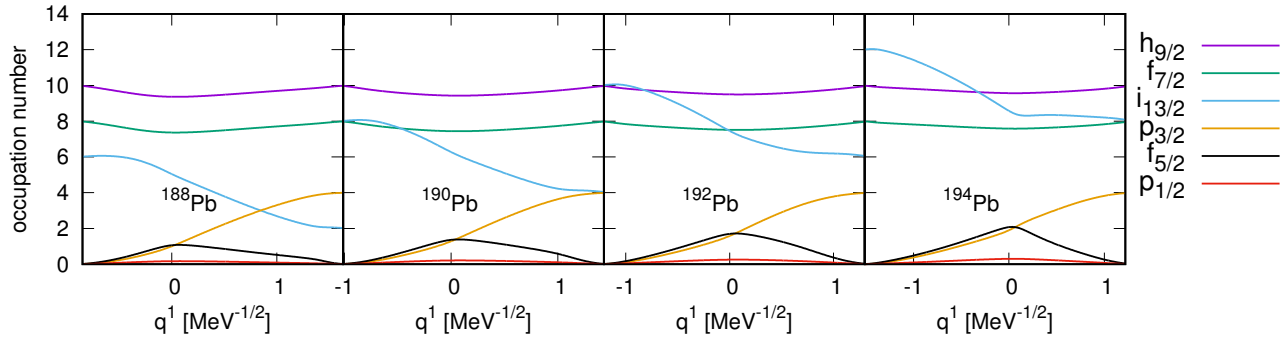

Figure 4.9: The same as described in the caption of Fig. 4.5 but for Pb isotopes. The figure is taken from Ref. [53].

It is more difficult to reproduce the absolute magnitude of interband transitions ($k \neq k'$), which are far smaller than the intraband transitions. Although the increasing (decreasing) trend for $B(P_{\rm ad}; 0_2^+ \to 0_1^+)$ ($B(P_{\rm ad}; 0_1^+ \to 0_2^+)$) as a function of the particle number is properly reproduced, the absolute magnitude is significantly underestimated in the ASCC+SPA. This is due to extremely small collectivity in the interband transitions. Almost all the strengths are absorbed in the intraband transitions. Even in the exact calculation, the pair addition strength is about two orders of magnitude smaller than the intraband strength. Remember that the non-collective limit ($g \to 0$) of this value is $B(P_{\rm ad}; 0_1^+ \to 0_2^+) = \Omega$. Therefore, the pairing correlation hinders the interband transitions by about one order of magnitude. For such tiny quantities, perhaps, the reduction to the 1D collective path is not well justified.

We remark here that there is a difficulty in the present ASCC+SPA requantization for weak pairing cases. In such cases, the potential minimum is close to the left end ($q^1 = q_L$) of the collective path, and the potential height at $q^1 = q_L$, $V(q_L) - V(0)$, becomes small. Then, a classical trajectory with $E > V(q_L)$ hits this boundary ($q^1 = q_L$). In construction of wave functions, the boundary condition at $q^1 = q_L$ significantly influences the result. In the present study, we choose a strong pairing case to avoid such a situation. As in Fig. 4.6, the potential height at $q^1 = q_L$ has about $10\epsilon_0$ which is larger

Table 4.2: Single-particle energies of Pb isotopes used in the calculation in units of MeV. These are obtained from the spherical Woods-Saxon potential with the parameters of Ref. [54]. The table is taken from Ref. [53].

orbit	$h_{9/2}$	$f_{7/2}$	$i_{13/2}$	$p_{3/2}$	$f_{5/2}$	$p_{1/2}$
energy(MeV)	-10.94	-10.69	-8.74	-8.44	-8.16	-7.45

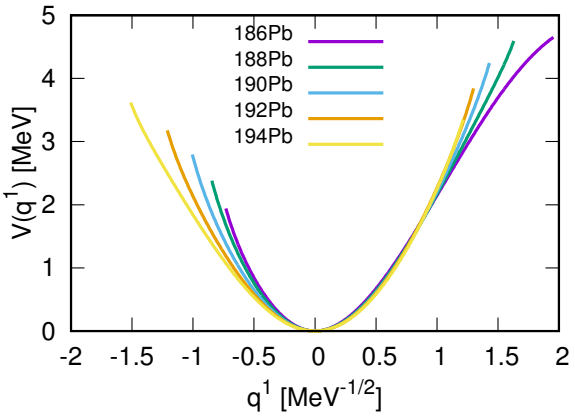

Figure 4.10: The same as described in the caption of Fig. 4.6 but for Pb isotopes. The figure is taken from Ref. [53].

than the excitation energies of the second excitation. Therefore, all the trajectories are "closed" in the usual sense. We discuss the possible approach for the weak pairing cases in Sec. 4.4.

4.3.3 Non-integrable case (2): Pb isotopes

We also apply our method to neutrons' pairing dynamics in neutron-deficient Pb isotopes. The spherical single-particle levels of neutrons between the magic numbers 82 and 126 are adopted and their energies are presented in Table 4.2. The coupling constant $g = 0.138$ MeV is determined to reproduce the experimental pairing gap given by the odd-even mass difference, $\Delta(N) = \frac{(-1)^{N+1}}{2}[B(N+1) - 2B(N) + B(N-1)]$ of ^{192}Pb. The even-even nuclei from ^{188}Pb to ^{194}Pb are studied.

The TDHFB dynamics is described by six degrees of freedom. Figure 4.8 shows eigenvalues of the moving-frame QRPA equation. Again, we find that there is a zero mode corresponding to the neutron pair rotation. Among the five vibrational modes, we choose the lowest one to construct the collective path in the ASCC. This lowest mode never crosses with other modes, though the spacing between the lowest to the next lowest mode can be very small, especially for ^{194}Pb. The evolution of the occupation numbers along the collective path is shown in Fig. 4.9. Similarly to the three-level model, the end points of the collective path indicate exactly the integer numbers, and the left end of each panel corresponds to the "Hartree-Fock"-like state. On the collective path, the occupation numbers of $i_{13/2}$, $p_{3/2}$, and $f_{5/2}$ mainly change.

The collective potentials for these isotopes are shown in Fig. 4.10. The heights of the potentials at the left end, $V(q_L) - V(0)$, are $2 \sim 3.5$ MeV. For ^{186}Pb, the height of the potential is not enough to satisfy the condition, $E < V(q_L)$, to have a closed trajectory for the first excited state (See the last paragraph in Sec. 4.3.2). We obtain the excited state for ^{186}Pb in a special boundary condition discussed in Sec. 4.4. We encounter another kind of problem for ^{196}Pb, which will be discussed in Sec. 4.4. Therefore, we calculate the first excited states in ^{188,190,192,194}Pb in the manner of the

Table 4.3: The same as described in the caption of Table 4.1 but for Pb isotopes. The energies are given in units of MeV. The value in parenthesis () is obtained in a special boundary condition discussed in Sec. 4.4. The table is adapted from Table III in Ref. [53].

	^{186}Pb	^{188}Pb	^{190}Pb	^{192}Pb	^{194}Pb	^{196}Pb
ASCC+SPA	(2.36)	2.31	2.21	2.12	2.04	–
Exact	2.58	2.44	2.34	2.25	2.20	2.15

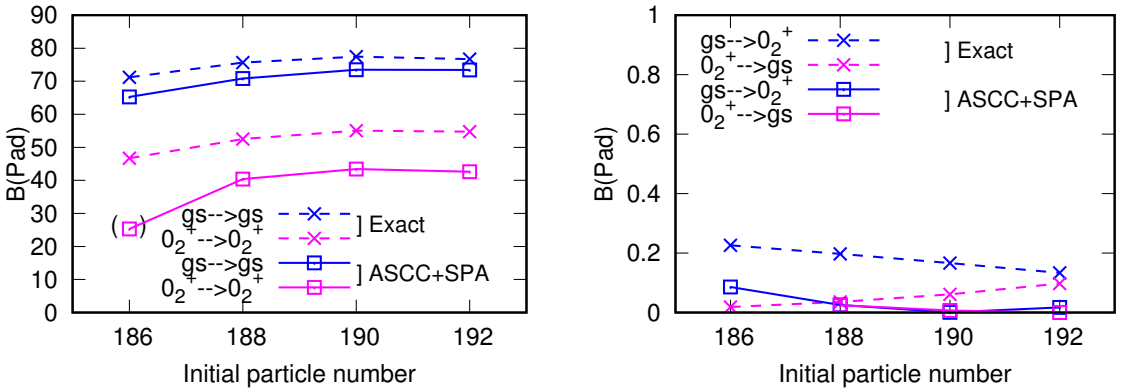

Figure 4.11: The same as described in the caption of Fig. 4.7 but for Pb isotopes. The value in parenthesis () is obtained in a special boundary condition discussed in Sec. 4.4. The figure is adapted from Fig. 11 in Ref. [53].

ASCC+SPA without any artificial assumption.

We show the calculated excitation energy of the first excited state in Table 4.3. Experimentally, this pair vibrational excited 0^+ state is fragmented into several 0^+ states due to other correlations, such as quadrupole correlation, not taken into account in the present model. We make a comparison with the exact solution of the multi-level pairing model. The ASCC+SPA method quantitatively reproduces the excitation energy of the exact solution.

The pair-addition transition strengths are shown in Fig. 4.11. The feature that is similar to the three-level case is observed: dominant intraband transition and very weak interband transitions. The accuracy from the ASCC+SPA method well reproduces $B(P_{\rm ad}; 0_1^+ \to 0_1^+)$ and qualitatively reproduces $B(P_{\rm ad}; 0_2^+ \to 0_2^+)$ as well. The deviation for the latter is about 25%, except the value in the parenthesis. The interband transitions are smaller than the intraband transitions by more than two orders of magnitude. This is also similar to the three-level model discussed in Sec. 4.3.2. For such weak transitions, the ASCC+SPA significantly underestimates the strengths. We may say that the ASCC+SPA gives reasonable results for the intraband transitions in the realistic values of the pairing coupling constant g and single-particle levels. The value of $B(P_{\rm ad}; 0_1^+ \to 0_2^+)$ for ^{186}Pb $\to$ ^{188}Pb, which is not shown in the Fig. 4.11, is 6.30, much larger than the exact value. We still need to develop the boundary condition for "unbound" states discussed in Sec. 4.4.

4.4 Remaining problems

Although we have constructed the basic framework of ASCC+SPA, there are two remaining problems for the non-integrable pairing models.

The first problem is the application of the ASCC+SPA to the open trajectories corresponding to the weak pairing case, as shown in Fig. 4.12. Because SPA is only available for the periodic trajectories, we need to assume that the collective momentum p_1 has a periodicity. Following the

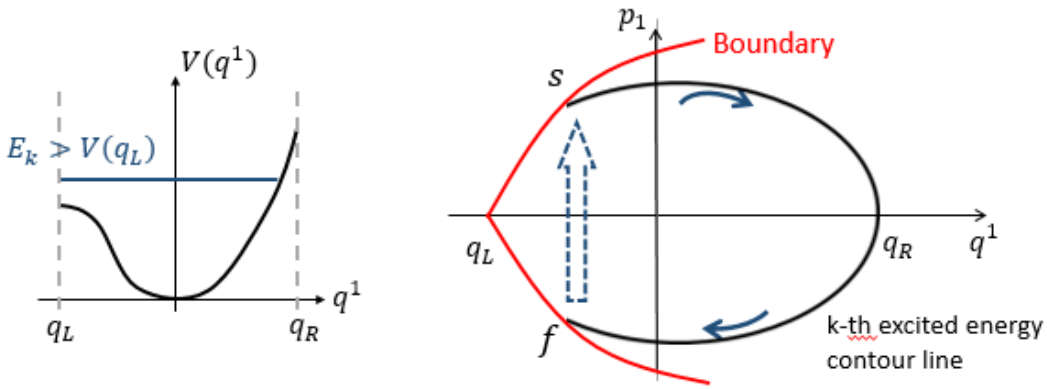

Figure 4.12: Schematic image for the open trajectory ($E_k > V(q_L)$). Left: schematic excitation energy and collective potential. Right: schematic classical trajectory in collective phase space. Red line represents a virtual boundary which connects the points s and f for the open trajectory.

periodicity $0 \leq \chi_\alpha \leq 2\pi$ for the original variables χ_α, we may construct an approximate periodic boundary condition for p_1.

We remember the open trajectories in two-level pairing models. As shown in Fig. 3.1, these open trajectories are connected at $\phi = \pm\pi$. From Eq. (3.1), the boundary with respect to χ_1, χ_2 becomes

$$\chi_1 - \Phi = \pm\frac{\pi}{2}, \qquad \chi_2 - \Phi = \mp\frac{\pi}{2}, \tag{4.42}$$

which lead to

$$e^{i\sum_{\alpha=1,2}|\chi_\alpha - \Phi|} = -1. \tag{4.43}$$

A possible construction of the approximate boundary for the multi-level pairing models is extending Eq. (4.43) to

$$e^{i\sum_{\alpha=1}^{L}|\phi_\alpha|} = -1, \tag{4.44}$$

where ϕ_α is defined in Eq. (4.36). Then, the boundary for p_1 is determined by

$$e^{i|p_1|\sum_{\alpha=1}^{L}|f^1_{,\alpha}|} = -1, \tag{4.45}$$

where $f^1_{,\alpha}$ is obtained from ASCC.

Using the above boundary condition, we try to calculate the excited states for open trajectories. We choose the same three-level system as discussed in Sec. 4.3, $\nu = 0$, $\Omega_1 = \Omega_2 = \Omega_3 = \Omega = 8$, $\epsilon_1 = -\epsilon_0$, $\epsilon_2 = 0$, $\epsilon_3 = 1.5\epsilon_0$, but with small coupling constant $g = 0.05\epsilon_0$. We discuss the result for $N = 18$. Fig. 4.13 shows the collective potential obtained from ASCC. The shallow energy minimum pocket cannot bind any excited states, $E_k > V(q_L)$. Next, we need to apply the EBK quantization condition. We assume the quantization condition for both open trajectory and closed trajectory as

$$\begin{aligned}\mathcal{T}_{\rm tot} &= \mathcal{T}_\circ + \mathcal{T}_{\rm corr} \\ &= \int_s^f \sum_\alpha j^\alpha d\chi_\alpha + \mathcal{T}_{\rm corr} = 2\pi k,\end{aligned} \tag{4.46}$$

where s and f are the starting and ending points for the open trajectory, respectively, as shown in Fig. 4.12 ($\int_s^f \to \oint$ for closed trajectory), and $\mathcal{T}_{\rm corr}$ is the correction to make the smooth change of $\mathcal{T}_{\rm tot}$ from closed to open trajectory by increasing the excitation energy. In closed trajectory, $\mathcal{T}_{\rm corr} = 0$.

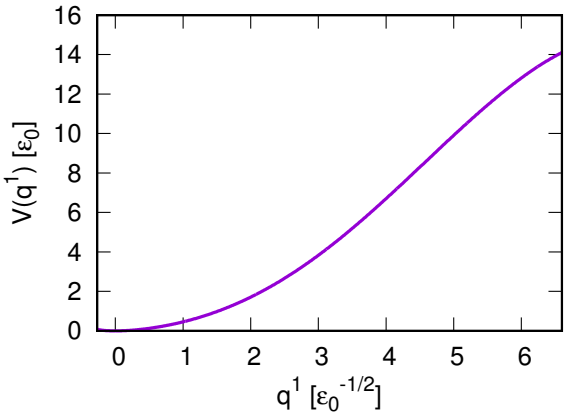

Figure 4.13: Collective potential $V(q^1)$ for $N = 18$ obtained from the ASCC. We adjust the energy minimum point as $q^1 = 0$ and $V = 0$.

Calculated $\mathcal{T}_{\rm tot}$ is shown in Fig. 4.14. The trajectory changes from closed to open at the excitation energy from 0.2 to 0.3. To cancel the large jump of $\mathcal{T}_\circ$ between closed and open trajectory the $\mathcal{T}_{\rm corr}$ has finite value for open trajectory. The classical trajectory of $|0_2^+\rangle$ fulfilling the Eq. (4.46) are shown in Fig. 4.15. Integrating the classical trajectory, we obtain the excited states. The excitation energy for $|0_2^+\rangle$ is 1.36, while 1.46 for exact solution, in units of ϵ_0. The occupation probability expanded in the SU(2) quasispin basis is represented in Fig. 4.16. We can find the result from ASCC+SPA with the boundary condition reasonably reproduce the exact solution.

We cannot convince that the boundary condition (4.45) well works in all multi-level pairing models. Actually, there is a certain deviation for the $|0_2^+\rangle$ in ^{186}Pb shown in Fig. 4.11. We need to consider more about the boundary condition. Moreover, we cannot calculate the excited states with normal ground state because the moving-frame QRPA equation in ASCC cannot give the eigenvectors associated with pairing vibrations at normal state.

Another problem occurs in the calculation of ^{196}Pb, in which we have encountered complex eigenvalues and eigenvectors of the moving-frame QRPA equation. This happens at $q \approx 0.1$ where the two eigen frequencies become identical, $\omega_1^2 = \omega_2^2$, as shown in Fig. 4.17. Because the complex values of f_α^1 the ASCC cannot determine the next point of the collective coordinate q^1. We do not have a problem for the crossing between the pairing rotational mode and the other modes. Currently, we do not know exactly when the complex solutions emerge.

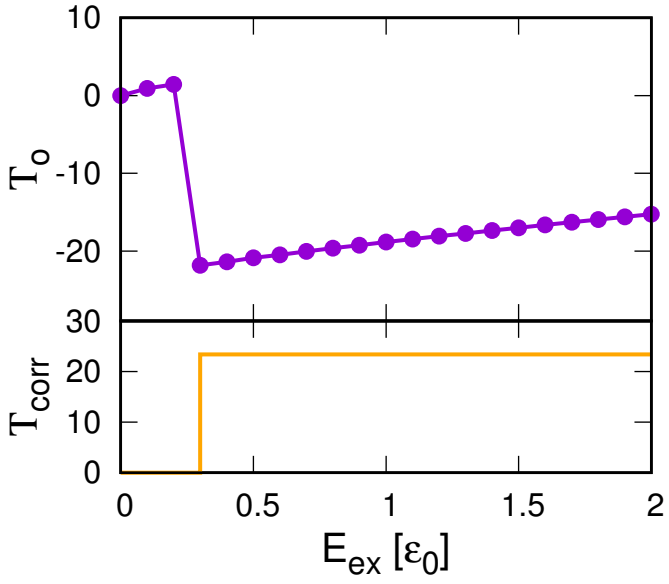

Figure 4.14: Action integral $\mathcal{T}_\circ$ and $\mathcal{T}_{\rm corr}$ for $N = 18$ in the EBK quantization condition Eq. (4.46) as a function of excitation energy $E_{\rm ex}$ below $2\epsilon_0$. See text for the definition of the two quantities.

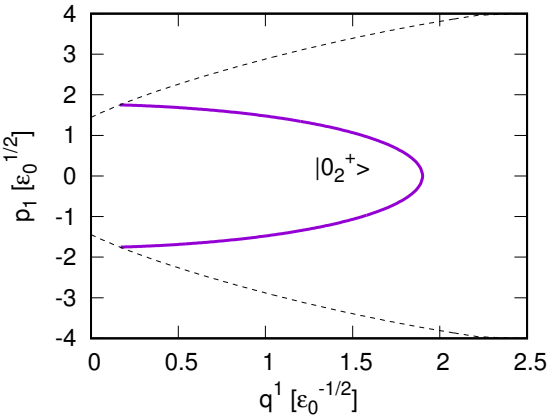

Figure 4.15: Classical trajectory for the $|0_2^+\rangle$, $N = 18$ in phase space. Black dashed lines are the approximate boundary defined in Eq. (4.45).

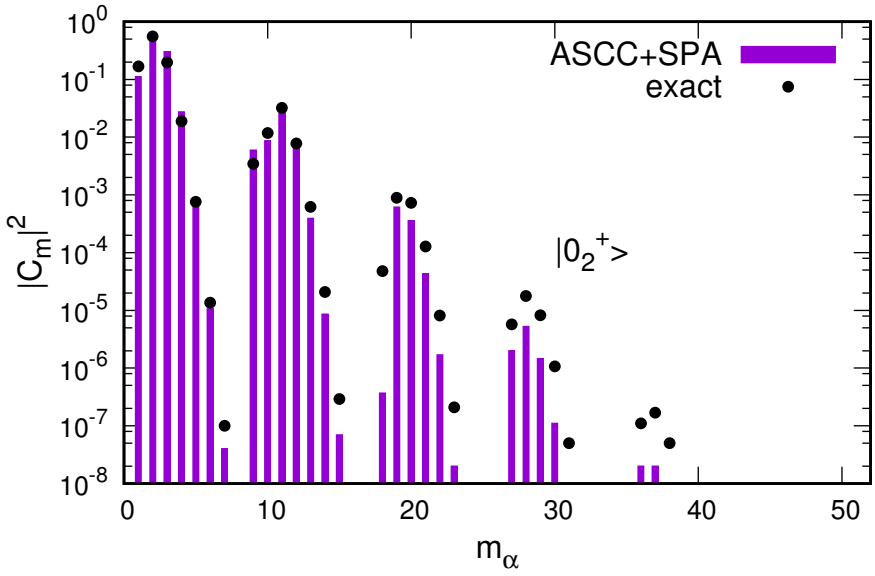

Figure 4.16: Occupation probability for $|0_2^+\rangle$, $N = 18$ in logarithmic scale as a function of $\{m_\alpha\} \equiv 9m_3 + m_2$. For example, $(m_1, m_2, m_3) = (8, 1, 0)$ at 1, $(m_1, m_2, m_3) = (7, 2, 0)$ at 2 in horizontal axis. The vertical bars and the circles at each $\{m_\alpha\}$ represent the squared components of the wave function from the ASCC+SPA and exact calculation, respectively.

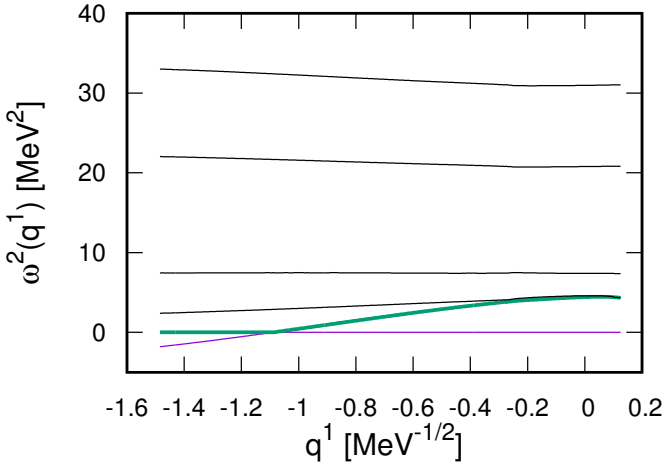

Figure 4.17: The same as described in the caption of Fig. 4.4 but for ^{196}Pb.

Chapter 5

Collective model treatment

The collective model has been proposed and utilized for the nuclear pairing dynamics [26, 27, 28, 29]. For those studies, the pairing collective Hamiltonian is constructed in terms of the pairing gap parameter Δ (or equivalent quantities) and the gauge angle Φ. This is analogous to the Bohr collective model, in which the collective coordinates are assumed to be the quadrupole deformation parameters, $\alpha_{2\mu}$. The 5D collective model has been extensively applied to analysis on numerous experimental data. On the contrary, there have been very few applications of the pairing collective model in comparison with experimental data. In this chapter, we examine the validity of the collective treatment of the pairing.

Because pairing rotation is trivial, we only consider the collective coordinate for pairing vibration. The deformation parameter is defined in $\alpha \equiv \langle \hat{S}^- \rangle$. To consider pairing vibration only, we fix the gauge angle as $\Phi = 0$. With $\Phi = 0$, the energy minimization with a fixed value of real α always leads to $\chi_\alpha = 0$.

$$\alpha(j) = \langle Z|\hat{S}^-|Z\rangle\Big|_{\chi=0} = \sum_\alpha \sqrt{j_\alpha(\Omega_\alpha - \nu_\alpha - j_\alpha)}. \tag{5.1}$$

The parameter α is equivalent to the pairing gap Δ, since the relation, $\Delta = g\alpha$, guarantees one-to-one correspondence between α and Δ.

5.1 Integrable system

In Chapter 3, we treat (ϕ, j) as canonical variables to describe pairing vibration. The collective model treatment is based on the choice, j as a coordinate and ϕ as a momentum, as discussed in Sec. 3.1.2.

$$\alpha(j) = \langle Z|\hat{S}^-|Z\rangle = \sqrt{j_1(\Omega_1 - \nu_1 - j_1)} + \sqrt{j_2(\Omega_2 - \nu_2 - j_2)}, \tag{5.2}$$

where j_1 and j_2 are the function of j as in (3.6).

The problem is that there is no one-to-one correspondence between j and α. If we examine the derivative of (5.2)

$$\frac{\partial \alpha}{\partial j} = \frac{-(\Omega_1 - \nu_1)/2 + j_1}{\sqrt{j_1(\Omega_1 - \nu_1 - j_1)}} + \frac{(\Omega_2 - \nu_2)/2 - j_2}{\sqrt{j_2(\Omega_2 - \nu_2 - j_2)}}, \tag{5.3}$$

we can find (5.3) is $+\infty$ for j_{min} and $-\infty$ for j_{max} in any two-level system. It indicates $\frac{\partial \alpha}{\partial j} = 0$ exists at $j = j_0$ ($j_{min} < j_0 < j_{max}$). For equal degeneracy case ($\Omega_1 - \nu_1 = \Omega_2 - \nu_2$), $j_0 = 0$. The relation between j and α are shown by dashed lines in Fig. 5.1 for $\Omega = 8$ mid-shell (a) and closed-shell (b) configurations discussed in Sec. 3.3.2. The deformation parameter α is largest at $j = 0$ (equal filling in both levels), and smallest at the end points of j. The constrained minimization with respect to α

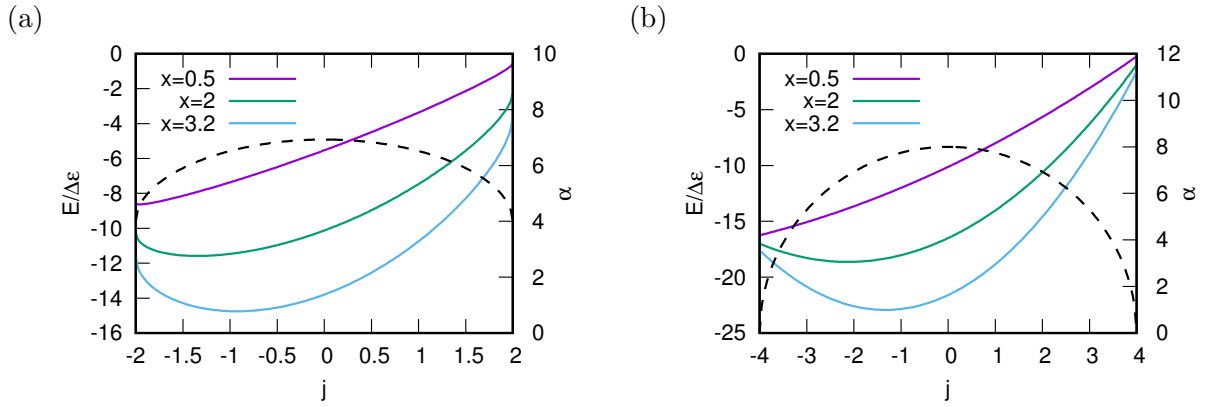

Figure 5.1: Potential surfaces as functions of j, Eq. (3.12) for $x = 0.5$, 2, and 3.2. Dashed line is the pairing deformation parameter α of Eq. (5.2) as a function of j. (a) mid-shell ($\Omega = N = 8$) and (b) closed-shell ($2\Omega = N = 16$). The figure is taken from Ref. [40].

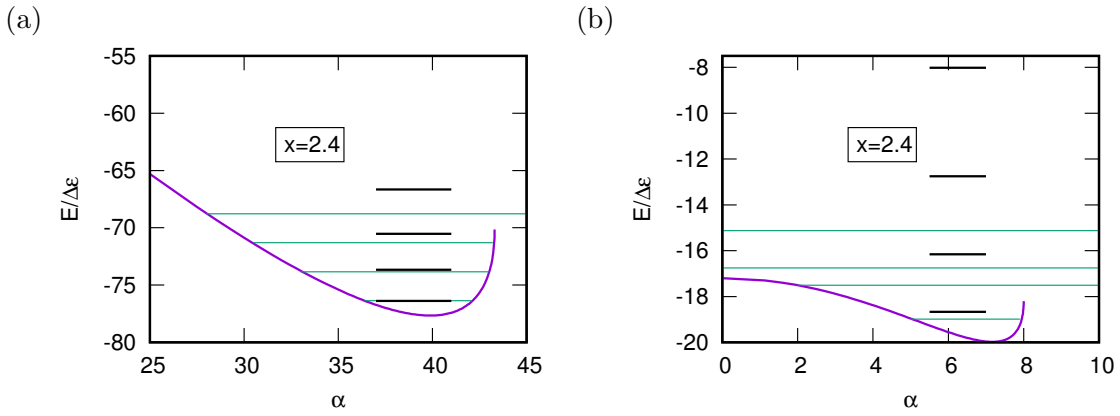

Figure 5.2: Potential energy surface as functions of α with $x = 2.4$; (a) $\Omega = N = 50$, (b) $2\Omega = N = 16$. Horizontal lines indicate energy spectra. Black lines are obtained from the potential energy surface, and green lines are obtained with the CQ method (Sec. 3.2.2). The figure is taken from Ref. [40].

cannot produce the states corresponding to $j > 0$. Apparently, we cannot map the entire region of j to α.

The collective model treatment requires the collective wave functions to be well localized in the $j < 0$ region. The potential energy, $V(j) = \mathcal{H}(\phi = 0, j; J = N/2)$ of Eq. (3.12), is also shown in Fig. 5.1. The restriction becomes more serious for the stronger pairing cases. For instance, the potential with $x = 3.2$ in Fig. 5.1(a) has only about 1 MeV depth at the minimum point, relative to the value at the boundary point ($j = 0$) corresponding to the maximum value of α (Δ).

To simulate the result of the collective model, we requantize the ATDHFB Hamiltonian in (3.11)-(3.13) by $\hat{\phi} = i\partial/\partial j$, with the ordering given by Pauli's prescription in Eq. (B.8). The range of the coordinate j is restricted to $j_{\min} \leq j \leq 0$ with the vanishing boundary condition $\psi(j_{\min}) = \psi(0) = 0$. Figure 5.2 shows two examples of the relationship between excitation energies and the potential energy surface. In the panel (a), we show the case of large Ω ($\Omega = 50$, $N = 50$, and $x = 2.4$), in which the excited 0^+ states are bound up to second excitation. From the collective model, the energies of the ground and the first excited states are well described, while the deviation becomes larger for higher excited states. For very large degeneracy, the pocket of energy surface is deep, hence the low-lying excited states may be described by α. However, in the small-Ω case ($\Omega = 8$, $N = 16$, and $x = 2.4$) of

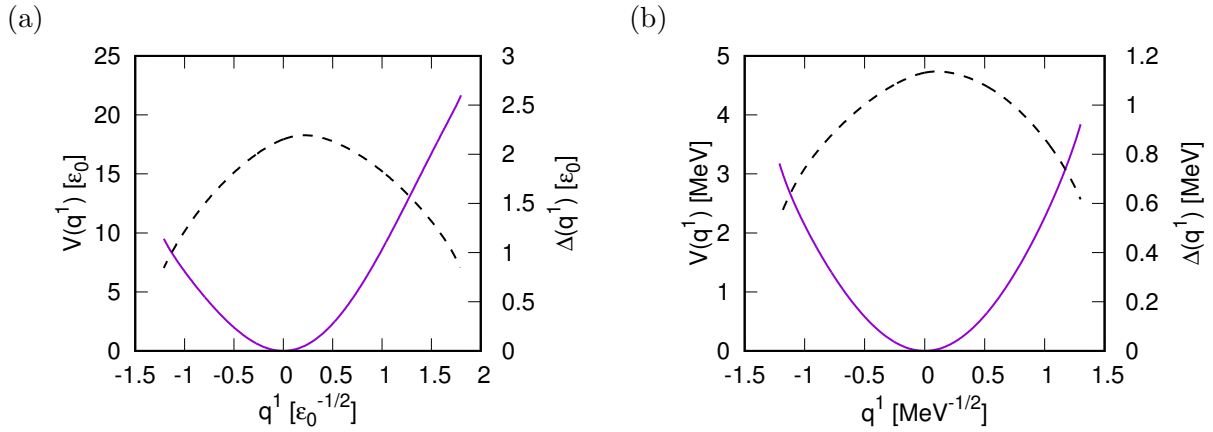

Figure 5.3: Potential surface as a function of q^1, in solid line. Dashed line is the pairing gap parameter Δ of Eq. (5.1) as a function of q^1. (a) $N = 20$ in three-level system ($\Omega_1 = \Omega_2 = \Omega_3 = 8$, $\epsilon_1 = -\epsilon_0$, $\epsilon_2 = 0$, $\epsilon_3 = 1.5\epsilon_0$, and $g = 0.2\epsilon_0$), (b) ^{192}Pb ($g = 0.138$ MeV and single-particle level shown in Table 4.2).

the panel (b), no excited states are bound by the potential as a function of α. None of the excited 0^+ states are properly described in the collective model. This shallow potential is a consequence of the improper choice of the collective coordinate α which represents only the $j < 0$ region. Therefore, the collective model treatment assuming α (Δ) as the collective coordinate is not applicable to small-Ω and strong-pairing cases.

5.2 Non-integrable system

In Chapter 4, the collective canonical variables (q^1, p_1) describing pairing vibration are obtained from ASCC. As far as there is a one-to-one correspondence between Δ and the collective variable q^1, we can transform the collective Hamiltonian in (q^1, Φ) into the one in (Δ, Φ). As integrable system, however, we cannot map the entire region of q^1 to Δ because the peak values of pairing gap parameter always appear around the middle of the collective path.

In Fig. 5.3, we show two examples of the behavior of pairing gap parameter as a function of the collective coordinate q^1. Panel (a) corresponds to the case of $N = 20$ in three-level system ($\Omega_1 = \Omega_2 = \Omega_3 = 8$, $\epsilon_1 = -\epsilon_0$, $\epsilon_2 = 0$, $\epsilon_3 = 1.5\epsilon_0$, and $g = 0.2\epsilon_0$), and panel (b) corresponds to the case of ^{192}Pb ($g = 0.138$ MeV and single-particle level shown in Table 4.2). In both panels, the peak in Δ is near $q^1 = 0$ and it is not a monotonic function of q^1, thus no one-to-one correspondence exists. Because the peak in Δ emerges near the energy minimum point, the potential surface of Δ is too shallow to bind the first excited state. The same behavior observed for all of the non-integrable systems. The situations are similar to the case in Fig. 5.2 (b), where the low-lying excited states cannot be properly described.

We conclude that the pairing gap parameter Δ (or equivalent quantities) is not a suitable collective coordinate to describe the pairing dynamics, in the multi-level pairing model.

Chapter 6

Conclusion and perspective

In order to construct a theoretical framework to describe large-amplitude collective motion associated with nuclear pairing, we studied the low-lying excited 0^+ states in multi-level pairing model. Based on the time-dependent Hartree-Fock-Bogoliubov (TDHFB) theory, we constructed the pairing collective excited states in two steps: (1) solve the TDHFB equation to obtain the TDHFB classical trajectories; (2) requantize the TDHFB trajectories to obtain the excited states. In these models, the TDHFB degrees of freedom consist of one constant of motion, pairing rotation described in variables (Φ, J), and $L-1$ degrees of freedom in the system with L single-particle levels. Therefore, the two-level system corresponds to the integrable system, and the system with more than two levels corresponds to the non-integrable system.

In the integrable two-level case, it is easy to find the coordinates to describe two types of collective motion, pairing rotation described by (Φ, J), and pairing vibration by variables (ϕ, j). With these canonical variables, we studied three different methods of requantization of TDHFB, the stationary-phase approximation (SPA) to the path integral, the canonical quantization (CQ), and the Fourier decomposition (FD) of the time-dependent observables. To test the performance of each requantization method, we applied them to systems with large particle numbers, and to small systems which are comparable with the valence orbits in realistic nuclear systems. In the former case, all the quantization methods reasonably reproduced the results of the exact calculation not only for excitation spectra, but also for two-particle transfer matrix elements. In the latter case, on the other hand, the agreement is less quantitative for the CQ and FD, especially for the two-particle transfer matrix elements. In contrast, the SPA keeps its accuracy for both cases in the entire range of pairing strengths. One of the reasons of its success is due to the inclusion of the off-diagonal parts of the pair transfer operator, by the explicit construction of the microscopic wave functions. The CQ and FD calculate the pair transfer matrix elements using only the diagonal part (expectation value) of the operator $\hat{S}^{\pm}$, based on Eqs. (3.40) and (3.41). This is a good approximation when the collectivity is so large that the diagonal parts dominate. However, the pairing collectivity may be too weak to justify this treatment. Thus, the SPA is the most accurate tool for description of the pairing collective motions in the large-amplitude regime.

The weak point of SPA is that the SPA is applicable only to the integrable TDHFB systems. To overcome this problem, we proposed the ASCC+SPA method for non-integrable systems. The concept is that the ASCC can decouple an integrable collective subspace from the original TDHFB phase space, then, the SPA is available for the collective subspace. In this approach, we use the ASCC method to extract the 2D collective subspace including the pairing rotation. In other words, we extract an approximate integrable system in the non-integrable system described by $(q^1, p_1; J, \Phi)$.

We applied the ASCC+SPA method to the multi-level pairing model. We investigated the three-level model and the multi-level model simulating Pb isotopes with a realistic pairing coupling constant g and single-particle levels. In both cases, the low-lying excited 0^+ states obtained with the ASCC+SPA well reproduce the exact solutions not only of the excitation energies but also of the wave functions.

In the ASCC+SPA, the calculation of any matrix elements is straightforward, because we have a microscopic wave function for every quantized state. This overcomes a disadvantage in the conventional canonical requantization in which we need to construct an effective expression of a given operator in terms of the collective variables only.

We also investigated the validity of the conventional treatment of the pairing collective model which assumes that the collective coordinate describing pairing vibration is the paring gap parameter Δ. In integrable (two-level) systems, the coordinate j describes the pairing vibration. We have found that there is no one-to-one correspondence between Δ and j in any two-level systems. In non-integrable systems, the coordinate q^1 obtained from ASCC describes the pairing vibration. The behavior of $\Delta(q^1)$ is very similar to $\Delta(j)$ in integrable systems. There is no one-to-one correspondence between Δ and q^1. The collective wave functions are not necessarily bound in the region where the variable Δ can represent. Thus, Δ is not a suitable coordinate to describe pairing vibration, at least in the pairing model.

This is the first attempt of the application of SPA into non-integrable systems, and we succeeded to describe the pairing dynamics quantitatively in the large-amplitude regime. In realistic nuclear systems, the competition between pairing and quadrupole correlations is important. The behavior of the pairing dynamics in such systems may be different from that in the pairing model we discussed in this thesis.

Thus, it is of significant interest to apply the SPA to systems with pairing and quadrupole correlations, such as multi-O(4) model [52] and P+Q model [55]. It is also important to extend the ASCC+SPA to the following cases: (1) "unbound" trajectories in shallow potential energy surface as discussed in Sec. 4.3; (2) trajectories in potential energy surface with multi energy minimum pockets, such as shape coexistence. In the former case, we need to find a proper boundary condition to guarantee the periodicity of the trajectories. In the latter case, the tunneling effect between the different energy minimum pockets is important, while the current version of SPA is based on classical trajectories which cannot take into account tunneling effect. Perhaps, it is possible to overcome the difficulty by extending the EBK quantization condition to multi-trajectories in each energy minimum pocket and imaginary-time trajectories in the classically forbidden region.

Ultimately, we aim at applying the ASCC+SPA to the realistic nuclear system with the density functional formalism. The numerical cost for solving the ASCC basic equations is extremely large in realistic systems. Recently, the ASCC has been applied to the realistic nuclear effective interaction [56, 57] employing an efficient method, finite amplitude method (FAM) [58, 59], in solution of the moving-frame QRPA equation. We expect in the near future, ASCC+SPA will be able to describe the low-lying excited states in nuclei, including the mysterious 0^+ states.

Acknowledgments

First, I would like to show my greatest appreciation to my supervisor, Takashi Nakatsukasa. I didn't have any knowledge about nuclear physics at all when I entered the graduated school. Even in such situation, his great instruction made me grow little by little. I was keeping positive condition for my research during my Ph.D. life because of his nice character. Also, his wealthy knowledge and experience always motivated me in the discussion. From my supervisor, I learned not only nuclear physics, but also the way of thinking for the problems.

I am grateful to all members in nuclear theory group. I am indebted to Kazuhiro Yabana for wide supports in my Ph.D. life. I really appreciate to Yukio Hashimoto. His kindness always encouraged me during the chat and discussion. I give a special thank to Nobuo Hinohara. I discussed a lot with him in the last two years. His nice suggestion always solved the serious problems I encountered in my research. I am particularly grateful to Kohei Washiyama. I was glad that he talked to me everyday. I cannot forget that he invited me to the eel restaurant twice.

The two seniors, Kazuyuki Sekizawa and Shunsuke Sato, are my idles for research. I really appreciate you teaching me a lot about physics and programming. Sekizawa-san held a seminar to study Bohr-Mottelson's textbook for me during my first-year. Thanks to the seminar, I understood the entire picture of nuclear physics. I often asked Sato-san when I encountered some problems related to the research. Surprisingly, his answer always satisfied me. I am very lucky to have met the two seniors.

I also thank to the DFT meeting per month. It improved my scientific English skill significantly. I especially appreciate to Haozhao Liang, Masayuki Matsuo, Kenichi Yoshida, and Koichi Sato, in DFT meeting group. They always gave me precious comments for my presentations. I cannot finish my research without a lot of discussion with them.

I would like to offer my special thanks to my family, girl friend, and special friends, Zhiheng Wang and Bin Zhou. They gave me a lot of emotional support during my Ph.D. life. Finally, I have to appreciate myself making honest efforts in the five years.

This work was supported in part by JASSO Honors Scholarship, JEES Scholarship, Interdisciplinary Computational Science Program in CCS, University of Tsukuba, JSPS KAKENHI Grants No. 18H01209, 17H05194, and 16K17680, and by JSPS-NSFC Bilateral Program for Joint Research Project on Nuclear mass and life for unravelling mysteries of r-process. Numerical calculations were performed in part using COMA at the CCS, University of Tsukuba.

Appendix A

Derivation of the action in pairing model

To obtain the TDHFB dynamics in pairing model, We need to derive the action $\mathcal{S}$ in explicit form. We give the detailed derivation in this Appendix.

A.1 Matrix elements of the spin-coherent state

The time-dependent coherent state classified into the spin-coherent state is employed in (2.16). We derive the necessary formula for the spin-coherent state in this subsection.

First, we consider the single-level case. With the commutation relation in (2.5), the SU(2) quasispin operators fulfill the following relations

$$\hat{S}^{\pm} |S, S^0\rangle = \sqrt{(S \mp S^0)(S \pm S^0 + 1)}\, |S, S^0 \pm 1\rangle \tag{A.1}$$

$$\hat{S}^0 |S, S^0\rangle = S^0 |S, S^0\rangle . \tag{A.2}$$

Using above relations, the coherent state can be expanded as

$$\begin{aligned} |Z\rangle &= (1 + |Z|^2)^{-S} e^{Z\hat{S}^+} |S, S^0 = -S\rangle \\ &= (1 + |Z|^2)^{-S} \sum_{n=0}^{2S} \sqrt{\frac{(2S)!}{n!(2S-n)!}} Z^n |S, -S + n\rangle . \end{aligned} \tag{A.3}$$

We can find the normalization condition is fulfilled

$$\begin{aligned} \langle Z|Z\rangle &= (1 + |Z|^2)^{-2S} \sum_{n=0}^{2S} \frac{(2S)!}{n!(2S-n)!} |Z|^{2n} \\ &= (1 + |Z|^2)^{-2S} \sum_{n=0}^{2S} {}_{2S}\mathrm{C}_n (|Z|^2)^n \\ &= (1 + |Z|^2)^{-2S} \times (1 + |Z|^2)^{2S} \\ &= 1. \end{aligned} \tag{A.4}$$

The overlap is

$$\langle \eta | Z \rangle = \frac{(1 + \eta^* Z)^{2S}}{(1 + |\eta|^2)^S (1 + |Z|^2)^S}. \tag{A.5}$$

We also calculate the expectation values of the operators. For $\hat{S}^0$,

$$\hat{S}^0 e^{Z\hat{S}^+} |S, S^0 = -S\rangle = \sum_{n=0}^{2S} (-S + n) \sqrt{\frac{(2S)!}{n!(2S-n)!}} Z^n |S, -S + n\rangle , \tag{A.6}$$

hence,

$$\begin{aligned}\langle Z|\hat{S}^0|Z\rangle &= (1+|Z|^2)^{-2S}\sum_{n=0}^{2S}(-S+n)\frac{(2S)!}{n!(2S-n)!}|Z|^{2n} \\ &= -S+2S\left(1-\frac{1}{1+|Z|^2}\right) \\ &= S\left(1-\frac{2}{1+|Z|^2}\right). \end{aligned} \tag{A.7}$$

From the first line to the second line, we used the differentiation for the both sides of

$$(1+|Z|^2)^{2S} = \sum_{n=0}^{2S} {}_{2S}\mathrm{C}_n (|Z|^2)^n \tag{A.8}$$

with respect to $|Z|^2$. With (A.7), the expectation values of occupation number is

$$\begin{aligned}\langle Z|\hat{n}|Z\rangle &= \langle Z|2\hat{S}^0+\Omega|Z\rangle \\ &= 2S\left(1-\frac{2}{1+|Z|^2}\right)+\Omega. \end{aligned} \tag{A.9}$$

The expectation values for $\hat{S}^+$ and $\hat{S}^-$ are the complex conjugate pair. For $\hat{S}^+$,

$$\hat{S}^+ e^{Z\hat{S}^+}\,|S,S^0=-S\rangle = \sum_{n=0}^{2S}\sqrt{(2S-n)(n+1)}\sqrt{\frac{(2S)!}{n!(2S-n)!}}Z^n\,|S,-S+n+1\rangle\,. \tag{A.10}$$

hence,

$$\begin{aligned}\langle Z|\hat{S}^+|Z\rangle &= (1+|Z|^2)^{-2S}\sum_{n=0}^{2S} Z^n\sqrt{(2S-n)(n+1)}\sqrt{\frac{(2S)!}{n!(2S-n)!}}\times(Z^*)^{n+1}\sqrt{\frac{(2S)!}{(n+1)!(2S-n-1)!}} \\ &= (1+|Z|^2)^{-2S}Z^*\sum_{n=0}^{2S}|Z|^{2n}\frac{(2S)!}{n!(2S-n-1)!} \\ &= \frac{2SZ^*}{1+|Z|^2}, \end{aligned} \tag{A.11}$$

and

$$\langle Z|\hat{S}^-|Z\rangle = \langle Z|\hat{S}^+|Z\rangle^* = \frac{2SZ}{1+|Z|^2}. \tag{A.12}$$

For the expectation value of $\hat{S}^+\hat{S}^-$,

$$\begin{aligned}\langle Z|\hat{S}^+\hat{S}^-|Z\rangle =&(1+|Z|^2)^{-2S}\|\hat{S}^- e^{Z\hat{S}^+}\,|S,S^0=-S\rangle\,\|^2 \\ =&(1+|Z|^2)^{-2S}\sum_{n=0}^{2S} n(2S-n+1)_{2S}\mathrm{C}_n|Z|^{2n} \\ =&(1+|Z|^2)^{-2S}\left\{(2S+1)2S(1+|Z|^2)^{2S-1}|Z|^2-2S(1+|Z|^2)^{2S}\right. \\ &\left.\times\left(\frac{(2S-1)|Z|^4}{(1+|Z|^2)^2}+\frac{|Z|^2}{1+|Z|^2}\right)\right\} \\ =&2S|Z|^2\frac{2S+|Z|^2}{(1+|Z|^2)^2}. \end{aligned} \tag{A.13}$$

From the second line to the third line, we need to calculate the term $\sum_{n=0}^{2S} n^2{}_{2S}\mathrm{C}_n|Z|^{2n}$. It can be obtained from the following relation

$$|Z|^2\frac{\partial}{\partial|Z|^2}|Z|^2\frac{\partial}{\partial|Z|^2}(1+|Z|^2)^{2S}=\sum_{n=0}^{2S}n^2{}_{2S}\mathrm{C}_n|Z|^{2n}. \tag{A.14}$$

When Z is time-dependent, the expectation value of $\frac{\partial}{\partial t}$ is also important quantity.

$$\begin{aligned}\langle Z|\frac{\partial}{\partial t}|Z\rangle &= \langle Z|\dot{Z}\frac{\partial}{\partial Z}+\dot{Z}^*\frac{\partial}{\partial Z^*}|Z\rangle \\ &= -\frac{S}{1+|Z|^2}(Z^*\dot{Z}+Z\dot{Z}^*)+\dot{Z}\langle Z|\hat{S}^+|Z\rangle \\ &= \frac{S}{1+|Z|^2}(Z^*\dot{Z}-Z\dot{Z}^*)\end{aligned} \tag{A.15}$$

From the second line to the third line, we used (A.11).

Next, we consider the multi-level case. For one-body operators, the extension from the single-level case is simple because we only sum over the index l for the single-particle levels. For two-body operators, we need to give the new derivations basically. For the expectation value of $\hat{S}^+\hat{S}^-$,

$$\langle Z|\hat{S}^+\hat{S}^-|Z\rangle=\sum_{\alpha\beta}\langle Z|\hat{S}^+_\beta\hat{S}^-_\alpha|Z\rangle\,. \tag{A.16}$$

When $\beta=\alpha$, the form is the same as in (A.13). When $\beta\neq\alpha$, from (A.11) and (A.12),

$$\langle Z|S^+_\beta S^-_\alpha|Z\rangle=\frac{2S_\alpha Z_\alpha}{1+|Z_\alpha|^2}\frac{2S_\beta Z^*_\beta}{1+|Z_\beta|^2}. \tag{A.17}$$

Therefore,

$$\langle Z|\hat{S}^+\hat{S}^-|Z\rangle=\sum_\alpha 2S_\alpha|Z_\alpha|^2\frac{2S_\alpha+|Z_\alpha|^2}{(1+|Z_\alpha|^2)^2}+\sum_{\alpha\neq\beta}\frac{2S_\alpha Z_\alpha}{1+|Z_\alpha|^2}\frac{2S_\beta Z^*_\beta}{1+|Z_\beta|^2}. \tag{A.18}$$

We conclude the useful formulae for the spin-coherent state as follows.

- Spin-coherent state

$$|Z\rangle=\prod_\alpha\left(1+|Z_\alpha|^2\right)^{-S_\alpha}e^{Z_\alpha\hat{S}^+_\alpha}\,|S_\alpha,S^0_\alpha=-S_\alpha\rangle\,. \tag{A.19}$$

- Normalization

$$\langle Z|Z\rangle=1 \tag{A.20}$$

- Overlap

$$\langle\eta|Z\rangle=\prod_\alpha\frac{(1+\eta^*_\alpha Z_\alpha)^{2S_\alpha}}{(1+|\eta_\alpha|^2)^{S_\alpha}(1+|Z_\alpha|^2)^{S_\alpha}}. \tag{A.21}$$

- Expectation value of $\hat{S}^0$

$$\langle Z|\hat{S}^0|Z\rangle=\sum_\alpha S_\alpha\left(1-\frac{2}{1+|Z_\alpha|^2}\right) \tag{A.22}$$

- Expectation value of $\hat{S}^+$

$$\langle Z|\hat{S}^+|Z\rangle = \sum_\alpha \frac{2S_\alpha Z_\alpha^*}{1+|Z_\alpha|^2} \tag{A.23}$$

- Expectation value of $\hat{S}^-$

$$\langle Z|\hat{S}^-|Z\rangle = \sum_\alpha \frac{2S_\alpha Z_\alpha}{1+|Z_\alpha|^2} \tag{A.24}$$

- Expectation value of $\hat{S}^+\hat{S}^-$

$$\langle Z|\hat{S}^+\hat{S}^-|Z\rangle = \sum_\alpha 2S_\alpha|Z_\alpha|^2\frac{2S_\alpha+|Z_\alpha|^2}{(1+|Z_\alpha|^2)^2} + \sum_{\alpha\neq\beta}\frac{2S_\alpha Z_\alpha}{1+|Z_\alpha|^2}\frac{2S_\beta Z_\beta^*}{1+|Z_\beta|^2} \tag{A.25}$$

- Expectation value of $\frac{\partial}{\partial t}$

$$\langle Z|\frac{\partial}{\partial t}|Z\rangle = \sum_\alpha \frac{S_\alpha}{1+|Z_\alpha|^2}(Z_\alpha^*\dot{Z}_\alpha - Z_\alpha\dot{Z}_\alpha^*) \tag{A.26}$$

A.2 Matrix elements in special canonical variables (χ, j) representation

In the text, we mostly use the transformed formulae derived in the previous section. We use (χ, j) representation. which is defined from the transformation of the complex number Z

$$Z_\alpha \equiv \tan\frac{\theta_\alpha}{2}e^{-i\chi_\alpha} \tag{A.27}$$

$$j_\alpha \equiv S_\alpha(1-\cos\theta_\alpha). \tag{A.28}$$

In such representation, most of matrix elements of spin-coherent state become concise. Because the derivations of the transformation for those matrix elements are simple, we omit the explanation here. We conclude the useful formulae as follows.

- Expectation value of $\hat{S}^0$

$$\langle Z|\hat{S}^0|Z\rangle = \sum_\alpha (j_\alpha - S_\alpha) \tag{A.29}$$

- Expectation value of $\hat{S}^+$

$$\langle Z|\hat{S}^+|Z\rangle = \sum_\alpha \sqrt{j_\alpha(2S_\alpha - j_\alpha)}e^{-i\chi_\alpha} \tag{A.30}$$

- Expectation value of $\hat{S}^-$

$$\langle Z|\hat{S}^-|Z\rangle = \sum_\alpha \sqrt{j_\alpha(2S_\alpha - j_\alpha)}e^{i\chi_\alpha} \tag{A.31}$$

- Expectation value of $\hat{S}^+\hat{S}^-$

$$\langle Z|\hat{S}^+\hat{S}^-|Z\rangle = \sum_\alpha \left(2S_\alpha j_\alpha - j_\alpha^2 + \frac{j_\alpha^2}{2S_\alpha}\right) + 2\sum_{\alpha\leq\beta}\sqrt{j_\alpha j_\beta(2S_\alpha - j_\alpha)(2S_\beta - j_\beta)}\cos\left(\chi_\alpha - \chi_\beta\right). \tag{A.32}$$

- Expectation value of $\frac{\partial}{\partial t}$

$$\langle Z|\frac{\partial}{\partial t}|Z\rangle = \frac{1}{i}\sum_\alpha j_\alpha\dot{\chi}_\alpha \tag{A.33}$$

A.3 Derivation of the path integral in spin-coherent state

We derive the path integral formulation for SU(2) spin-coherent state. First, we consider the case of one degree of freedom corresponding single-level system. Using the coherent state $|Z\rangle$, the time development from t' to t'' of the system is described by the propagator

$$K(Z'',t'';Z',t') = \langle Z''|\exp\left\{-\frac{i}{\hbar}\hat{H}(t''-t')\right\}|Z'\rangle \tag{A.34}$$

$$= \lim_{n\to\infty}\int\prod_{k=1}^{n-1}d\mu(Z_k)\prod_{k=1}^{n}\langle Z_k|\exp\left\{-\frac{i}{\hbar}\hat{H}\epsilon\right\}|Z_{k-1}\rangle\,, \tag{A.35}$$

where we set $Z_n = Z''$, $Z_0 = Z'$, and $\epsilon = \frac{t''-t'}{n}$. Because ϵ is infinitesimal quantity, we can expand (A.35) with respect to ϵ up to first order

$$\begin{aligned}\langle Z_k|\exp\left\{-\frac{i}{\hbar}\hat{H}\epsilon\right\}|Z_{k-1}\rangle &\approx \langle Z_k|1 - \frac{i}{\hbar}\epsilon\hat{H}|Z_{k-1}\rangle \\ &\approx \langle Z_k|Z_{k-1}\rangle\exp\left\{\frac{i}{\hbar}\epsilon\frac{\langle Z_k|\hat{H}|Z_{k-1}\rangle}{\langle Z_k|Z_{k-1}\rangle}\right\} \\ &\approx \langle Z_k|Z_{k-1}\rangle\exp\left\{\frac{i}{\hbar}\epsilon\,\langle Z_k|\hat{H}|Z_{k-1}\rangle\right\}.\end{aligned} \tag{A.36}$$

In addition, we expand the overlap up to first order

$$\begin{aligned}\langle Z_k|Z_{k-1}\rangle &= \exp(\log\kappa(Z_k,Z_k^*;Z_{k-1},Z_{k-1}^*)) \\ &\approx \exp\left\{\frac{i}{\hbar}\left(\frac{\hbar}{i}\left(\frac{\partial\kappa}{\partial Z_k}\Delta Z_k + \frac{\partial\kappa}{\partial Z_k^*}\Delta Z_k^*\right)\right)\right\},\end{aligned} \tag{A.37}$$

where we set $\Delta Z_k = Z_k - Z_{k-1} = \dot{Z}_k\epsilon$. Using (A.21), the differentiations of κ become

$$\left.\frac{\partial\kappa}{\partial Z_k}\right|_{Z_k=Z_{k-1}} = -\frac{SZ_k^*}{1+|Z_k|^2} \tag{A.38}$$

$$\left.\frac{\partial\kappa}{\partial Z_k^*}\right|_{Z_k^*=Z_{k-1}^*} = \frac{SZ_k}{1+|Z_k|^2} \tag{A.39}$$

Therefore, the propagator is written in path integral formulation

$$K(Z'',t'';Z',t') = \int \mathcal{D}\mu(Z(t))e^{\frac{i}{\hbar}\mathcal{S}} \tag{A.40}$$

$$\mathcal{D}\mu(Z(t)) = \lim_{n\to\infty}\prod_{k=1}^{n-1} d\mu(Z_k) \tag{A.41}$$

$$\mathcal{S} = \int dt \left\{ \frac{i\hbar S}{1+|Z|^2}(Z^*\dot{Z} - Z\dot{Z}^*) - \langle Z|\hat{H}|Z\rangle \right\} \tag{A.42}$$

Of course, the action $\mathcal{S}$ is identical to the definition

$$\mathcal{S} = \int dt \, \langle Z|i\hbar\frac{\partial}{\partial t} - \hat{H}|Z\rangle \, . \tag{A.43}$$

It can be easily checked by using (A.26).

The extension to the multi-level system is straightforward. The action $\mathcal{S}$ becomes

$$\mathcal{S} = \int \mathcal{L}(t)dt, \quad \mathcal{L}(t) = i\hbar\sum_\alpha \frac{S_\alpha}{1+|Z_\alpha|^2}(Z_\alpha^*\dot{Z}_\alpha - Z_\alpha\dot{Z}_\alpha^*) - \langle Z|H|Z\rangle \tag{A.44}$$

A.4 Action in pairing model

We derived the action in the previous sections. Using the formula in Sec. A.1, the expectation value of pairing Hamiltonian is

$$\begin{aligned}\langle Z|\hat{H}|Z\rangle =& \sum_\alpha \epsilon_\alpha \left\{ 2S_\alpha \left(1 - \frac{2}{1+|Z_\alpha|^2}\right) + \Omega_\alpha \right\} \\ & - g\sum_\alpha 2S_\alpha|Z_\alpha|^2\frac{2S_\alpha+|Z_\alpha|^2}{(1+|Z_\alpha|^2)^2} + \sum_{\alpha\neq\beta}\frac{2S_\alpha Z_\alpha}{1+|Z_\alpha|^2}\frac{2S_\beta Z_\beta^*}{1+|Z_\beta|^2}.\end{aligned} \tag{A.45}$$

Using the canonical variables (χ, j), we can obtain the tractable form of the action based on Sec. A.2. The Lagrangian in (χ, j) representation becomes

$$\mathcal{L}(t) = \sum_\alpha j_\alpha\dot{\chi_\alpha} - \mathcal{H}(\chi, j), \tag{A.46}$$

$$\begin{aligned}\mathcal{H}(\chi,j) \equiv& \langle Z|H|Z\rangle \\ =& \sum_\alpha \epsilon_\alpha\nu_\alpha + \sum_\alpha 2\epsilon_\alpha j_\alpha - g\sum_\alpha\left((\Omega_\alpha-\nu_\alpha)j_\alpha - j_\alpha^2 + \frac{j_\alpha^2}{\Omega_\alpha-\nu_\alpha}\right) \\ & - 2g\sum_{\alpha\leq\beta}\sqrt{j_\alpha j_\beta(\Omega_\alpha-\nu_\alpha-j_\alpha)(\Omega_\beta-\nu_\beta-j_\beta)}\cos(\chi_\alpha-\chi_\beta).\end{aligned} \tag{A.47}$$

Appendix B

Extra discussion in two-level pairing model

B.1 Phase transition point

We consider the phase transition point between the superfluid state and the normal state. The superfluid ground state corresponds to the local minimum point in potential energy surface. The time-dependent coherent state (2.16) attributes to BCS trail wave function in $\chi_\alpha = 0$. For the sake of simplicity, here, we only consider the even-particle system with $\nu = 0$ (without Pauli blocking).

With fixed expectation value of the total particle number $N = 2J$, the superfluid ground state correspond to the local minimum point in (3.5)

$$\left.\frac{\partial \mathcal{H}(\phi, j; J)}{\partial j}\right|_{\phi=0} = 0. \tag{B.1}$$

The explicit form of (B.1) is

$$\frac{2(\epsilon_2 - \epsilon_1)}{g} = 2(S_2 q_2 - S_1 q_1) - (q_2 - q_1) + 2\left(\frac{q_2}{\sqrt{1-q_2^2}} S_1 \sqrt{1-q_1^2} - \frac{q_1}{\sqrt{1-q_1^2}} S_2 \sqrt{1-q_2^2}\right), \tag{B.2}$$

where

$$q_\alpha = \cos\theta_\alpha = \frac{\Omega_\alpha - J - 2(-1)^l j}{\Omega_\alpha} \quad \text{for } \alpha = 1, 2 \tag{B.3}$$

with the range $-1 \le q_\alpha \le 1$. $q_\alpha = 1$ corresponds to empty occupation and $q_\alpha = -1$ corresponds to full occupation.

(B.2) has solution only for the superfluid state. In open shell, (B.2) always have solution. In closed shell, substituting $q_1 = -1$ and $q_2 = 1$ into (B.2) leads the phase transition point between normal state and superfluid state. The last term of right side in (B.2) becomes

$$\begin{aligned}
& 2\left(\frac{q_2}{\sqrt{1-q_2^2}} S_1 \sqrt{1-q_1^2} - \frac{q_1}{\sqrt{1-q_1^2}} S_2 \sqrt{1-q_2^2}\right) \\
= \; & 2\left(\frac{S_2 - j_2}{\sqrt{j_2(2S_2 - j_2)}} \sqrt{j_1(2S_1 - j_1)} - \frac{S_1 - j_1}{\sqrt{j_1(2S_1 - j_1)}} \sqrt{j_2(2S_2 - j_2)}\right) \\
= \; & 2\left(\frac{S_2 - j_2}{\sqrt{2S_2 - j_2}} \sqrt{j_1} - \frac{S_1 - j_1}{\sqrt{j_1}} \sqrt{2S_2 - j_2}\right) \\
\xrightarrow[j_2 \to 0]{j_1 \to 2S_1} \; & 4\sqrt{S_1 S_2}.
\end{aligned}$$

From second line to the third line, we used the fact of closed shell $J = 2S_1$. With $\Omega_\alpha = 2S_\alpha$, the phase transition point in closed shell is

$$g_c = \frac{2\Delta\epsilon}{\Omega_1 + \Omega_2 + 2\sqrt{\Omega_1 \Omega_2} - 2}, \tag{B.4}$$

where $\Delta\epsilon = \epsilon_2 - \epsilon_1$. When $\Omega_1 = \Omega_2 = \Omega$, (B.4) becomes

$$g_c = \frac{\Delta\epsilon}{2\Omega - 1}, \tag{B.5}$$

In the textbook [60], the dimensionless coupling constant x is defined in

$$x = 2g\frac{\Omega}{\Delta\epsilon}. \tag{B.6}$$

We can find the phase transition occurs at

$$x_c = 2g_c\frac{\Omega}{\Delta\epsilon} = \frac{2\Omega}{2\Omega - 1} \approx 1. \tag{B.7}$$

The last approximation well performs for $\Omega \gg 1$. We often use the dimensionless coupling constant x in the text.

B.2 Canonical quantization in Pauli's prescription

In Sec. 3.1.2, we derived the TDHFB Hamiltonian in adiabatic approximation. The canonical quantization in Pauli's prescription is available for Eq. (3.11). Using Pauli's prescription, Eq. (3.11) becomes

$$H\left(j, i\frac{\partial}{\partial j}\right) = V(j) - \frac{1}{2}\sqrt{B^{-1}(j)}\frac{\partial}{\partial j}\sqrt{B^{-1}(j)}\frac{\partial}{\partial j}, \tag{B.8}$$

and we can obtain the requantized states by solving the Schrödinger equation

$$H\left(j, i\frac{\partial}{\partial j}\right)\psi(j) = E\psi(j). \tag{B.9}$$

Because the range of j is limited ($j_{\min} \leq j \leq j_{\max}$), we have to care about the boundary condition for the end points $j_{\min}$ and $j_{\max}$. We show the potential surfaces in the range of $j_{\min} \leq j \leq j_{\max}$ in Fig. B.1. The boundary condition is negligible for the strong pairing correlation. On the other hand, the boundary condition is important for the weak pairing correlation because the potential cannot bind the states at $j_{\min}$. Actually, we obtain proper states in strong pairing correlations and improper states in weak correlations from Pauli's prescription for the canonical variables (ϕ, j) (Fig. B.3).

We reconsider the coordinate system for the phase space (ϕ, j) (Fig. B.2). It is natural to utilize a cylindrical coordinate system because ϕ is periodic. In cylindrical coordinate system, the points at $j_{\min}$ and $j_{\max}$ are singular. Instead of the cylindrical coordinate system, we bring an another coordinate system, geographic coordinate system, which assumes the phase space collapsing at $j_{\min}$ and $j_{\max}$, such as north pole and south pole. We think this assumption is correct from the following reason. The (adiabatic) TDHFB Hamiltonian is independent of ϕ at $j_{\min}$ and $j_{\max}$. In addition, we can white down the coherent state as $|Z\rangle = e^{i\Theta\hat{J}}|Z_0\rangle$, where Θ is an arbitrary phase depends on ϕ and $|Z_0\rangle$ is independent of ϕ, at $j_{\min}$ and $j_{\max}$.

Under the geographic coordinate system, we try to find a new set of canonical variables to obtain the requantized states in weak pairing correlation. In $x \to 0$ limit, the excitation energies are $2n\Delta\epsilon$ with equivalent energy spacing because the excited states are pure $2n$-particle-$2n$-hole configurations. We aim to obtain harmonic oscillator Hamiltonian by canonical transformation from (ϕ, j) to (Q, P) at $x = 0$. We utilize Type III generating function

$$G_3(P, \phi) = \frac{P^2}{2\tan\phi} - \phi j_{\min}. \tag{B.10}$$

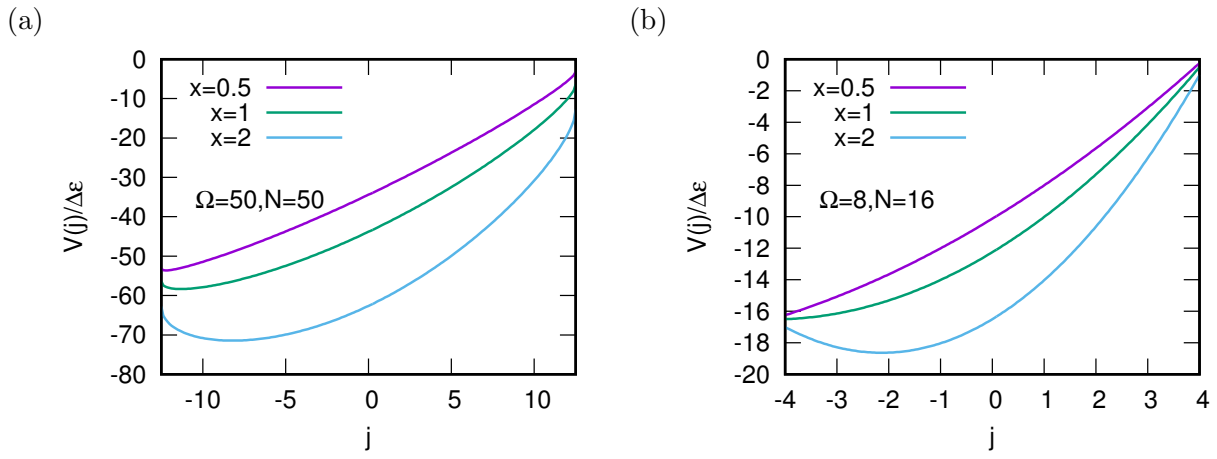

Figure B.1: Potential surfaces as functions of j, Eq. (3.12) for $x = 0.5$, 1, and 2. (a) mid-shell in large degeneracy ($\Omega = 50$, $N = 50$) and (b) closed-shell in small degeneracy ($\Omega = 8$, $N = 16$).

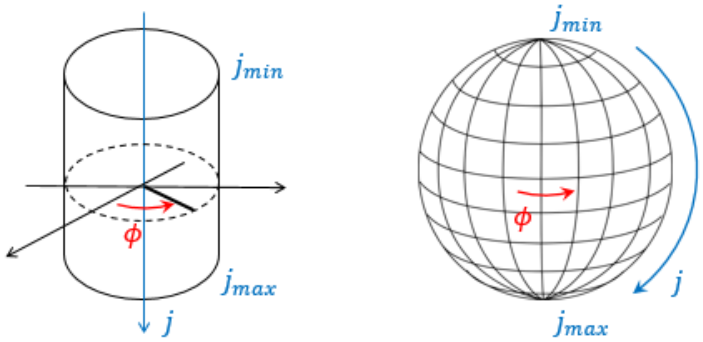

Figure B.2: Coordinate systems of the phase space (ϕ, j) in two-level pairing model. Left figure: cylindrical coordinate system; right figure: geographic coordinate system.

The first term is known as the harmonic oscillator generating function, and the second term is to determine the original point $(Q, P) = (0, 0)$ at $j = j_{\min}$. The new canonical variables can be straightforward derived from

$$Q = -\frac{\partial G_3}{\partial P} = -\frac{P}{2\tan\phi}$$
$$j = -\frac{\partial G_3}{\partial \phi} = \frac{P^2}{2\sin\phi} + j_{\min},$$

which lead to

$$Q(\phi, j) = \pm\sqrt{2}\sqrt{j - j_{\min}}\cos\phi$$
$$P(\phi, j) = \mp\sqrt{2}\sqrt{j - j_{\min}}\sin\phi, \tag{B.11}$$

and

$$j(Q, P) = \frac{Q^2 + P^2}{2} + j_{\min}$$
$$\phi(Q, P) = \arccos\left(\frac{Q^2}{\sqrt{Q^2 + P^2}}\right). \tag{B.12}$$

Under the new canonical variables, we can avoid the singularity at $j = j_{\min}$. The transformed TDHFB Hamiltonian $\tilde{\mathcal{H}}(Q, P; J)$ is

$$\tilde{\mathcal{H}}(Q, P; J) = \tilde{V}(Q) + \frac{1}{2}\tilde{B}^{-1}(Q)P^2, \tag{B.13}$$

where

$$\tilde{V}(Q) = \tilde{\mathcal{H}}(Q, P = 0; J) = \mathcal{H}(\phi(Q, P = 0), j(Q, P = 0); J) \tag{B.14}$$

$$\tilde{B}^{-1}(Q) = \left.\frac{\partial^2 \tilde{\mathcal{H}}}{\partial P^2}\right|_{P=0}. \tag{B.15}$$

We can also utilize the Pauli's prescription (B.8) for the transformed TDHFB Hamiltonian. Especially at $x = 0$, the TDHFB Hamiltonian becomes

$$\begin{aligned}\mathcal{H}(\phi, j; J) &= (\epsilon_1 + \epsilon_2)J + 2(\epsilon_2 - \epsilon_1)j \\ &= (\epsilon_1 + \epsilon_2)J + 2\Delta\epsilon j_{\min} + \Delta\epsilon(Q^2 + P^2),\end{aligned} \tag{B.16}$$

which perfectly reproduce the excitation energies $2n\Delta\epsilon$.

We apply the canonical quantization in Pauli's prescription for both canonical variables $(j, -\phi)$ and (Q, P). The boundary conditions are determined in $\psi'(j_{\min}) = 0$ and $\psi(j_{\max}) = 0$ for $(j, -\phi)$, and $\psi(Q_{\min}) = \psi(Q_{\max}) = 0$ for (Q, P). Calculated excitation energies are shown in Fig. B.3. For the canonical variables $(j, -\phi)$, the requantized energies well reproduce the exact solution in strong pairing correlation, while the deviation becomes larger and larger toward $x = 0$. The reason is that the singular point $j_{\min}$ influences the requantized states significantly. However, it may be difficult to know the proper boundary condition at $j_{\min}$. For the canonical variables (Q, P), on the other hand, the requantized energies well reproduce the exact solution in weak pairing correlation, while the deviation becomes larger and larger toward the strong pairing correlation in the panel (b). We cannot obtain the result after a certain x because the mass parameter $\tilde{B}^{-1}(Q)$ have the negative signs.

We find that the canonical variables $(j, -\phi)$ can well describe the strong pairing systems, while (Q, P) can well describe the weak pairing systems. We think that the choice of canonical coordinates is especially important for the canonical quantization in Pauli's prescription. In a sense, $(j, -\phi)$ is the best canonical variables in $x \to \infty$, and (Q, P) is the best canonical variables in $x \to 0$. Best canonical variables in the intermediate pairing correlation should also exist in proper canonical transformations. We need to be careful for this problem if we choose the canonical quantization in Pauli's prescription for the requantization of TDHFB.

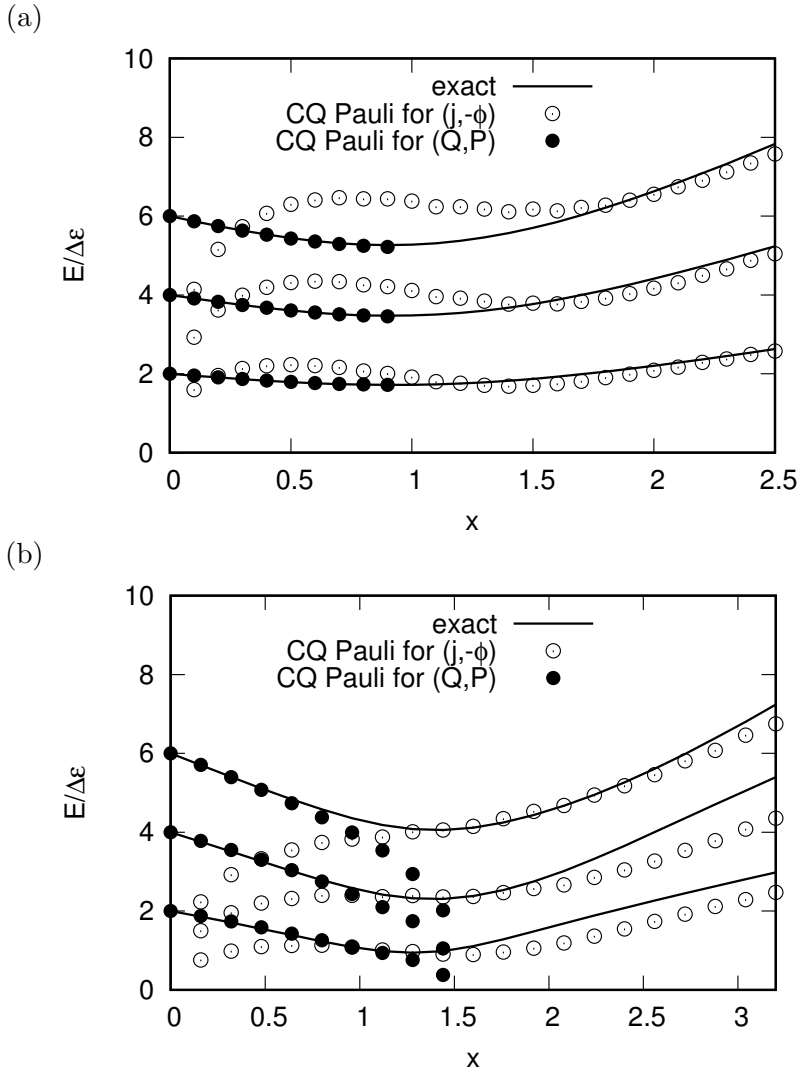

Figure B.3: Excitation energies of $|0_2^+\rangle$, $|0_3^+\rangle$ and $|0_4^+\rangle$ in canonical quantization with Pauli's prescription. (a) $\Omega = 50$, $N = 50$ and (b) $\Omega = 8$, $N = 16$ as functions of the dimensionless parameter x of Eq. (B.6). Open circles correspond to the canonical variables $(j, -\phi)$ and filled circles correspond to the transformed canonical variables (Q, P) in (B.11).

Appendix C

Derivation of semiclassical wave function in SPA

C.1 Derivation of Eq. (3.27)

We give a derivation of the semiclassical wave function of Eq. (3.27). The explicit form of coherent state in two-level system is

$$\begin{aligned}
|Z\rangle &= \prod_{\alpha=1}^{2}(1+|Z_\alpha|^2)^{-S_\alpha}e^{Z_\alpha\hat{S}_\alpha^+}\,|0\rangle \\
&= \prod_{\alpha=1}^{2}\left(1+\tan^2\frac{\theta_\alpha}{2}\right)^{-S_\alpha}\sum_k\frac{1}{k!}\sum_{m=0}^{k}\binom{k}{m}\left(\tan\frac{\theta_1}{2}e^{-i\phi_1}\hat{S}_1^+\right)^m\left(\tan\frac{\theta_2}{2}e^{-i\phi_2}\hat{S}_2^+\right)^{k-m}|0\rangle \\
&= \prod_{\alpha=1}^{2}\left(1+\tan^2\frac{\theta_\alpha}{2}\right)^{-S_\alpha}\sum_k\frac{1}{k!}\sum_{m=0}^{k}\binom{k}{m}\tan^m\frac{\theta_1}{2}\tan^{k-m}\frac{\theta_2}{2}e^{-ik\Phi}e^{-i(k/2-m)\phi}(\hat{S}_1^+)^m(\hat{S}_2^+)^{k-m}\,|0\rangle
\end{aligned} \tag{C.1}$$

Inserting (C.1) into (3.26) under fixed J and E_k, it becomes

$$\begin{aligned}
|\psi_k^J\rangle &\propto \oint d\Phi\oint dt e^{i\mathcal{T}_{J,E_k}(\Phi,t)}\,|\Phi,t\rangle_{J,E_k} \\
&\propto \sum_k\frac{1}{k!}\sum_{m=0}^{k}\binom{k}{m}\int_0^{2\pi}d\Phi e^{i(J-k)\Phi}\int_0^T dt e^{i\int\pi(t')\dot{\phi}(t')dt'-i(k/2-m)\phi} \\
&\quad\times\left\{\prod_{\alpha=1}^{2}\left(1+\tan^2\frac{\theta_\alpha}{2}\right)^{-S_\alpha}\right\}\tan^m\frac{\theta_1}{2}\tan^{k-m}\frac{\theta_2}{2}(\hat{S}_1^+)^m(\hat{S}_2^+)^{k-m}\,|0\rangle \\
&\propto \sum_{m=0}^{J}\binom{J}{m}\int_0^T dt\exp\left(i\int\pi(t')\dot{\phi}(t')dt'-i(J/2-m)\phi\right) \\
&\quad\times\left\{\prod_{\alpha=1}^{2}\left(1+\tan^2\frac{\theta_\alpha}{2}\right)^{-S_\alpha}\right\}\tan^m\frac{\theta_1}{2}\tan^{J-m}\frac{\theta_2}{2}(\hat{S}_1^+)^m(\hat{S}_2^+)^{J-m}\,|0\rangle\,.
\end{aligned} \tag{C.2}$$

We find that the integration over Φ is nothing but the number projection. In SU(2) quasi-spin representation, the vacuum state is written as $|0\rangle = |S_1,-S_1;S_2,-S_2\rangle$, which leads to

$$(\hat{S}_1^+)^m(\hat{S}_2^+)^{J-m}\,|0\rangle = \sqrt{\frac{(2S_1)!m!}{(2S_1-m)!}}\sqrt{\frac{(2S_2)!(J-m)!}{[2S_2-(J-m)]!}}\,|S_1,-S_1+m;S_2,-S_2+(J-m)\rangle\,. \tag{C.3}$$

For convenience, we define coefficients

$$\begin{aligned} A(q,S,m) &\equiv \frac{\tan^m\frac{\theta}{2}}{\left(1+\tan^2\frac{\theta}{2}\right)^{-S}}\sqrt{\frac{(2S)!m!}{(2S-m)!}} \\ &= \left(\frac{j}{2S}\right)^{m/2}\left(\frac{2S-j}{2S}\right)^{S-m/2}\sqrt{\frac{(2S)!m!}{(2S-m)!}} \end{aligned} \tag{C.4}$$

where $j = S(1-\cos\theta)$. Inserting Eq. (C.4) into Eq. (C.2), we reach Eq. (3.27).

C.2 Derivation of Eq. (4.34)

To obtain the semiclassical wave function Eq. (4.37) via ASCC, we give the derivation of Eq. (4.34).

$$\begin{aligned} |Z\rangle &= \prod_\alpha (1+|Z_\alpha|^2)^{-S_\alpha} e^{Z_\alpha \hat{S}_\alpha^+}|0\rangle \\ &= \prod_\alpha \left(1+\tan^2\frac{\theta_\alpha}{2}\right)^{-S_\alpha}\sum_{m_\alpha=0}^{2S_\alpha}\frac{1}{m_\alpha!}\left(\tan\frac{\theta_\alpha}{2}e^{-i\chi_\alpha}\hat{S}_\alpha^+\right)^{m_\alpha}|0\rangle \\ &= \left[\prod_\alpha \left(1+\tan^2\frac{\theta_\alpha}{2}\right)^{-S_\alpha}\right]\sum_{\{m_\alpha\}}\prod_\alpha\frac{1}{m_\alpha!}\left(\tan\frac{\theta_\alpha}{2}e^{-i\chi_\alpha}\hat{S}_\alpha^+\right)^{m_\alpha}|0\rangle \\ &= \left[\prod_\alpha \left(1+\tan^2\frac{\theta_\alpha}{2}\right)^{-S_\alpha}\right]\sum_{\{m_\alpha\}}\prod_\alpha\left(\tan\frac{\theta_\alpha}{2}e^{-i\chi_\alpha}\right)^{m_\alpha}\sqrt{\frac{(2S_\alpha)!}{m_\alpha!(2S_\alpha-m_\alpha)!}}\,|\cdots;S_\alpha,-S_\alpha+m_\alpha,\cdots\rangle\,, \end{aligned} \tag{C.5}$$

where the summation is taken over all possible combinations of integer values of $\{m_\alpha\}$. For convenience, we define coefficients

$$\begin{aligned} B_{m_\alpha}(q,p) &= \prod_\alpha \left(1+\tan^2\frac{\theta_\alpha}{2}\right)^{-S_\alpha}\left(\tan\frac{\theta_\alpha}{2}e^{-i(\chi_\alpha-\Phi)}\right)^{m_\alpha}\sqrt{\frac{(2S_\alpha)!}{m_\alpha!(2S_\alpha-m_\alpha)!}} \\ &= \prod_\alpha \left(\frac{j_\alpha}{2S_\alpha}\right)^{m_\alpha/2}\left(\frac{2S_\alpha-j_\alpha}{2S_\alpha}\right)^{S_\alpha-m_\alpha/2}\sqrt{\frac{(2S_\alpha)!}{m_\alpha!(2S_\alpha-m_\alpha)!}}e^{-im_\alpha\phi_\alpha}, \end{aligned} \tag{C.6}$$

where $\phi_\alpha \equiv \chi_\alpha - \Phi$ and $j_\alpha = S_\alpha(1-\cos\theta_\alpha)$. Using the coefficients $B_{m_\alpha}(q,p)$, Eq. (C.5) becomes

$$|Z\rangle = \sum_{\{m_\alpha\}} e^{-i\Phi\sum_\alpha m_\alpha} B_{m_\alpha}(q,p)\,|\cdots;S_\alpha,-S_\alpha+m_\alpha,\cdots\rangle\,. \tag{C.7}$$

Also,

$$\begin{aligned} |Z\rangle &= e^{-i\Phi\hat{J}}\sum_{\{m_\alpha\}} B_{m_\alpha}(q,p)\,|\cdots;S_\alpha,-S_\alpha+m_\alpha,\cdots\rangle \\ &= e^{-i\Phi\sum_\alpha(\hat{S}_\alpha^0+S_\alpha)}\sum_{\{m_\alpha\}} B_{m_\alpha}(q,p)\,|\cdots;S_\alpha,-S_\alpha+m_\alpha,\cdots\rangle \\ &= \sum_{\{m_\alpha\}} e^{-i\Phi\sum_\alpha m_\alpha} B_{m_\alpha}(q,p)\,|\cdots;S_\alpha,-S_\alpha+m_\alpha,\cdots\rangle\,. \end{aligned} \tag{C.8}$$

Comparing Eq. (C.7) with (C.8), therefore, we reach Eq. (4.34).

Appendix D

Exact energy spectra in multi-level pairing model

D.1 Two-level system

We give the energy spectra with various coupling constant g in $\Omega_1 = \Omega_2 = 8$, $\epsilon_1 = -\epsilon_0$, and $\epsilon_2 = 0\epsilon_0$. We fix the seniority as $\nu = 0$. The level spacing is $\Delta\epsilon = \epsilon_2 - \epsilon_1 = \epsilon_0$. We use a dimensionless coupling constant x as in Eq. (B.6) instead of g. $N = 16$ corresponds to the closed shell.

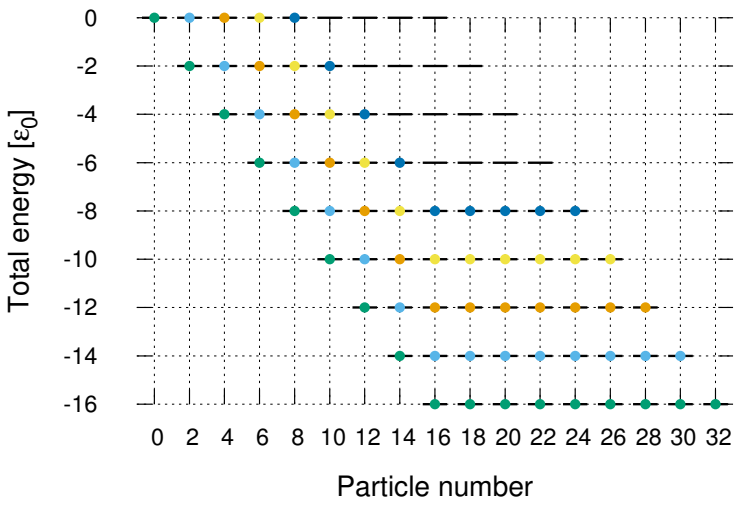

Figure D.1: Energy spectra in $x = 0$ (no pairing correlation). Horizontal line is total particle number and Vertical line is total energy in units of ϵ_0. Green, light blue, orange, yellow, and deep blue dots correspond to $|0_1^+\rangle \sim |0_5^+\rangle$, respectively.

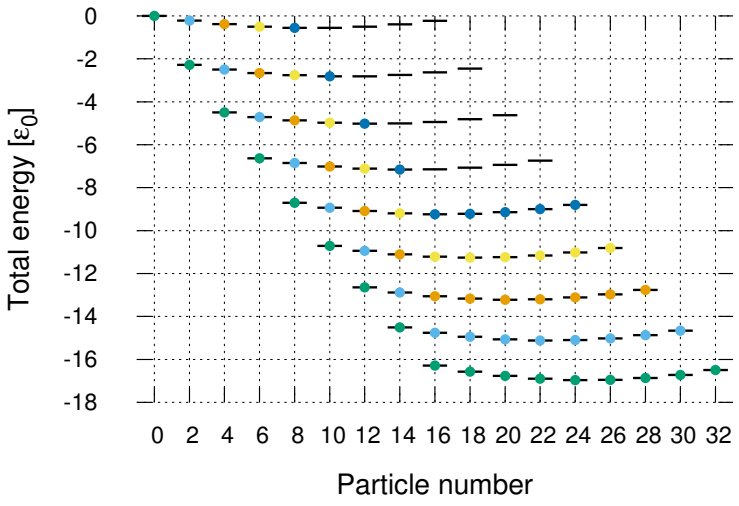

Figure D.2: The same as described in the caption of Fig. D.1 but for $x = 0.5$.

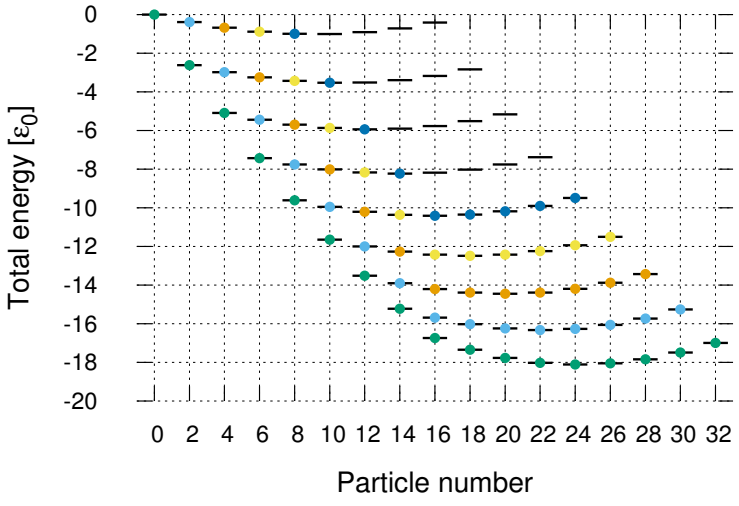

Figure D.3: The same as described in the caption of Fig. D.1 but for $x = 1$.

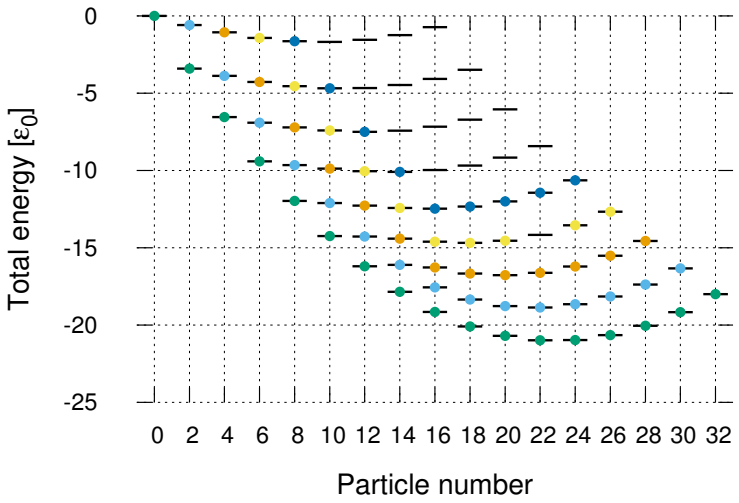

Figure D.4: The same as described in the caption of Fig. D.1 but for $x = 2$.

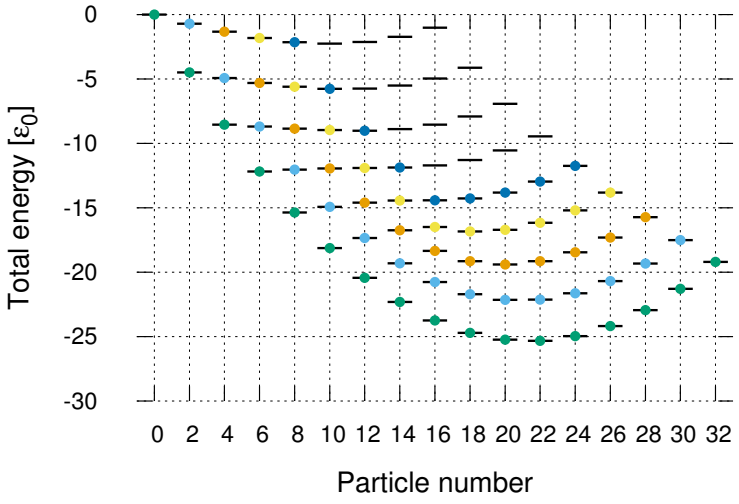

Figure D.5: The same as described in the caption of Fig. D.1 but for $x = 3.2$.

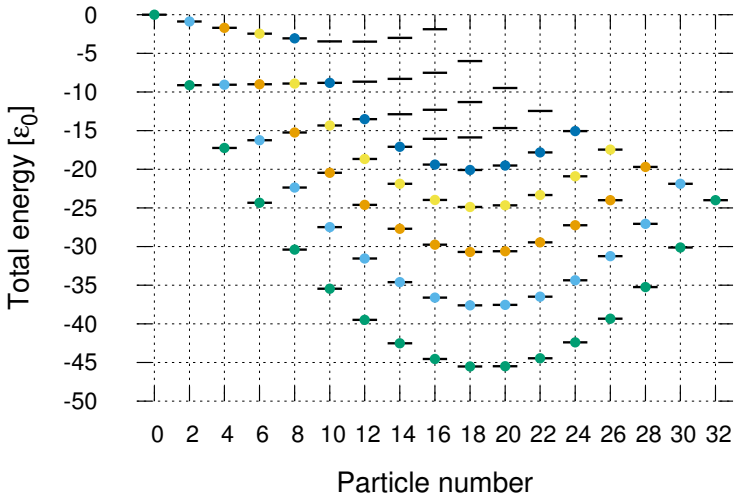

Figure D.6: The same as described in the caption of Fig. D.1 but for $x = 8$.

D.2 Three-level system

We give the energy spectra with various coupling constant g in $\Omega_1 = \Omega_2 = \Omega_3 = 8$, $\epsilon_1 = -\epsilon_0$, $\epsilon_2 = 0\epsilon_0$, and $\epsilon_3 = 1.5\epsilon_0$. We fix the seniority as $\nu = 0$. $N = 16$ and $N = 32$ correspond to the closed shell.

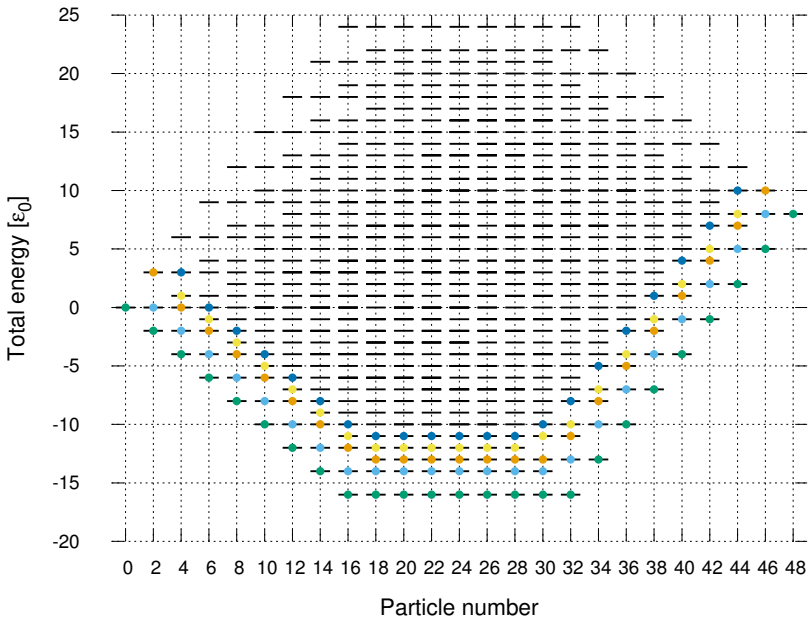

Figure D.7: The same as described in the caption of Fig. D.1 but for $g = 0\epsilon_0$.

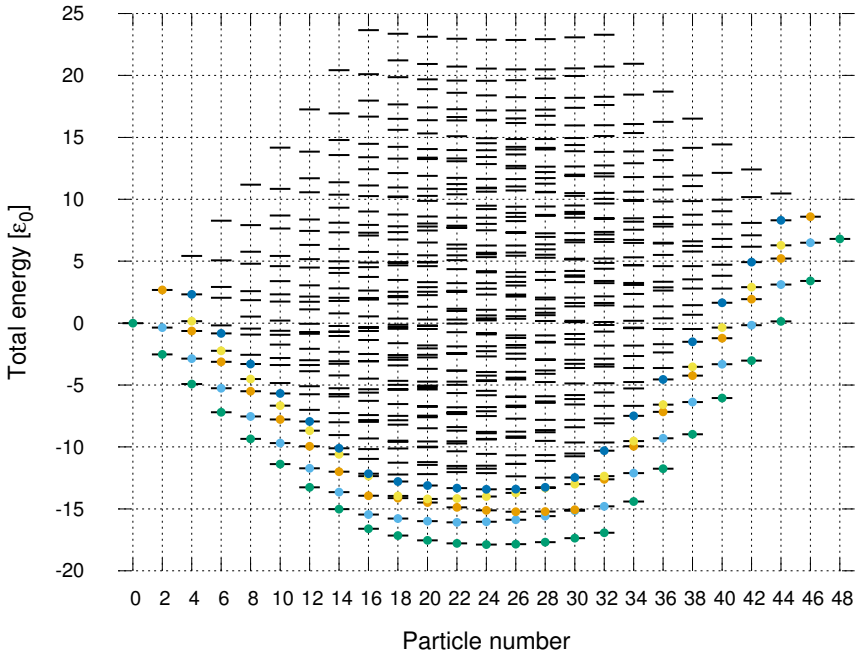

Figure D.8: The same as described in the caption of Fig. D.1 but for $g = 0.05\epsilon_0$.

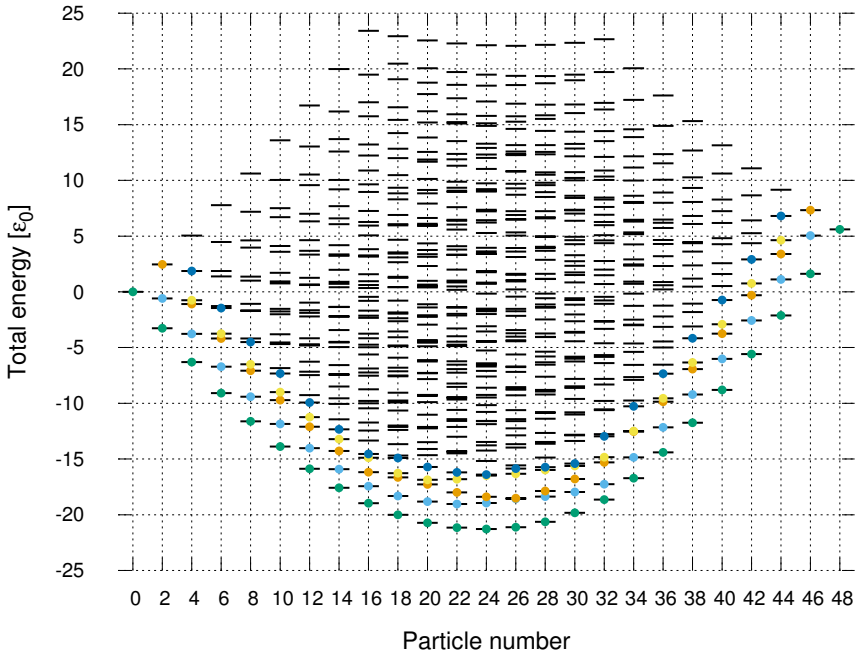

Figure D.9: The same as described in the caption of Fig. D.1 but for $g = 0.1\epsilon_0$.

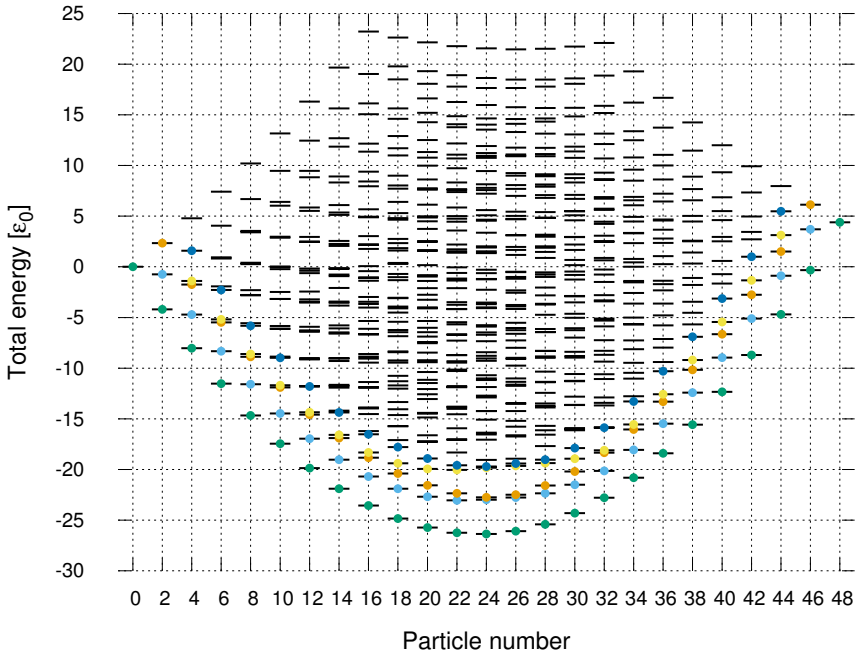

Figure D.10: The same as described in the caption of Fig. D.1 but for $g = 0.15\epsilon_0$.

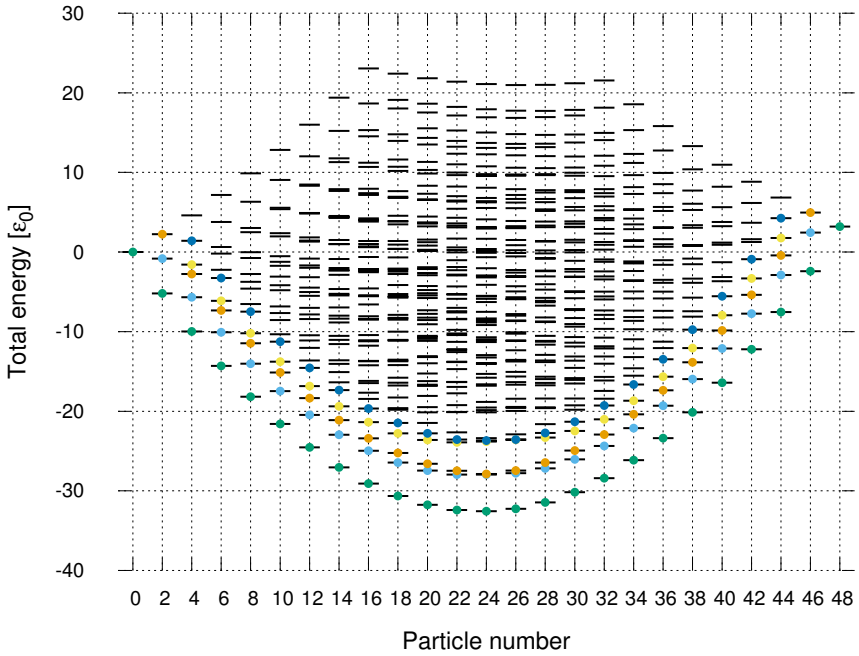

Figure D.11: The same as described in the caption of Fig. D.1 but for $g = 0.2\epsilon_0$.

Bibliography

[1] A. Kankainen, J. Äystö, and A. Jokinen. J. Phys. G 39, 093101 (2012).

[2] G. Potel, F. Barranco, F. Marini, A. Idini, E. Vigezzi, and R. A. Broglia. Phys. Rev. Lett 107, 092501 (2011).

[3] N. Hinohara and W. Nazarewicz. Phys. Rev. Lett 116, 152502 (2016).

[4] D. J. Thouless and J. G. Valatin. Nucl. Phys. 31, 211 (1961).

[5] R. A. Broglia, O. Hansen, and C. Riedel. Adv. Nucl. Phys. 6, 287 (1973).

[6] K. Heyde and J. L. Wood. Rev. Mod. Phys. 83, 1467 (2011).

[7] D. R. Bès and R. A. Broglia. Nucl. Phys. A 80, 289 (1966).

[8] J. V. Maher, J. R. Erskine, A. M. Friedman, J. P. Schiffer, and R. H. Siemssen. Phys. Rev. Lett. 25, 302 (1970).

[9] J. V. Maher, J. R. Erskine, A. M. Friedman, R. H. Siemssen, and J. P. Schiffer. Phys. Rev. C 5, 1380 (1972).

[10] R. F. Casten, E. R. Flynn, J. D. Garrett, O.Hansen, T. J. Mulligan, D. R. Bessab, R. A. Broglia, and B. Nilsson. Phys. Lett. B 40, 333 (1972).

[11] R. E. Griffin, A. D. Jackson, and A. B. Volkov. Phys. Lett. B 36, 281 (1971).

[12] W. I. v. Rij and S. H. Kahana. Phys. Rev. Lett. 28, 50 (1972).

[13] I. Ragnarsson and R. A. Broglia. Nucl. Phys. A 263, 315 (1976).

[14] A. Bohr and B. R. Mottelson. *Nuclear Structure, Vol. II.* W. A. Benjamin, New York (1975).

[15] P. E. Garrett. J. Phys. G: Nucl. Part. Phys. 27, R1 (2001).

[16] W. D. Kulp, J. L. Wood, P. E. Garrett, C. Y. Wu, D. Cline, J. M. Allmond, D. Bandyopadhyay, D. Dashdorj, S. N. Choudry, A. B. Hayes, H. Hua, M. G. Mynk, M. T. McEllistrem, C. J. McKay, J. N. Orce, R. Teng, and S. W. Yates. Phys. Rev. C 77, 061301(R) (2008).

[17] J. F. Sharpey-Schafer, S. M. Mullins, R. A. Bark, J. Kau, F. Komati, E. A. Lawrie, J. J. Lawrie, T. E. Madiba, P. Maine, A. Minkova, S. H. T. Murray, N. J. Ncapayi, and P. A. Vymers. Eur. Phys. J. A 47:, 5 (2011).

[18] P. E. Garrett and J. L. Wood. J. Phys. G: Nucl. Part. Phys. 37, 064028 (2010).

[19] T. Nakatsukasa, K. Matsuyanagi, M. Matsuo, and K. Yabana. Rev. Mod. Phys. 88, 045004 (2016).

[20] S. Ebata, T. Nakatsukasa, T. Inakura, K. Yoshida, Y. Hashimoto, and K. Yabana. Phys. Rev. C 82, 034306 (2010).

[21] K. Yoshida and T. Nakatsukasa. Phys. Rev. C 83, 021304 (2011).

[22] K. Yoshida and T. Nakatsukasa. Phys. Rev. C 88, 034309 (2013).

[23] G. Scamps and D. Lacroix. Phys. Rev. C 88, 044310 (2013).

[24] T. Nakatsukasa, T. Inakura, and K. Yabana. Phys. Rev. C 76, 024318 (2007).

[25] J. Terasaki and J. Engel. Phys. Rev. C 83, 021304(R) (2011).

[26] D. R. Bès, R. A. Broglia, R. P. J. Perazzo, and K. Kumar. Nucl. Phys. A 143, 1 (1970).

[27] A. Góźdź, K. Pomorski, M. Brack, and E. Werner. Nucl. Phys. A 442, 50 (1985).

[28] K. Zajac, L. Prochniak, K. Pomorski, S. G. Rohozinski, and J. Srebrny. Nucl. Phys. A 653, 71 (1999).

[29] K. Pomorski. Int. J. Mod. Phys. E. 16, 237 (2007).

[30] P. Ring and P. Schuck. *The nuclear many-body problems*. Springer-Verlag, New York (1980).

[31] M. Matsuo, T. Nakatsukasa, and K. Matsuyanagi. Prog. Theor. Phys. 103, 959 (2000).

[32] T. Nakatsukasa. Prog. Theor. Exp. Phys. 2012, 01A207 (2012).

[33] K. Kumar and M. Baranger. Nucl. Phys. A 92, 608 (1967).

[34] R. W. Richardson. Phys. Lett. 3, 277 (1963).

[35] R. W. Richardson and N. Sherman. Nucl. Phys. 52, 221 (1964).

[36] R. W. Richardson and N. Sherman. Nucl. Phys. 52, 253 (1964).

[37] R. W. Richardson. Phys. Rev. 141, 949 (1966).

[38] R. W. Richardson. J. Math. Phys. 6, 1034 (1965).

[39] C. Qi and T. Chen. Phys. Rev. C 92, 051304(R) (2015).

[40] F. Ni and T. Nakatsukasa. Phys. Rev. C 97, 044310 (2018).

[41] J. W. Negele. Rev. Mod. Phys. 54, 913 (1982).

[42] S. Levit. Phys. Rev. C 21, 1594 (1980).

[43] S. Levit, J. W. Negele, and Z. Paltiel. Phys. Rev. C 21, 1603 (1980).

[44] H. Kuratsuji and T. Suzuki. Phys. Lett. B 92, 19 (1980).

[45] H. Kuratsuji. Prog. Theor. Phys. 65, 224 (1981).

[46] H. Reinhardt. Nucl. Phys. A 346, 1 (1980).

[47] T. Suzuki and Y. Mizobuchi. Prog. Theor. Phys, 79, 480 (1988).

[48] M. Cambiaggio, G. Dussel, and M. Saraceno. Nucl. Phys. A 415, 70 (1984).

[49] L. D. Landau and E. M. Lifshitz. *Quantum Mechanics.* A Course of Theoretical Physics. Pergamon Press, Oxford (1965).

[50] T. Marumori, T. Maskawa, F. Sakata, and A. Kuriyama. Prog. Theor. Phys. 64, 1294 (1980).

[51] K. Sato. Prog. Theor. Exp. Phys. 2018, 103D01 (2018).

[52] H. Nobuo, N. Takashi, M. Masayuki, and M. Kenichi. Prog. Theor. Phys. 117, 451 (2007).

[53] F. Ni, N. Hinohara, and T. Nakatsukasa. Phys. Rev. C 98, 064327 (2018).

[54] A. Bohr and B. R. Mottelson. *Nuclear Structure, Vol.1: Single-Particle Motion.* W. A. Benjamin (1969).

[55] H. Nobuo, N. Takashi, M. Masayuki, and M. Kenichi. Prog. Theor. Phys. 119, 59 (2008).

[56] K. Wen and T. Nakatsukasa. Phys. Rev. C 94, 054618 (2016).

[57] K. Wen and T. Nakatsukasa. Phys. Rev. C 96, 014610 (2017).

[58] T. Nakatsukasa, T. Inakura, and K. Yabana. Phys. Rev. C 76, 024318 (2007).

[59] N. Hinohara, M. Kortelaine, and W. Nazarewicz. Phys. Rev. C 87, 064309 (2013).

[60] D. Brink and R. A. Broglia. *Nuclear Superfluidity, Pairing in Finite Systems.* Cambridge University Press, Cambridge (2005).